ZULF NMR

Zero and Ultra-Low Fields NMR, Innovative Training Network

UNIVERSITÀ DEGLI STUDI DI TORINO

Scuola di Dottorato in Scienze della Natura e Tecnologie

Innovative Dottorato in Scienze Farmaceutiche e Biomolecolari

(XXXIV ciclo)

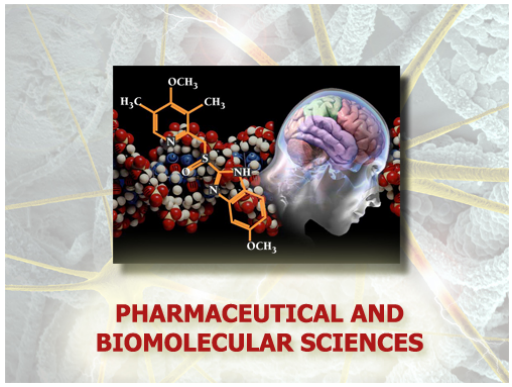

Para-Hydrogen Hyperpolarization of metabolic substrates for Zero and Ultra-Low Field (ZULF) NMR detection

Candidata: Tutor:

Oksana Bondar **Prof. Francesca Reineri**

2022

Dedicata a coloro che
ci provano ogni giorno.

TO MY LOVELY SON DAVYD

ABSTRACT

Sensitivity is a central issue in Magnetic Resonance based techniques, i.e. NMR spectroscopy and Magnetic Resonance Imaging (MRI). Different Hyperpolarization methods have been developed in the last few decades in order to increase the intensity of NMR signal thousands of times, with respect to thermal equilibrium. As far as the application of hyperpolarized substrates to medical diagnostics is concerned, d-DNP (dissolution-Dynamic Nuclear Polarization) is the gold-standard method and several clinical studies are currently ongoing. Among all the metabolites that have been hyperpolarized by means of d-DNP, pyruvate is the most widely applied and the only one that has been translated to clinical research. Unfortunately, the cost of purchase and maintenance of d-DNP polarizers is quite high and the polarization cycles are rather time-consuming. These features strongly limit the application of this powerful diagnostic tool to few research sites. ParaHydrogen Induced Polarization (PHIP) is a hyperpolarization method significantly less technically demanding than d-DNP and the polarization cycles are much faster. The work reported in

this thesis deals with the development of PHIP hyperpolarization of metabolites for in-vivo MRI and MRS studies. After an introduction to the MR hyperpolarization methods in general, the first experimental chapter is dedicated to the hyperpolarization of pyruvate by means of PHIP-SAH (PHIP and Side Arm Hydrogenation), a strategy introduced by this laboratory a few years ago. The main factors that determine the hyperpolarization level on the product and the strategies that can be applied to increase it are described. The second and third experimental chapters (Chapters 3 and 4) are focused on the application of this metabolite, hyperpolarized by means of PHIP, to biological studies. In particular, in chapter 3, HP-pyruvate has been used for the investigation of metabolism in prostate cancer cells characterized by different aggressiveness while in chapter 4 the work has been dedicated to improve the biocompatibility of the solutions of HP-pyruvate. The last chapter is dedicated to the use of Zero and Ultra Low Field (ZULF) NMR for the detection of PHIP polarized metabolites. ZULF-NMR is an emerging field of MR based techniques, based on the detection of MR signals without the application of a strong magnetic field, which is usually employed in conventional NMR and MRI machines. The use of ultra low magnetic field (below geomagnetic field) reduces the size and the cost of NMR, but also the intensity of MR signals, therefore hyperpolarization is an ideal partner for ZULF detection. In this chapter, the fundamentals of ZULF NMR are briefly discussed and the studies carried out using two metabolites (fumarate and pyruvate) are reported.

ACKNOWLEDGEMENTS

I am grateful to a large number of people who have made this work as a great journey to the academia word and help me got the best experience.

Foremost, I would like to thank my advisers Francesca Reineri and Silvio Aime for the choosing me for the ZULF project and for their directing me during whole my PhD.

I am immensely grateful to Francesca for her patience, understanding and help throughout the entire project. She introduced me new and magic world of hyperpolarization and MRI. The knowledge I've got during my education in Torino University and practical experience are extremely important for my future building the career as a scientist.

I also want to thank Eleanora Cavallari and Carla Carrera, who were not only my mentors, but also friends all time I've spent in Italy, as well as all Aime's group, who were so kind to me during this three year.

I am gratefully thankful for Malcolm Levitt for so important knowledge in NMR I've got during my secondment, for his support during the difficult

time for me and for the possibility work at the magnificent environment as his group, which made my time in Southampton wonderful. I want thank all people with whom I were working in Southampton, especially Laurynas Dagys and Johannes Colell for their help in the implementation of the project and friendly relations.

Additionally, I would like to thank James Eills who has also mentoring me and helped a lot during my PhD study; as well as I want to thank John Blanchard, Román Picazo Frutos and Dima Budker for the great collaboration and wonderful results obtained during it.

I am indebted to Szymon Pustelny who implemented such an important and interesting project, bringing together many universities and wonderful people working in different fields of science, but at the same time trying to achieve one goal.

I would also like to thank all the people directly or indirectly involved to the project generally or to the research that contributed to this thesis: Krystian Sycz, Ginevra Di Matteo, Erika Cerutti, Giuseppe Digilio, Kirill Sheberstov, Seyma Alcicek, Piotr Put, James Whipham and Marcel Utz.

Lastly, let me extend my thanks to the most important people in my life. I am greatly indebted to my parents and my family for all their support over the years. Finally, the main thank to my son Davyd, who has been my inspiration and source of strength all this time, and without him, this dissertation will not exist.

None of this would have been possible without all of them!

CONTENTS

CHAPTER 1

INTRODUCTION: HYPERPOLARIZATION IN NMR.

1.1 INTRODUCTION

Important characteristic of the atom and nuclei is the magnetic moment μ. Only nuclei for which mass number M and number of protons Z are even have no magnetic moments ($\mu = 0$). They include an even number of protons and neutrons (^{12}C, ^{16}O, ^{28}Si, ^{32}S, and others). These nuclei cannot be studied by NMR. All other nuclei (118 stable isotopes, 104 known chemical elements of the Periodic Table) have magnetic moments, and NMR can be observed for them. These magnetic nuclei differ in the magnitude of the magnetic moments and in the value of the nuclear spin I. Spin is the intrinsic angular momentum of a particle, electron, or atomic nucleus.

To understand better angular momentum, let's discuss situation when we have two particles with spin $I_1 = I_2 = 1/2$ (as example it could be two proton atoms at the hydrogen molecule). Hydrogen consists from two spins 1/2 that are magnetically equivalent and couplet through J-coupling interaction. In this situation total angular momentum (J) will be $J = \left|I_1 - I_2\right| = 0$ or $J = \left|I_1 + I_2\right| = 1$. In case of the total angular momentum $J = 1$ we can tell about parallel spins and antiparallel in case of 0 angular momentum.

These states have different energy with the azimuthal quantum number M_z ranging from $-J$ to J (total number of states are calculated by the formula $2J + 1$). At the isotropic environmental as a result will be obtained triplet state (three similar energy level) for total angular momentum equal one and singlet in case of $J = 0$, that explains different states of the hydrogen molecule (more will be describing later).

The presence of spin in the particles also leads to the existence of a magnetic moment in it, with which magnetic resonance deals. Nuclear magnetic resonance is the phenomenon of resonant absorption of electromagnetic radiation (radio frequency range) by a system of nuclear magnetic moments

placed in an external magnetic field. Atom with the spin $I = 1/2$ after placement to the external magnetic field has two energy levels that can be labeled α and β and are called eigenstates of angular momentum or *Zeeman eigenstates*:

$$|\alpha\rangle = |\frac{1}{2}, +\frac{1}{2}\rangle$$

$$|\beta\rangle = |\frac{1}{2}, -\frac{1}{2}\rangle$$

As magnetic field is applied along the z - axis the state $|\alpha\rangle$ is also polarized along the z - axis (positive axis direction) and the state $|\beta\rangle$ is polarized along the $-z$ - axis (negative axis direction). Applied magnetic field has magnitude B^0 and the spins precess in this field with the speed determined by the Larmor frequency (ω^0) proportional to the magnetic field strength and the magnetogyric ratio (γ) for these spins. So, for the 1/2 spin the eigenvalues $\pm\frac{1}{2}\omega^0$ are the energies of the states. If we are talking about energy level splitting of the spin at the magnetic field we can talk about *Zeeman splitting*, that is equal to the Larmor frequency, where $|\alpha\rangle$ is lower energy state and $|\beta\rangle$ is the state with the higher energy.

The intensity of the NMR signal is directly proportional to the spin polarization - the relative difference in the populations of this two energy levels of nuclear spins and prescribed by Boltzmann distributions (in this equation shown for α and β levels):

$$\frac{P_\beta}{P_\alpha} = e^{\frac{-\Delta E}{k_B T}} \tag{1.1}$$

where P_β and P_α are populations of these levels, ΔE is the Energy difference between the levels, k_B is the Boltzmann constant and T is the system temperature.

Despite numerous advantages, a main limitation of NMR spectroscopy is due to the low sensitivity. At thermal equilibrium, the difference between the populations of the nuclear spin states is only a few ppm, in other words,

only one nuclear spin in 10^6 is polarized in a NMR magnet. Hyperpolarization methods allow to temporarily increase the level of nuclear spin polarization up to several thousand times.[1] (Fig. 1.1)

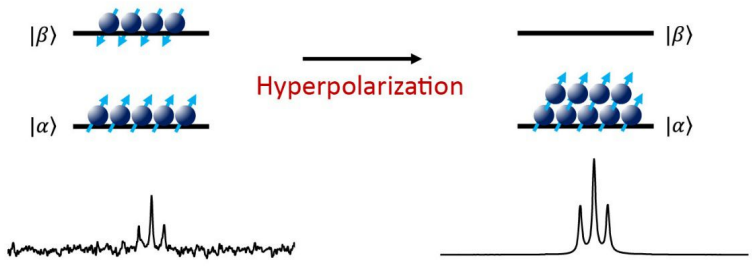

Figure 1.1: *Schematic representation of thermal equilibrium (left) and hyperpolarization in a system of isolated nuclear spins. At thermal equilibrium the two states (α and β states) are almost equally populated, while, following to hyperpolarization, one state is more populated than the other (in this case, the most stable state is more populated that the less stable one). This leads to a significant enhancement of the NMR signal.*

Here are described the main methods to obtain hyperpolarization.

1.2 Spin Exchange Optical Pumping (SEOP).

Spin-Exchange Optical Pumping (SEOP) allows the production of spin-polarized ^{3}He and ^{129}Xe gases.[2]

Conventional magnetic resonance imaging based on proton signals is not suitable for examining the lungs due to low proton density and changes in sensitivity between tissues and airspace. Therefore, the use of hyperpolarized noble gases (^{3}He and ^{129}Xe) was first introduced to obtain MR images of the

anatomy of the air space for indirect imaging of the pathological condition[3], in addition, noble gases are characterized by a very long T1, which allows long storage before their use. The hyperpolarization of ^{3}He, ^{129}Xe and ^{83}Kr is achieved using a procedure based on laser polarization of gaseous alkali atoms, which transfer polarization to noble gas nuclei due to van der Waals forces (Figure 1.2).

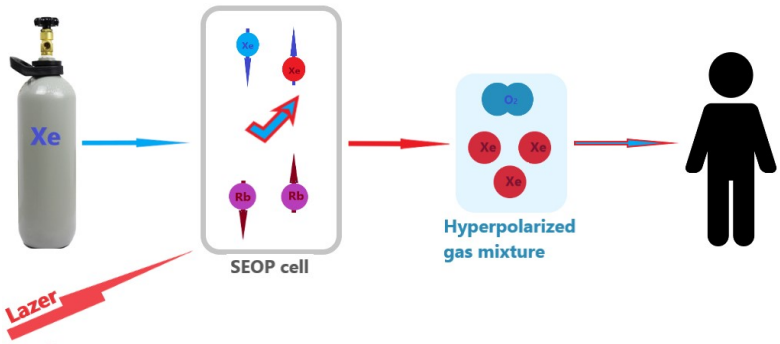

Figure 1.2: *Xenon is polarized using Spin Exchange Optical Pumping (SEOP). In SEOP, xenon flows into a chamber containing rubidium gas vapor in the presence of a magnetic field. The rubidium is excited by a laser. Xe colliding with the Rb results in a spin exchange, whereby a greater proportion of Xe atoms are in the lower energy spin state*

Noble gas nuclei, which have a non-zero nuclear spin, can be optically hyperpolarized to a degree several orders of magnitude greater than that corresponding to the thermal equilibrium distribution. The otherwise inert noble gas becomes extremely sensitive to magnetic resonance detection. A hyperpolarized gas is obtained by transferring angular momentum from circularly polarized light to a noble gas nucleus through interatomic collisions between the inert gas nuclei and an alkali metal, which absorbs this angular

momentum. In spin-exchange optical pumping, circularly polarized light is absorbed by a saturated vapor of alkali metal atoms contained in a glass cuvette. Part of the spin moment of the absorbed photons is transferred to the alkali metal atoms, and the valence electrons of the alkali metal atoms are polarized. Subsequent collisions between alkali metal atoms and noble gas atoms transfer part of the electron spin polarization to noble gas nuclei.

1.3 Dynamic Nuclear Polarization (DNP).

The fundamental concept of DNP was originally proposed by Overhauser in 1953, and is based on the transfer of the large electron spin polarization to nuclear spins $\gamma_e / \gamma_n > 657$ through microwave irradiation. In 1993–1995 high field, solid state MAS DNP experiments, utilizing gyrotron microwave sources, were described by Griffin and coworkers.[4,5] Subsequently, in 2003 the Nycomed/ Amersham group reported the possibility of polarizing samples at very low temperatures followed by fast dissolution, heating, and observation of the liquid state spectrum.[6] The first paper on dissolution-DNP reported a signal enhancement in the liquid sate of 10,000 compared to thermal polarization at 7 T and opened up to new possibilities of using hyperpolarized substances in the liquid state as diagnostic probes.[6,7] In particular, metabolic imaging has been made possible by the availability of hyperpolarized metabolic substrates.[7–10] D-DNP developed at rapid pace and moved, in less than two decades, from pre-clinical studies to clinical trials. Hyperpolarized [1-^{13}C] pyruvate is the substrate that has been most widely applied for the investigation of metabolism and its alterations in different diseases.[11]

D-DNP hyperpolarization (Fig. 1.3) is made by the following steps : 1) mixing the targeted ^{13}C labelled compound with a free radical (a source of unpaired electrons) or glass-forming agent (such as glycerol that is effective in

reducing ice crystal formation during freezing), 2)placing the mixture in a high magnetic field (3-7 T), 3) cooling to 1-2 K, and 4)irradiating with microwaves for a time delay that ranges from 20 min to a few hours. By choosing the monochromatic microwave irradiation at the off-resonans frequency with the electron spin, the high degree of electron polarization can be transferred to nearby nuclear spins. During the dissolution step, to the sample is rapidly heated and dissolved via the injection of a hot solvent, while maintaining a high level of polarization. However, hyperpolarization is a non-stable state and thermal polarization is restored in a time that is dictated by the T_1 relaxation time, therefore the hyperpolarized substrate must be quickly used, after the dissolution step.

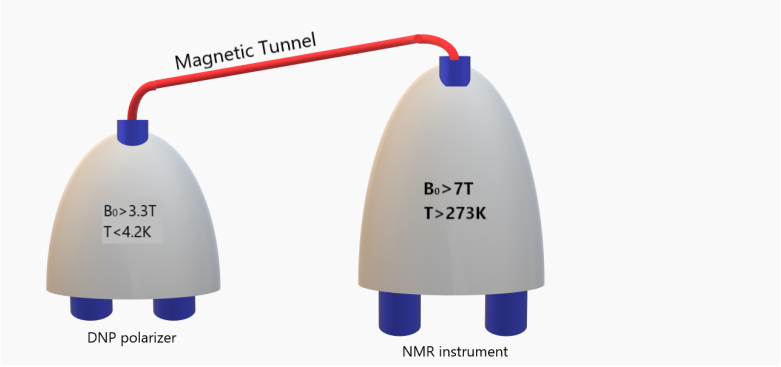

Figure 1.3: *Schema of the principle setup for d-DNP experiment. The DNP apparatus (left) typically operates at comparable or slightly lower magnetic fields than the NMR spectrometer used for detection (right).*

1.4 Parahydrogen Induced Polarization (PHIP).

PHIP is a chemistry-based hyperpolarization method based on the addition of hydrogen in the para-spin isomer to the unsaturated substrate. In order to understand how hyperpolarization can derive from parahydroge, it is necessary to define what parahydrogen is and how it can be obtained. The two spins of the hydrogen molecule (H_2) can combine in four different spin states (as were mentioned in Introduction), as follows:

$$|S_0\rangle = \frac{1}{\sqrt{2}} \times \left(|\alpha\beta\rangle - |\beta\alpha\rangle\right)$$
$$|T_{+1}\rangle = |\alpha\alpha\rangle$$
$$|T_0\rangle = \frac{1}{\sqrt{2}} \times \left(|\alpha\beta\rangle + |\beta\alpha\rangle\right)$$
$$|T_{-1}\rangle = |\beta\beta\rangle$$

The first state has total spin angular momentum J=0 and is a singlet state ($|S_0\rangle$), the other three states have J=1 and give a triplet state ($|T\rangle$). The singlet state is antisymetric with respect to spin exchange, while the triplet states are symmetric, therefore a nonequilibrium state containing a population imbalance between singlet and triplet states cannot be brought into equilibrium by symmetric interaction of the two spins (e.g. intramolecular DD interactions or application of rf radiation) because of the symetry reason[12]. The singlet state $J = 0$ in this case is a long-lived state[13]. In the case of molecular hydrogen, these two states (singlet and triplet states) are so well isolated one from the other that they behave as chemically different substances, named para- (pH_2) and ortho-hydrogen (o-H_2). At high temperature (T ˜ 298 K), all four states are equally populated, resulting in a mixture of 25% p-H_2 and 75% o-H_2.

Conversely, at low temperature, the para-hydrogen isomer is more stable than the ortho- isomers and the para-isomer percentage is higher, at equilibrium.

Enrichment in para-H_2 is obtained by flowing normal-H_2 through a catalyst (Fe_2O_3) at low temperature. As can be observed in Fig. 1.4, the parahydrogen fraction is about 50% at 77 K (liquid N_2 temperature) while it is increased to almost 100% at temperature lower than 32 K.

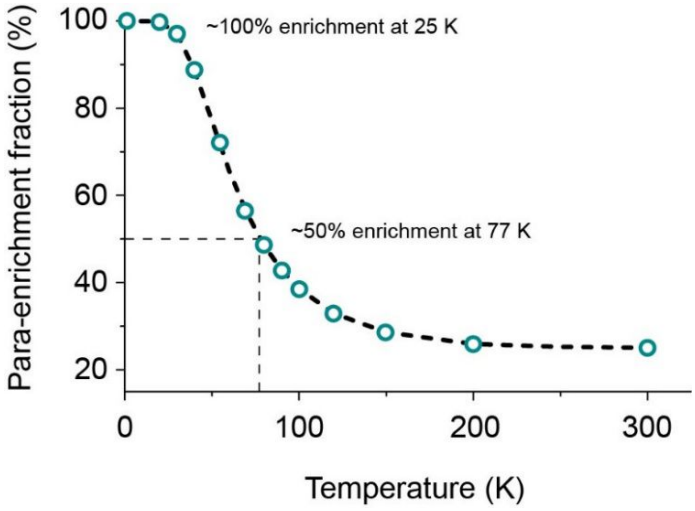

Figure 1.4: *para-H_2 percentage at different temperatures (equilibrium condition)*

The enrichment can be maintained, at high temperature, provided that the conversion catalyst is removed and para-hydrogen is stored in a bottle without any paramagnetic impurities or surfaces that can catalyse the para-ortho conversion.

Parahydrogen is non-magnetic, therefore is NMR silent, but the non-equilibrium condition thus obtained can be exploited to obtain hyperpolarization. In the first two decades since its discovery, PHIP was

observed uniquely following to the chemical addition of parahydrogen to unsaturated bonds (double or triple bonds). This effect can be referred to as hydrogenative-PHIP (h-PHIP), in contrast to the non-hydrogenative-PHIP effect (i.e. SABRE) that discovered later, in 2009, by S.Duckett and coworkers.[14–17] In this thesis only h-PHIP will be applied in the experiments, but here both methods are quickly described.

1.4.1 Signal Amplification by means of Reversible Exchange (SABRE).

In 2009, a non-hydrogenative variant of PHIP was discovered and introduced as SABRE.[14–17]Since the discovery of SABRE, the fundamental aspects of spin physics and chemical mechanisms have been of primary interest. Regarding spin physics, many theoretical descriptions of polarization transfer to various nuclei at low and high magnetic fields have been presented on the example of various compounds and their isotopes.

The spin dynamics depend obviously on the structure and chemistry of the SABRE complex. SABRE employs a reversible interaction of the ligand, an Iridium-based active catalyst ([Ir(COD)IMes]Cl, (IMes = 1,3-bis(2,4,6-trimethylphenyl)imidazol-2-ylidene; COD = cyclooctadiene)] as a precatalyst, which forms a ternary labile octahedral complex after activation) and p-H_2. Because of this reversible interaction, a labile complex of p-H_2, catalyst and the ligand is formed (Fig. 1.5). In such a complex, high spin polarization is transferred from p-H_2 to the ligand via the catalyst. Finally, the active complex splits up, but the released ligand is hyperpolarized.

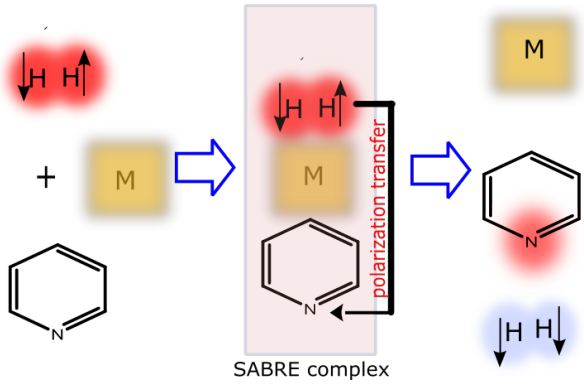

Figure 1.5: *Schematic view of the SABRE reaction and the hyperpolarization process, where pH_2 and substrate (py) exchange reversibly with a polarization transfer complex (SABRE complex) and spin order is transferred to the substrate via electron mediated J-couplings.*

In SABRE method, para-hydrogen molecules and substrate molecules are in the process of molecular chemical exchange on a hexacoordinated iridium complex. Polarization transfer is mediated by a scalar J-couplings network of active SABRE catalyst bonds and is the most effective in very weak magnetic fields in the range of 0–10 mT. With synchronization of the exchange rate, spin-spin interactions and a constant magnetic field (as were explained before in milli- and micro-Tesla modes), the singlet state of parahydrogen can be spontaneously transformed into hyperpolarization on the nuclei of the substrate, and some works are concerned with the level anticrossing[18], which is one of the most critical factors responsible for the polarization transfer from p-H_2 to the ligand, which can be used as a contrast agent for tomography metabolism.

Regarding molecular systems, which were SABRE hyperpolarized, it is worth noting that the pyridine (Py) molecule has been routinely employed as a molecular model for SABRE investigation. Thus, Py is a benchmark molecule in

SABRE NMR. Its use is considerably facilitated by easy handling and access of Py, including the different spin-labeled Py. Apart from Py, which is very toxic, many biorelevant molecular systems have also been hyperpolarized. Several of these molecules are of central importance in MRI, where they can serve as the contrast agents. For example one of the biorelevant molecule that comes to mind for SABRE is the pyridine derivative molecule - isonicotinic acid, one of the ingredients of vitamin B_3 [19]. Next compound, which is worth to mention is metronidazole [20–22], which belongs to the nitroimidazloes [23]. These compounds are also employed in PET as a tracer for hypoxia sensing. Their applications in for medical purpose is still increasing -in particular, in cancer therapy.

1.4.2 h-PHIP.

When the enriched para-H_2 is used in a catalytic hydrogenation, the resulting products can have substantially enhanced NMR signals, provided that the two protons are added pairwise to the substrate and that the symmetry of the hydrogen molecule is broken.

When the two protons are added to chemically different positions and the symmetry of the H_2 molecule is lost, only the states that overlap with the para-spin state become over-populated, thanks to the para-enrichment. As a consequence, the transitions from these states to the other states are hyperpolarized due to the large population difference. For simplicity, let's assume that the hydrogenation substrate does not contain protons and the two para-hydrogen atoms form an isolated two-spin system on the product molecule (Fig. 1.6).

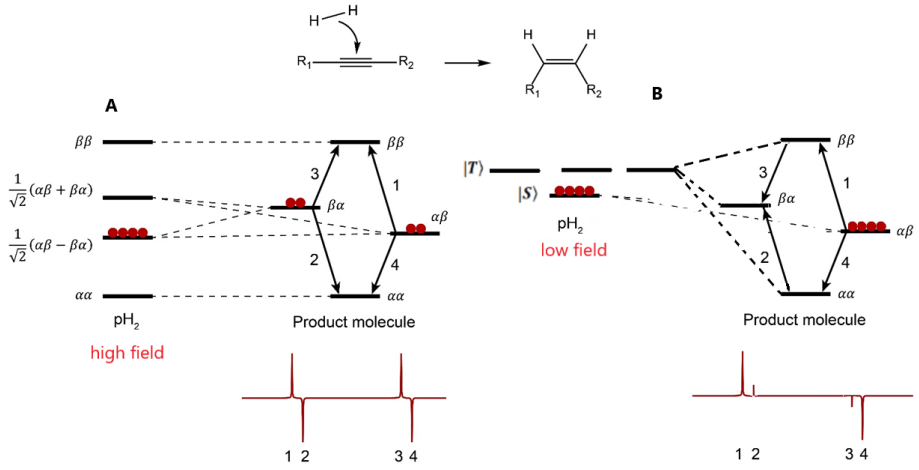

Figure 1.6: *Schematic showing a (A) PASADENA and (B) ALTADENA experiment. After a chemical reaction the parahydrogen protons end up in chemically different positions and an AX spin system is formed. This leads to an overpopulation of the $\alpha\beta$ and $\beta\alpha$ states in case of PASADENA and the $\alpha\beta$ state at the ALTADENA type experiment*

There are two different experiments using parahydrogen: PASADENA and ALTADENA. The PASADENA mechanism (para-hydrogen and synthesis can dramatically increase nuclear alignment) is observed when the hydrogenation reactions are carried out in strong magnetic fields[24]. When molecular hydrogen is added to the substrate, the two-spin system of the H_2 molecule is suddenly transformed in an AX spin system and, among the newly formed four states, only $\alpha_A\beta_X$ *and* $\alpha_X\beta_A$ equally overlap with the parahydrogen state and are overpopulated (Figure 1.6A). As a consequence, the transitions from these two states to the other states $\alpha_A\alpha_X$ *and* $\beta_X\beta_A$ are hyperpolarized due to the large population difference between the states and we expect to observe two antiphase hyperpolarized signals in the ^{1}H-NMR spectrum[25,26] as

shown at the Fig.1.6A.

While in the ALTADENA experiment (adiabatic longitudinal transfer after dissociation produces pure alignment), hydrogenation occurs in weak magnetic fields (Earth's field) outside the magnetometer with subsequent adiabatic transfer and subsequent detection in strong magnetic fields[27]. In this case, the two para-protons are the only two spins in the product and the singlet state of parahydrogen. When the symmetry is broken, the superposition of the singlet state occurs. However, the generated spin system of the product, due to the weak magnetic field of the Earth, is a strongly coupled system, which in the approximation can be considered as spin A_2 of the system. Only the energy level, which has singlet symmetry at present conditions, is populated during hydrogenation with p-H_2. This leads to selective population of one energy level and its corresponding absorption and emission peaks in the NMR spectrum (Figure 1.6B).

Synthesis of hyperpolarized contrast agents to specifically target disease tracers in vivo allows easy and fast medical diagnostics that could be one of the most promising future applications of para-hydrogen. The best contrast agent should possess a high degree of polarization and a long spin–lattice relaxation time T_1. As proton has short relaxation times (in the order of 1 - 10 s), the use of proton NMR as potential contrast agents has not been very useful[28–30], but heteronuclei such as ^{13}C and ^{15}N in biologically active material were found to possess longitudinal relaxation times that range from several seconds to several minutes, thereby significantly increasing the time available for substrate tracing in vivo[31–33]. So, using of hyperpolarized contrast agents with heteronuclei polarization would increase signal enhancement of naturally abundant thermally polarized heteronuclei such as ^{13}C[34]. That's why the logical step for producing contrast agents is reacting biochemically relevant, isotopically labelled compounds with para-hydrogen thereby polarizing the labelled species

as highly as possible and subsequently making use of high polarization and long relaxation times in the experiment of choice.

For this purpose hyperpolarization from parahydrogen protons can also be transferred to heteronuclei, such as ^{13}C or ^{15}N, through scalar couplings with parahydrogen protons. One of method of hyperpolarization, based on the chemical interaction of para-hydrogen with a substrate and, using simple and inexpensive manipulations, produces hyperpolarization on the ^{13}C atom is PHIP-SAH (para hydrogen induced polarization side arm hydrogenation), which makes it possible to obtain a pure aqueous solution of hyperpolarized substrates, especially pyruvate. More detailed this method will be described at next chapters, especially at the chapter 2.

CHAPTER 2

HYPERPOLARIZATION OF PYRUVATE USING H-PHIP

2.1 INTRODUCTION

Among the hyperpolarized substrates that can be used for metabolic studies, [1-^{13}C]pyruvate is the most widely applied because its fast metabolic transformation into lactate can give relevant diagnostic information about pathologies.[11] Hydrogenative-PHIP (h-PHIP) relies on the catalytic hydrogenation, using hydrogen enriched in the para-spin isomer, of unsaturated precursors of the target molecule, therefore hyperpolarization of pyruvate by means of h-PHIP seems precluded by the fact that an unsaturated precursor of pyruvate does not exsist. The Side-Arm Hydrogenation strategy[35,36] allowed to circumvent this issue through the syntehsis of an ester derivative of pyruvate (Fig. 2.1) that contains an unsaturated bond (double or triple bond) on the alcoholic moiety. The para-hydrogenation of this substrate and the following spin-order transfer from the parahydrogen protons to the ^{13}C carboxylate spin allow to obtain net ^{13}C magnetization on the carboxylic moiety of the ester (i.e. on pyruvate). Hydrolysis of the ester is, then, carried out quickly by means of the addition of an aqueous base (sodium hydroxide). Being the hydrogenation reaction carried out in a hydrophobic solvent (e.g. chloroform), the aqueous base does not mix with the organic phase and, after the formation of an unstable emulsion, the two phases split quickly. The carboxylate salt (sodium [1-^{13}C]pyruvate) is extracted in the aqueous phase while the metal catalyst is retained in the organic phase.

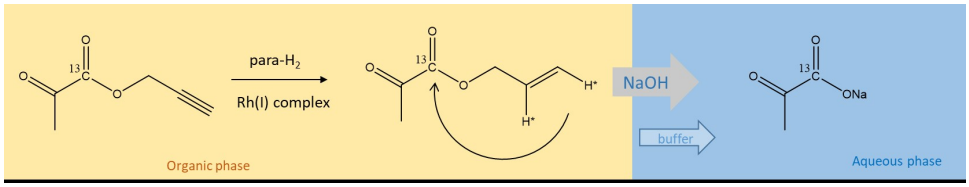

Figure 2.1: *PHIP-SAH method*: the hydrogenation reaction is hydrogenated in an organic solvent (orange background), while the sodium salt is extracted in aqueous phase (blue background).

This chapter is focused on the investigation of the different factors that determine the polarization level on the ^{13}C carboxylate signal of the final product. These factors are:

- para-hydrogen enrichment;
- polarization level on the ^{1}H-NMR signal of the para-hydrogen protons added to the product molecule;
- efficiency of the polarization transfer by means of magnetic field cycling;
- polarization losses during hydrolysis.

2.2 Materials and Methods

2.2.1 Samples preparation

The propargylic ester of pyruvate was hydrogenated using the commercial catalyst ([1,4-bis(diphenylphosphino)butane](1,5- cyclooctadiene)rhodium(I) tetrafluoroborate], Sigma Aldrich, ($1{\cdot}10^{-3}$ g). The catalyst was dissolved in $CDCl_3$ (100 µL), then the hydrogenation substrate (3 µL, $24{\cdot}10^{-6} mol$) was added. The 5mm NMR tubes used as hydrogenation reactor were pressurized

with 2.1 bar of para-enriched hydrogen (92% enriched), while keeping the NMR tube in a liquid nitrogen bath, to prevent starting of the hydrogenation reaction. The sample was kept frozen in liquid nitrogen until the start of the hyperpolarization experiment.

2.2.2 ^{1}H-hyperpolarization (ALTADENA experiment)

In order to initiate the para-hydrogenation reaction, the NMR tube was heated, using a water bath, at 353 K for 7 seconds, then shaken for 3s and kept out of the hot water bath for 7 more seconds. Then the NMR tube was opened to release the para-hydrogen pressure, 200 µL $CDCl_3$ were added in order to provide a sufficient volume for the acquisition of an NMR spectrum and immediately placed in the 600 MHz NMR-instrument and a single-scan ^{1}H-NMR spectrum was acquired.

After thermal polarization was re-established, a ^{1}H NMR reference spectrum was acquired.

2.2.3 ^{13}C hyperpolarization (allyl-pyruvate)

The hydrogenation reaction was carried out as reported in the ALTADENA experiments, but, in the experiments, after hydrogenation completion, MFC was applied to transfer the hyperpolarization from pH_2 to ^{13}C (Fig. 2.2). The equipment for the magnetic field cycle consisted of a magnetic field shield (Bartington TLMS-C200 capped-end magnetic shield, three-layers mu-metal) containing a solenoid coil (i.d.180 mm, 350 mm eight) fed with electric current provided by a Keysight Arbitrary Waveform Generator (33220A 20 MHz waveform generator, Keysight Technologies, Santa Rosa, CA, U.S.A.). The electric current in the solenoid is controlled by a custom-written function (Microsoft Visual Basic) and allows a precise control of the magnetic

field strength during the overall procedure. The magnetic field profile applied to all the experiments (Fig. S2) consists in a diabatic step from1.5 µT (starting magnetic field) to 50 nT and an adiabatic re-magnetization (exponential) to 10 µT in 4 seconds. The amplitude of the field is measured by means of a three-axis fluxgate magnetometer (Mag-03, Bartington, Witney, UK).

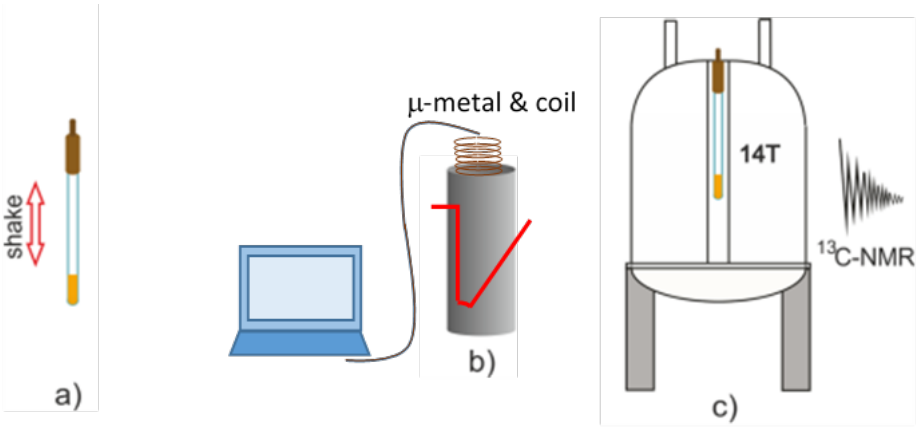

Figure 2.2: *Schematic representation of the experimental procedure: (a) the NMR tube, charged with the hydrogenation mixture and pressurized with Para-hydrogen, is vigorously shaken (3s); (b) the laboratory's magnetic field is shielded by µ-metal cylinders, and magnetic field cycle is carried out using a computer controlled current; (c) the sample is placed in the NMR spectrometer, and a single scan ^{13}C NMR spectrum is acquired*

2.2.4 Hydrolysis of the ester

Hydrogenation reactions was carried out as reported in the previous section. After the application of MFC, hydrolysis was carried out as follows: a base solution (260 µL of NaOH 0.1 M and Sodium Ascorbate 50 mM), pressurized in a home-made apparatus (Fig. S1) using argon (2bar) and heated

at ˜353 K, was injected into the organic solution to hydrolyse the hyperpolarized allyl-ester. Then an acidic buffer solution (100 µL HEPES 144 mM, pH 5.4) was added to the aqueous phase to reach the physiological pH (7.2 ± 0.2 were measured). Following to hydrolysis, we have a phase separation and the catalyst is retained in the organic solvent while the HP pyruvate is transferred to the aqueous solution. The aqueous solution of the HP product (250 µL) was taken up into a syringe and diluted with 300 µL of distilled H_2O and then transported to the NMR spectrometer for the acquisition of the single scan ^{13}C-NMR spectrum.

2.3 Experimental results

2.3.1 Para-hydrogen enrichment.

The enrichment is parahydrogen is the first fundamental step to observe PHIP and the hyperpolarizaton level is closely related to the enrichemnt in the para isomer. In our experiment we use a para-hydrogen generator (BPHG Bruker Para-Hydrogen Generator) that operates at 36K and the percentage of para-hydrogen is, nominally, 92%.

Para-hydrogenation experiments are carried out in NMR tube that are charged with the hydrogenation mixture (metal catalyst, substrate and solvent) and pressurized with para-hydrogen. Although the NMR tubes are kept frozen in liquid nitrogen until the hydrogenation is carried out, the para-H_2 enrichment can be partly lost, during the time delay between the sample preparation and the experiment, due to the conversion catalysed by the hydrogenation mixture and by the NMR tube itself.

In order to obtain information about this possible depleting of para-enrichment, we have measured the p-H_2 percentage immediately after

filling the NMR tube with parahydrogen and at increasing time delays, in order to get measurement of the decay rate of p-H_2 in the NMR tubes.

Since p-H_2 is NMR silent, the signal of the ortho- isomer is obsderved. In the Fig. 2.3 are reported the signals of hydrogen (normal-H_2 and para-enriched) after filling 5mm NMR tube tubes equipped with PTFE gas valves with the hydrogen mixtures, at the same pressure.

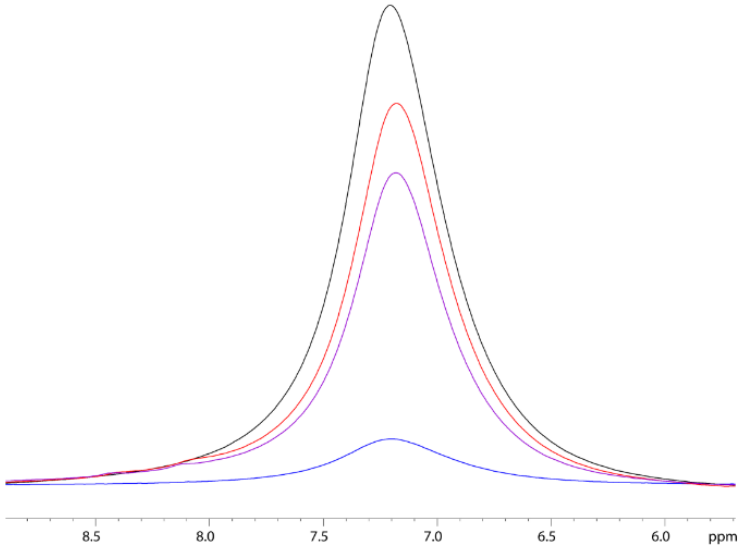

Figure 2.3: *o-H_2 signals from a sample of 92% p-H_2 enriched (blue line), from normal-H_2 (black line) and after heating and shaking the sample as during the hyperpolarization experiments (red and purple lines). In all the experiments the gas pressure was 1950±50mbar, the signal has been precisely normalized to the gas pressure.*

As can be observed from Fig. 2.4, the speed of para-hydrogen decay in the NMR test tubes, used for the reactions, changes from one NMR tube to another, probably due to the fact that traces of oxygen enter the tubes during para-H_2

pressurization. Nevertheless, the parahydrogen percentage is almost constant for about two hours after that the NMR tubes have been filled. Therefore, it can be assumed that the parahydrogen enrichment is maintained during the delay between the preparation of the NMR tubes and the starting of the experiment baced on PHIP method.

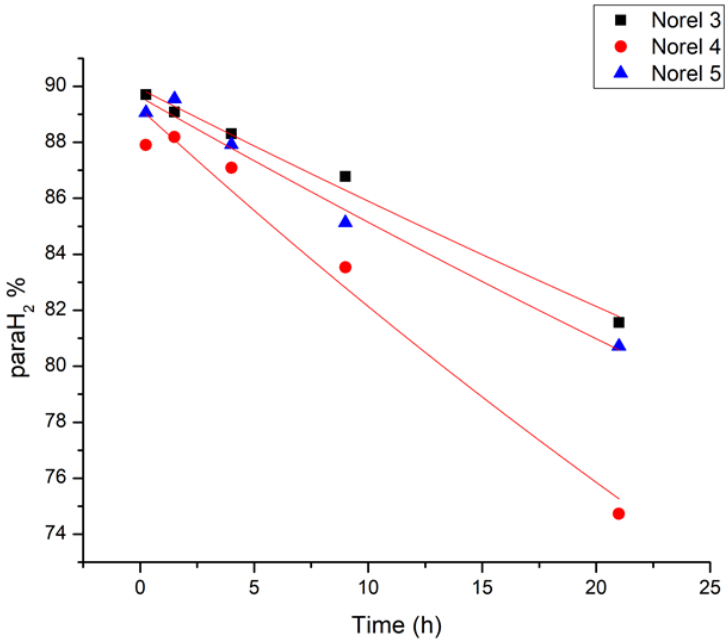

Figure 2.4: *Para-Hydrogen decay in three different NMR test tubes. Tube number 1 is not shown at the picture as it was filled with normal hydrogen for reference calculation and regarding the tube number 2, it is not present at the graph as were found that it's cap connection was leaking.*

2.3.2 ^{1}H hyperpolarization on parahydrogenated propargyl-pyruvate.

The polarization level on ^{1}H-NMR signals of parahydrogenation products depends from the fact that the singlet state of p-H_2 is transferred to the product "as is", without that mixing with the triplet state occurs on intermediates. According to the "sudden approximation", pure singlet state is added to the product, without any effect of reaction intermediates on singlet-triplet mixing. In that case, the polarization level on the ^{1}H signals of the parahydrogen protons would correspond to the para-enrichment.

In order to investigate if the reaction intermediates have any effect on the ^{1}H polarization, hyperpolarized ^{1}H-NMR spectra have been acquired, immediately after the hydrogenation reaction, according to the procedure reported in the experimental methods (ALTADENA experiments) (Fig. 2.5).

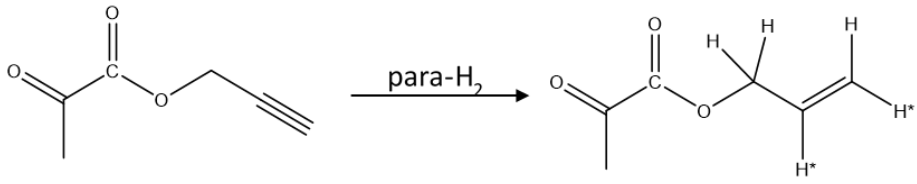

Figure 2.5: *Para-hydrogen is added to the triple bond. In the product molecule, the p-H_2 protons are evidenced with an asterisk.*

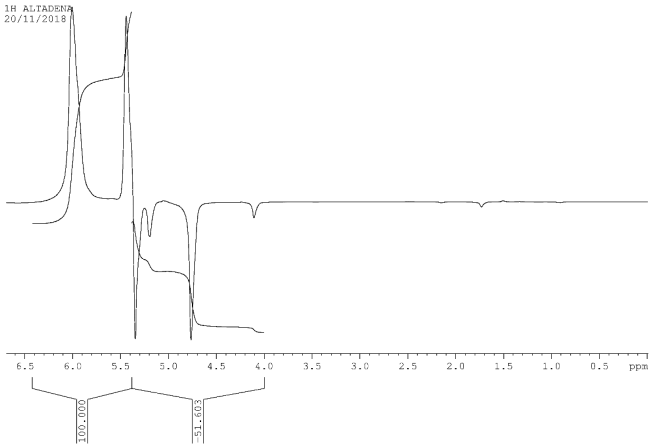

Figure 2.6: *^{1}H-NMR spectrum (1 scan) of HP allyl-pyruvate (the enhanced signals are from the olefinic protons and from CH_2.*

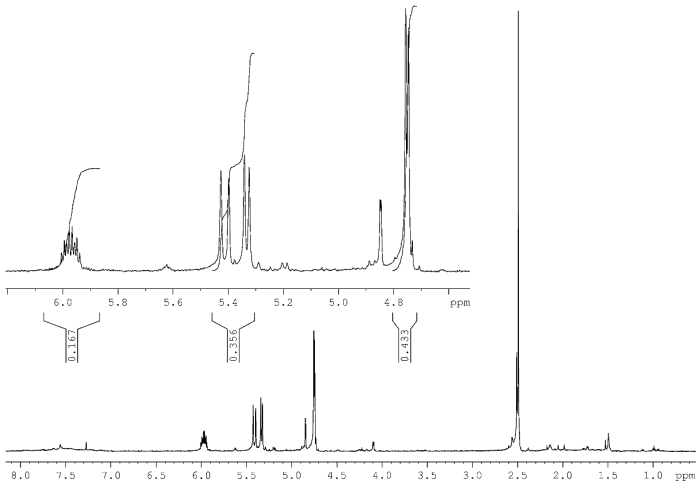

Figure 2.7: *thermally polarized ^{1}H-NMR (4 scan)*

The ^{1}H polarization level has been calculated using the following equation:

$$P_{obs} = \frac{S_{HP}}{S_{therm}} \times P_{therm}(H) = 4 \times \frac{5}{2} \times \frac{S_{SH}}{S_{therm}} \times 4.847 \times 10^{-5} \tag{2.1}$$

Where S_{HP} is given by the sum of the integrals of all the ^{1}H hyperpolarized signals (absolute value of positive and negative signals of the olefinic and -CH_2 protons), (Fig. 2.6), S_{therm} is the sum of the integrals of all the ^{1}H thermal signals, $P_{therm}(H)$ is the thermal polarization of protons at 14.1T and 298 K and coefficient 4 takes into account that the thermally polarized signal has been acquired with 4 transients (Fig. 2.7). Factor 5/2 takes into account that thermally polarized signals are originated from 5 protons whereas hyperpolarized signals correspond to two para-H_2 protons.

Since ^{1}H hyperpolarization decays quickly, due to the short T_1 of ^{1}H spins, nascent polarization has also been back-calculated. To do that, several different samples have been observed, at different delays between the end of hydrogenation and acquisition (Fig. 2.8). The experimental data have been defined by a mono-exponential decay function:

$$P_{obs} = P_{t_0} exp\left(\frac{-t}{T_1}\right) + y_0 \tag{2.2}$$

where the y_0 parameter is the y-offset of the exponential fit, i.e., the value reached at infinity. We have to provide the y-offset value in order to use a linear solution, so if you take the log, a non-zero y_0 value will make the line to be not straight.

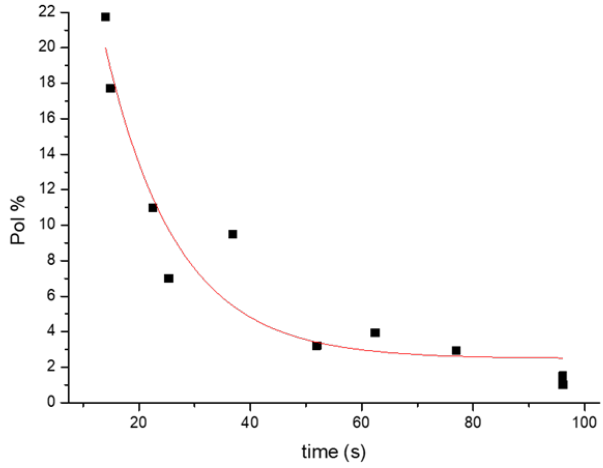

Figure 2.8: *^1H polarization (y axis) observed in different ALTADENA experiments, in which the time delay (x axis) between the end of hydrogenation and the acquisition has been increased.*

The nascent polarization (at time zero) on protons has been thus calculated to be 35.5 +/- 6.7 % while the T_1 decay was 17.6+/- 4.6s.

2.3.3 ^{13}C polarization on the carboxylate signal of pyruvate ester

In order to transfer the proton spin order to the ^{13}C carboxylate spin, magnetic field cycle (MFC) has been applied .

During MFC, the magnetic field at the parahydrogenated sample is, first, switched diabatically from geomagnetic field (30 µT), where the weak coupling condition between protons and heteroatoms occurs, to nearly zero field (50 nT), at which isotropic mixing between heteronuclei and protons takes place. Then

it is increased adibatically from nearly zero to geomagnetic field. The zero magnetic field is obtained using a mu-metal shield and the speed of the passages is controlled using an electric current circulating in a solenoid placed in the μ-metal shield.

In order to explain how MFC works, we can consider how the population of the spin states is re-distributed during MFC in a three spins system formed by the two parahydrogen protons and one heteroatom (^{13}C). The eight spin states of the AA'X spin system and their population during MFC are represented in Fig. 2.9. On the left of the figure, the geomagnetic field applies, the difference between the Larmor frequencies of protons and ^{13}C is about 1.5KHz (weak coupling between heteronuclei).

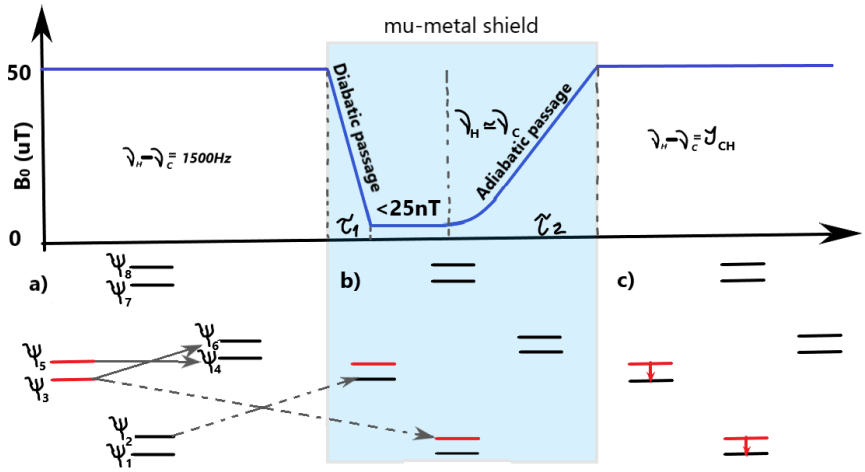

Figure 2.9: *Schematic principle of the MFC process with explanation of the spin states populations: a) after hydrogenation with Para-hydrogen of the substrate at geomagnetic field, b) at zero field, after the diabatic passage (τ1), and c) after the adiabatic passage (τ2) from zero to Earth's field, where the red arrows correspond to transition, in emission, that will be seen in the NMR spectrum*

In the central part of the figure, the ^{1}H and ^{13}C Larmor frequencies are almost equal, isotropic mixing between protons and ^{13}C occurs and the population of the spin states is redistribuited, due to the diabatic passage. In the end the adiabatic (slow) re-magnetization allows to preserve the spin state population achieved at nearly zero field. ^{13}C polarization on the carboxylate signal of pyruvate ester has been measured after the application of the polarization transfer procedure based on magnetic field cycling using the formula:

$$P_{obs} = \frac{S_{HP}}{Stherm} \times P_{therm}(^{13}C) = 8 \times \frac{S_{SH}}{S_{therm}} \times 1.219 \times 10^{-5} \qquad (2.3)$$

Where S_{HP} is the ^{13}C-hyperpolarized signal, S_{therm} is the thermal signal of ^{13}C and the P_{therm} (C) is the thermal polarization at 14.1T and 300K and coefficient 8 considers that the thermally polarized signal has been acquired with 8 transients.

The average polarization thus obtained on ^{13}C was 4,7±0,3%.

2.3.4 ^{13}C polarization on the carboxylate signal of sodium pyruvate after hydrolysis.

The last passage of the PHIP-SAH method, i.e. the hydrolysis of the ester, is carried out by means of the injection of an aqueous base solution (NaOH 0.1 M) containing sodium ascorbate (50 mM) into the organic solution of the hyperpolarzied ester. A suspension of droplets of the organic phase into the aqueous phase if formed instantaneously. After a few seconds (3-5 s) the two phases tends to separate, the catalyst is retained in the organic solvent while the HP pyruvate is transferred to the aqueous solution. An acidic buffer (HEPES solution, 100 µL), is added, in order to reach physiological pH. The addition of the buffer also facilitates the separation of the organic and the aqueous phases.

The aqueous solution is separated form the organic phase and is transferred into a NMR tube, diluted with H_2O and placed into the NMR spectrometer for the ^{13}C-NMR acquisition. The time delay between the end of the hydrogenation reaction and the acquisition of the ^{13}C-NMR spectrum is about 30 s and the ^{13}C observed polarization is 2.2 $\pm$ 0.2 %. In order to extrapolate the nascent ^{13}C polarization, i.e. the polarization level at time zero, immediately after hydrolysis, several hyperpolarization experiments have been carried out at increeasing delay between the hydrolysis and acquisition of the ^{13}C-MR spectrum. The ^{13}C polarization in these experiments are reported in figure 2.10.

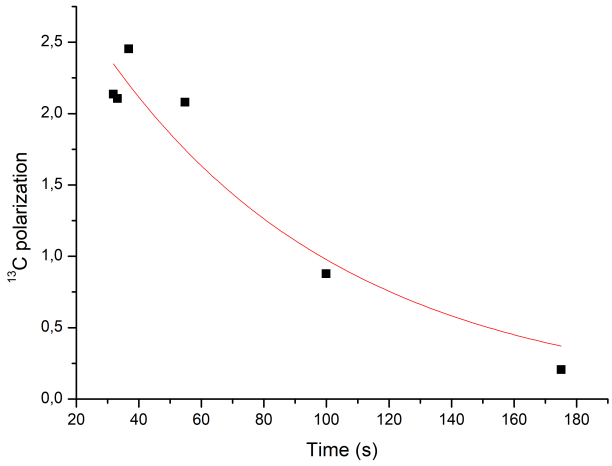

Figure 2.10: *^{13}C Polarization, observed on the carboxylate signal of sodium pyruvate after hydrolysis was carried out using an aqueous base solution (NaOH 0.1M). Different samples were used and the Polarization has been reported as a function of the delay between hydrolysis and acquisition of the ^{13}C-MR specrum.*

During the time delay between hydrolysis and acquisition of the ^{13}C-NMR spectra, the aqueous solution of HP pyruvate has been kept at geomagnetic field, therefore an estimate of the ^{13}C relaxation rate at this magnetic field. The polarization level at time zero has been extrapolated ($^{13}C(t_0) = 3.5 \pm 0.5$ %) and the decay constant (T_1) have been derived (77 $\pm$ 20 s).

2.4 DISCUSSION and CONCLUSIONS

The experimental results show that the parahydrogen enrichment is maintained during the time delay between the sample preparation and the starting of the PHIP experiment. Conversely, the hyperpolarization level observed on ^{1}H-NMR signals in the ALTADENA experiments is only about 20 % and the nascent polarization (obtained from back-calculation) can be estimated around 35 %. Although the value obtained from back calculation might not be precise, due to the fast decay of the proton polarization, the proton polarization is significantly lower than expected, considering that 92% enriched parahydrogen is used. The singlet loss during the hydrogenation reaction may be due to the singlet/triplet mixing that occurs on reaction intermediates. Therefore, testing different hydrogenation catalysts, in particular Rh(I) complexes that contain different phosphine ligands, can be useful to increase the singlet state percentage transferred to the product molecule.

A significant polarization loss is also observed in the spin order transfer passage, carried out by means of MFC, in fact the ^{13}C polarization observed on the ester derivative is 4,7 $\pm$ 0,3 %, while the nascent proton polarization has been estimated to approximately 35 %. Therefore it may be deduced that only 13 % of the ^{1}H polarization is transferred to the ^{13}C spin, and the ^{13}C polarization level can be increased using a more efficient polarization transfer

method, for instance an optimized MFC profile. Hyperpolarization is also decreased during the hydrolysis step to about 50 % of that observed on the ester, in fact it is reduced from 4,7 ± 0,3 % to 2,2 ± 0,2 %. This can be due, in part, to the time needed to carry out hydrolysis and phase separation, nevertheless the back-calculated ^{13}C polarization, immediately after hydrolysis, is only 3.5 %, therefore it can be deduced that fast relaxation processes occur during mixing of the organic and the water phase. In conclusion, the herein reported studies show that several steps of the hyperpolarization procedure still need to be improved in order to reach a higher polarization level on ^{13}C, suitable for in-vivo diagnostic applications.

CHAPTER 3

IN-CELLS METABOLIC STUDIES USING PHIP POLARIZED [1-^{13}C]PYRUVATE

The results presented in this chapter have been previously published as the following article:

Cavallari E, Carrera C, Di Matteo G, **Bondar O**, Aime S and Reineri F/ In-vitro NMR Studies of Prostate Tumor Cell Metabolism by Means of Hyperpolarized[1-13C]Pyruvate Obtained Using the PHIP-SAH Method/ Front. Oncol., April 2020, doi: 10.3389/fonc.2020.

3.1 INTRODUCTION

[1-^{13}C]pyruvate is the substrate that has been used most widely for the study of cellular metabolism and its alterations in diseases such as cancer, heart failure and stroke.[8,37–40] Pyruvate plays a central role in cellular metabolism as it can be converted into a number of metabolites, depending on cellular conditions. In most normal tissues, pyruvate dehydrogenase catalysis the decarboxylation of the pyruvate that enters the TCA cycle. Pyruvate can also be transaminated by alanine aminotransferase or reduced to lactate by lactate dehydrogenase. The presence of disease can alter metabolic fluxes through the different enzymes and an increased glycolytic flux is often observed in tumours. The use of hyperpolarized pyruvate has shown a marked upregulation in the exchange of the ^{13}C hyperpolarized label, mediated by the LDH enzyme, between pyruvate and lactate in tumour cells[41]. Hyperpolarized [1-^{13}C]pyruvate is currently under intense scrutiny as a potential probe with which to assess the presence and grading of prostate cancer in humans[42].

At the moment the gold-standard method for the hyperpolarization of molecules in the liquid state is d-DNP[6]. d-DNP in our days is the method that is used not just for preclinical study, but also for clinical MRI for human.

Unfortunately, d-DNP is an inherently slow, technologically demanding and extremely expensive technique that limits the application of this powerful tool to few laboratories worldwide.

Para-Hydrogen Induced Polarization (PHIP) allows to obtain hyperpolarized substrates in few seconds at much lower costs than d-DNP[43,44]. This hyperpolarization method is based on the hydrogenation, catalysed by metal complexes, of an unsaturated precursor of the target molecule. On this basis the number of PHIP-polarizable substrates appears to be limited by the availability of the proper unsaturated precursor and concern about

the biological applications of the obtained hyperpolarized products relies on the presence of residual metal catalyst and other impurities associated to the hydrogenation reaction. The PHIP- side-arm hydrogenation (PHIP-SAH) approach[35] represented a good step ahead as it circumvents both issues and provides aqueous solutions of hyperpolarized pyruvate, or other metabolites[44], that can be safely used for in vivo and in-cells studies[45].

In the herein reported work, the toxicity of the aqueous solutions of the HP metabolites was studied, by performing in-vitro cytotoxicity analysis, and HP [1-^{13}C]pyruvate has been used for metabolic investigations in different prostate carcinoma cell lines. Since I contributed mainly to the experiments carried out using HP-pyruvate on cells, the citotoxicity tests and the in-cells metabolomic measurements reported in the main manuscript have been omitted in this thesis.

3.2 Materials and Methods

The aqueous solution of HP pyruvate was prepared according to the PHIP-SAH procedure, as reported in Chapter 2. The concentration and hyperpolarization of [1-^{13}C]pyruvate were measured at the end of each experiment by acquiring a ^{13}C-NMR spectrum of the thermally polarized product with the addition of ^{13}C-urea as an internal reference. The pyruvate concentration in the cell suspensions was found to be 5.0 $\pm$ 0.4 mM.

3.2.1 ^{13}C-NMR Experiment: Set-Up

In order to carry out the in-cells experiments, a set-up for the perfusion of the cells, suspended in their grow medium and placed into the NMR spectrometer, was assembled. To do that, a standard 5 mm-OD Wilmad NMR tube was equipped with a cap modified with a central hole (inner diameter

2mm) and a glass tube (2 mm OD, 1.75 mm ID, 8 mm L) was inserted into the cap. A PTFE tube (1 mm OD, 0.75 mm ID, 750 mm L) was placed inside the glass capillary tube and kept in the axial position, a few mm above the cells suspension. The quick injection of the aqueous solution of the hyperpolarized substrate through the PTFE injection line allowed the cell suspension to mix with the HP pyruvate. The PTFE tube was removed immediately after the addition of the HP-pyruvate in order to avoid B_0 inhomogeneities during the acquisition of the ^{13}C-NMR spectra.

3.2.2 ^{13}C-NMR Experiments: Cells Preparations

The metabolic transformation of [1-^{13}C]pyruvate, hyperpolarized through the PHIP-SAH procedure, into [1-^{13}C]lactate, was assessed using the following samples: (I) prostate cancer cells suspended in their growth medium; (II) intact cells suspended in lactate-enriched medium; (III) lysed cells.

The samples were prepared as follows:

I. Pyr/Lac tests in cells suspension: cells were harvested from plates (2 ml of warm 0.25 % Trypsin 0.53 mMEDTA solution), counted using a Burker chamber and then centrifuged in the growth medium for 5 min at 125 $\times$ g-force. Once the supernatant was removed, 9.2 $\pm$ 0.2 M cells for each experiment were suspended in 300 µL of culture medium and transferred into a 5 mm NMR test tube.

II. Pyr/Lac test in cells suspension with added Lac: the cell-containing sample was prepared as in I, L-lactate was then added to the culture medium and left to equilibrate for 10 min in the NMR spectrometer before the injection of the HP-pyruvate. At the end of the experiment, after the addition of the aqueous solution of the HP metabolite, the final lactate concentration was 5.94 $\pm$ 0.14 mM.

III. Pyr/Lac test in Lysed cells: for each experiment, the lysed cell solution was obtained by twice freeze-thawing cell suspension in liquid nitrogen. The sample-containing cells were prepared as in II. In this set of experiments L-lactate (10mM) was also added to the growth medium and left to equilibrate for 10min in the NMR spectrometer before the HP experiment.

The acquisitions of the ^{13}C-NMRspectra were carried out using a small flip angle (18°). A 2 s delay was applied between successive acquisitions. The first acquisition started a few seconds before the injection of the HP substrate.

The samples (volume of 300 µL) were placed in the 5mm NMR tube equipped with the Teflon transfer line ready to receive the addition of the HP substrate. The NMR tube was positioned into the NMR spectrometer (600 MHz Bruker Avance) where it was kept at 310 K. The cells viability at the end of the hyperpolarized experiment was checked using the trypan blue exclusion test. The viability in all of the experiments was 95%. At the end of the experiment the number of cells was checked via the quantification of Bradford proteins, using the specific calibration line for each cell line. The ^{13}C NMR spectra were acquired on a Bruker Avance 14.1 T NMR spectrometer using a 5mm BBO probe equipped with ^{1}H and ^{13}C coils.

3.2.3 Cells Cultures

The PC3, DU145, and LNCaP (prostate carcinoma) cell lines were purchased from American Type Culture (ATCC^{R}). Cells were kept for 72 h in 175 cm^2 flasks at 310 K in a humidified atmosphere with 5 % CO_2 in the recommended culture media as suggested by ATCC, in particular: LNCaP: RPMI1640 (D-glucose 25.0 mM); PC3: F-12K (D-glucose 7.0 mM); DU145: EMEM (D-glucose 5.6 mM). All the cells were used within the first 10 passages

from unfreezing.

3.2.4 In vitro cytotoxicity

[1]

To assess adverse effects of the aqueous solutions derived from the PHIP-SAH hyperpolarization procedure, the MTT test (based on the enzymatic reduction of the tetrazolium salt MTT [3-(43-dimethylthiazol-2-yl)-2,5-diphenyl-tetrazoliumbromidein]) in living, metabolically active cells was carried out on both prostate cancer cell lines.

For these tests, cells were harvested by trypsinization, resuspended in fresh medium, and plated in a volume of 0.1 ml in the wells of 96-well microtiter plates. Routinely 7,000-16,000 cells, depending on the cell lines growth curve, were plated in each well. After 24 hours, to ensure the cells adhesion, the culture medium was removed and replaced with a fresh medium of the same composition as the one used in the hyperpolarization procedure, i.e. 15% of the aqueous solution in the final volume (0.1 ml).

At the end of the incubation period (1, 6 and 24 hours), the medium was replaced with 0.1 ml of a 5 mg/ml solution of MTT (purchased from Sigma, St. Louis, MO) in phosphate-buffered saline (PBS 1X). After 4 hours of incubation with MTT at 310 K, the supernatant was carefully sucked off and a solubilization solution, 0.15 ml of dimethyl sulfoxide, was added to dissolve the insoluble purple formazan product into a coloured solution and the absorbance at 570 nm was read by a spectrophotometer.

Cells were plated in triplicates to minimize the variability of the results. In each plate, 3 control wells for each cell line were included.

The PC3 and DU145 cells were treated with the following solutions:

[1] Cytotoxicity tests as well as extracellular and itracellular lactate concentration measurements were performed by E. Cavallari and G. Di Matteo

1) aqueous solution of the product of the PHIP-SAH procedure, prepared as described in the [1-^{13}C]pyruvate hyperpolarization paragraph (i.e. the aqueous phase resulting after step **c**).

2) aqueous solution obtained from the injection of the pressurized and heated base through a chloroform solution of the hydrogenation catalyst, without the addition of propargyl-pyruvate. The solution is analogous to 1 but is expected to contain only residues of chloroform and catalyst impurities.

3) aqueous solution obtained from the injection of the pressurized and heated base through chloroform, without the hydrogenation catalyst. The aqueous solution is expected to contain only traces of chloroform.

4) aqueous solution of allyl-alcohol, at the same concentration as that obtained from the hyperpolarization procedure.

5) aqueous solution of the product of the PHIP-SAH procedure, prepared with the addition of ethanol (5 µL) to the organic phase. In this case the composition of the aqueous solution is analogous to 1, but with an excess of ethanol. As this composition was the one used in a previous *in vivo* study[46], its toxicity was tested in this work for completeness.

3.2.5 Lactate dehydrogenase assay

A commercial kit (Sigma-Aldrich MAK066) has been used to measure the LDH activity in the two cell lines. The kit has been used according to the manufacturer's instructions. Briefly, 1x10^6 cells per sample were rapidly homogenized by sonication (30 % power, 21Watt, for 30 seconds) on ice in 500 µL of cold LDH Assay buffer, centrifuged at 10000 g for 15 minutes at 277 K to remove insoluble material.

To ensure the readings are within the linear range of the standard curve, 4-10µL samples were added into duplicate wells of a 96 well plate, bringing the sample to the final volume of 50 µL with LDH Assay Buffer. After the addition of 50 µL of the Master Reaction Mix the NADH production kinetics were measured via absorbance of the specific probe at 450 nm.

3.2.6 Extracellular lactate assessment.

To determine the concentration of lactate in the supernatant, cells were seeded on 75mm^2 plates. After overnight adhesion in standard conditions (310K and 5 % CO_2), the culture medium was replaced with a new one. In order to determine the concentration of lactate in the medium at three different times, three sets of plates (three plates for each time point) have been prepared and left in the incubator for 24, 48 or 72h, respectively. At the three selected times, the medium was collected, the cells harvested by trypsinization and counted. The applied procedure allows to normalize the amount of lactate measured in the culture medium to the number of cells that have produced it.

In order to immediately quench any possible residual metabolism, one volume of culture medium was mixed with two volumes of cold methanol in a vial, snap-frozen and left 2 hours in liquid nitrogen. Proteins were then allowed to precipitate at 250 K for 30 min and the sample was centrifuged at 16000 g at 277 K for 20 minutes. The supernatant was then collected and immediately lyophilized to remove the methanol for subsequent measurements and reconstituted with 0.6 ml of phosphate buffer (0.15 M K_2HPO_4, pH=7.0) in deuterated water (D_2O) for the ^{1}H NMR quantification.

The amount of extracellular lactate was determined using NMR ^{1}H spectrometry (Fig. 3.1). Experiments were carried out in triplicates and the lactate concentration in the samples (μmol/cell) was calculated

based on internal standard reference. A known amount (0.35 mM) of 3-(trimethylsilyl)-propionic-d_4 acid sodium salt (TSP-d_4) was added to act as chemical shift reference for the calibration of the NMR data (at 0.0 ppm) as well as internal standard for quantitation.

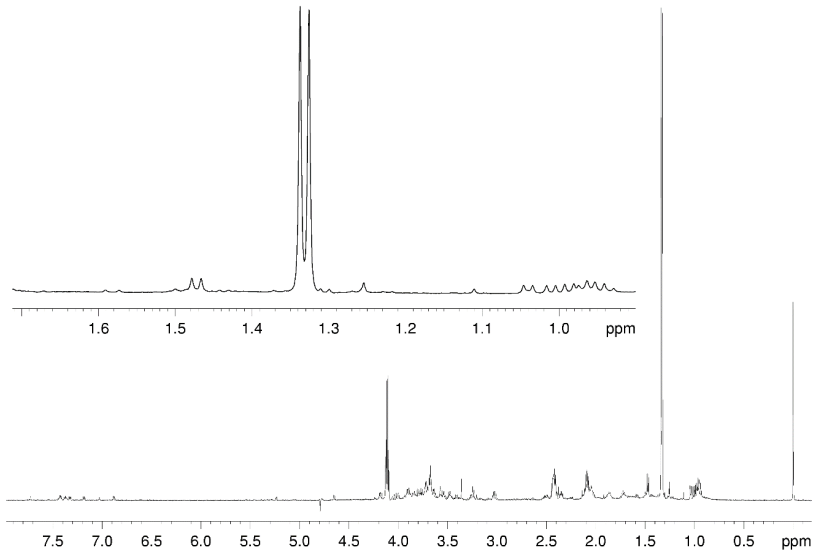

Figure 3.1: *1D ^{1}H NMR spectra of extracellular metabolites from DU145 cells cultured in this medium for 72 hours. The 1.33 ppm signal is the one originating from the methyl lactate protons. At 0.0 ppm the 3-(trimethylsilyl)-propionic-d4 acid sodium salt (TSP-d4) protons (0.35 mM).*

3.2.7 Intracellular lactate concentration.

Methanol-chloroform-water extraction (M/C) was used to extract metabolites from cells. Briefly, cell pellets were promptly quenched in liquid nitrogen followed by the addition of 0.5 ml of cold methanol-chloroform solution

in a ratio of 2:1. After thawing on ice, samples were vortexed for 60 s and sonicated. After 15 minutes of contact to the M/C solution, 0.25 ml of chloroform and 0.25 ml of distilled water were added to the mixture to yield an emulsion, which was vortexed and centrifuged at 13000 g for 20 min at 277 K. The upper layer containing water-soluble metabolites was collected, lyophilized and reconstituted with 0.6 ml of phosphate buffer (0.15 M K_2HPO_4, pH 7.0) in deuterated water (D_2O) for the ^{1}H NMR quantification.

A concentration of 0.03 mM of the internal standard (TSP-d_4) was used as reference (Fig. 3.2, 3.3).

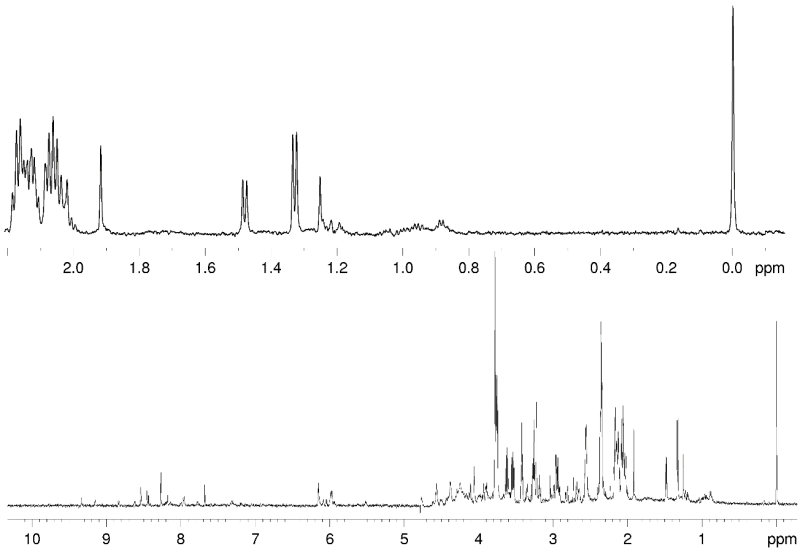

Figure 3.2: *1D ^{1}H NMR spectra of intracellular metabolites from DU145 cells cultured for 72 hours. The 1.33 ppm signal is the one originating from the methyl lactate protons. At 0.0 ppm the 3-(trimethylsilyl)-propionic-d4 acid sodium salt (TSP-d4) protons (0.03 mM).*

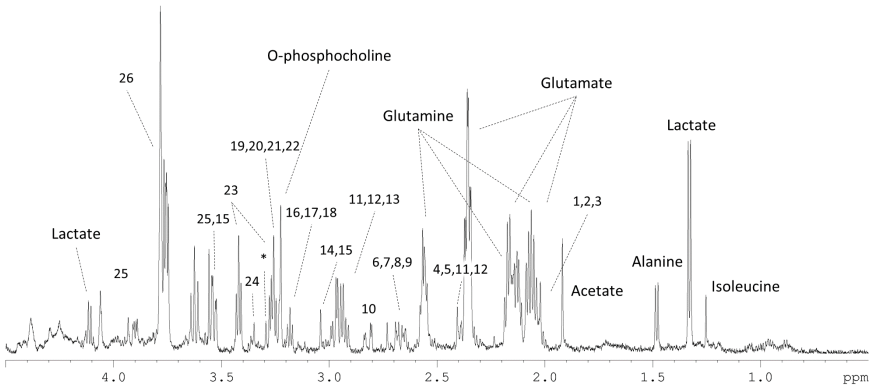

Figure 3.3: *1D ^{1}H NMR spectra of intracellular metabolites from DU145 cells extract. The characteristic peaks from most of the identified metabolites for this cell line are annotated with names and numbers: 1 N-acetylaspartate, 2 N-acetylglutamine, 3 Proline, 4 Pyruvate/Oxaloacetate, 5 Glutathion/Aspargine, 6 Citrate, 7 Methionine, 8 Hypotaurine, 9 Malate, 10 Aspartate, 11 Lysine, 12 α-ketoglutarate, 13 Glutathion, 14 Creatine, 15 Phosphocreatine, 16 Phenylalanine, 17 Histidine, 18 Choline, 19 Taurine, 20 Betaine, 21 Trimethylamine-N-oxide, 22 Myoinositol, 23 Taurine, 24 D-glucose, 25 Myoinositol, 26 Overlapped peaks from D-glucose, D-galactose, Fructose, GSH and several amino acids (-CαH-), * Methanol (residual extraction solvent).*

3.3 RESULTS

When HP-[1-^{13}C]pyruvate was added to the cells suspended in their growth medium, kept in the NMR spectrometer at physiological temperature, build-up of the lactate signal was observed immediately, in the series of the ^{13}C-NMR spectra, due to the rapid exchange of the ^{13}C hyperpolarized label between pyruvate and lactate that occurs in the intracellular compartment (Fig. 3.4). The lactate signal reaches a maximum at about 20 s, then it

decays due to the T_1 relaxation processes. The ^{13}C signals corresponding to pyruvate and lactate were integrated and the time dependent signal intensities of lactate and pyruvate were interpolated using a set of functions, in order to obtain information about the kinetics of the metabolic process. The experimental results might be interpolated using a four pools model that takes into account intra- and extra-cellular pyruvate and lactate, all mutually exchanging[47,48]. However, in the present case, the spectral resolution did not allow to discriminate between the intra and extracellular metabolites' signals, therefore the two compartments model was used, in order to avoid errors due to the use of too many parameters for fittings[49].

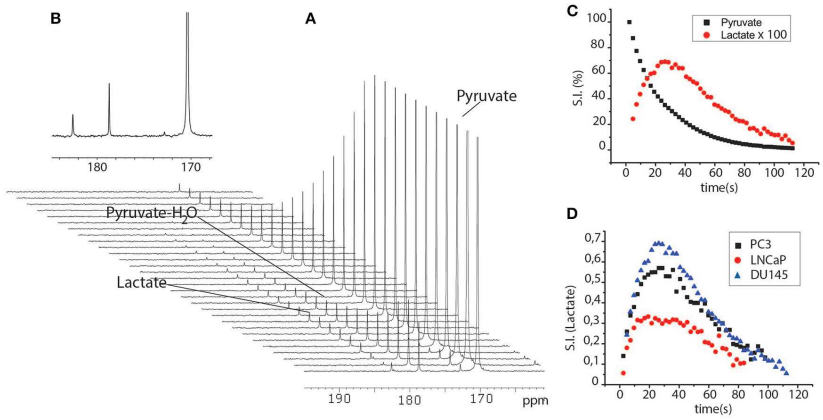

Figure 3.4: *Series of ^{13}C-NMR spectra acquired after the perfusion of a cells suspension (PC3 cells, 10M) with the aqueous solution HP-[1-^{13}C]pyruvate. Spectra were acquired using small flip angle pulse (18°) and 2 s delays between one scan and another.* ***B****) expanded ^{13}C-NMR spectrum at maximum intensity of the lactate signal;* ***(C)****Time dependent pyruvate and lactate curves obtained from the integrals of the signals of the two metabolites in the ^{13}C-NMR spectra reported in* ***A****.* ***D)*** *time dependent lactate curves obtained after the addition of HP-pyruvate to a suspension of DU145, PC3, and LNCaP cells.*

The observed pyruvate and lactate peak intensities can be fitted to a simple two sites exchange model

$$\mathbf{Pyr} \rightleftharpoons \mathbf{Lac} \tag{3.1}$$

according to which , the ^{13}C-NMR signals of [1-^{13}C]pyruvate and [1-^{13}C]lactate are described by the coupled differential equations[11]

$$\frac{dP_{Pyr}}{dt} = -k_{PL}Pyr(t) + k_{PL}Lac(t) - \frac{1}{T_{1P}}Pyr(t) \tag{3.2}$$

$$\frac{dP_{Lac}}{dt} = +k_{PL}Pyr(t) - k_{PL}Lac(t) - \frac{1}{T_{1L}}Lac(t) \tag{3.3}$$

where k_{PL} and k_{LP} are the kinetic constants of the pyruvate to lactate conversion and T_1 is the decay time constants of the ^{13}C carbonyl sites. It has already been shown that the model can be further simplified by setting the back-conversion rate (k_{LP}) to zero. It follows that one deals with a two compartment model characterized by a unidirectional flow with the kinetic constant k_{PL} being an apparent overall pyruvate to lactate conversion rate. We must also be considering that the small flip angle pulses (18^0) that were used lead to further loss of polarization. In order to take into account this factor, an envelope function exp(-λt) was added to the observed signal intensity, where

$$\lambda = \frac{ln(cos\varphi)}{\Delta t} \tag{3.4}$$

and t is the time interval between successive pulses[50]

$$Pyr' = Pyr \cdot exp(\lambda t) \tag{3.5}$$

$$Lac' = Lac \cdot exp(\lambda t) \tag{3.6}$$

The kinetic constants obtained from the fittings were normalized to the number of cells and the pyruvate-to-lactate conversion rate was calculated as follows:

$$\vartheta = \frac{k_{PL} \cdot [Pyr]_{t0} \cdot \vartheta}{n_{cells}} \tag{3.7}$$

where υ_{PL} is the volume of the sample.

From the interpolation of the ^{13}C-NMR time-dependent signals LNCaP cells resulted to be less glycolytic than the other two (PC3 and DU145), in agreement with the fact that LNCaP cells have a more oxidative metabolic phenotype than the other two[51], while DU145 were significantly more glycolytic than PC3 cells (Fig. 3.5.A).

In the second set of experiments, lactate was added to the medium in which cells were suspended, during the ^{13}C-NMR experiment, as reported by Day et al.[52] In this case, the pyruvate-to-lactate conversion rate become significantly faster in PC3 than in DU145 cells, while the apparent glycolytic efficiency of the LNCaP cells was still significantly lower than in the other two cell lines (Fig. 3.5B).

In order to get more information about the differences in the metabolic phenotype of the two, more aggressive cell lines (PC3 and DU145), another series of experiments has been carried out on lysed cells. In these experiments, the exchange kinetics became higher in both cell lines (PC3 and DU145) and were still slightly, even if not significantly, faster in DU145 than in PC3 cells (Fig. 3.5C).

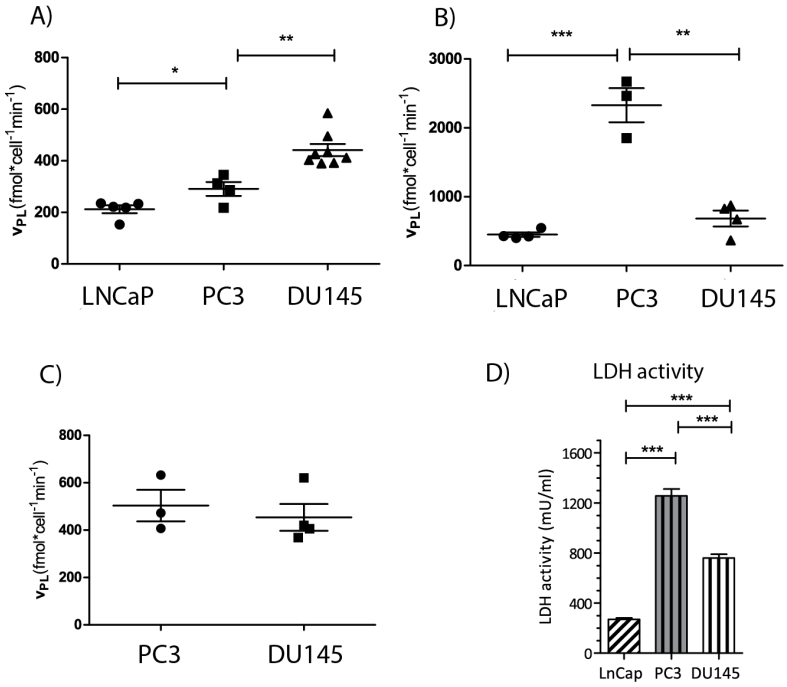

Figure 3.5: *Rate of pyruvate to lactate conversion obtained from the experiments carried out using HP [1-^{13}C]pyruvate on cells, in different conditions: A) intact cells (DU145, PC3 and LNCaP cells) cultured in their proper culture medium; B) intact cells suspended in the medium with added lactate; C) lysed cells and D) results of the LDH activity biochemical assay carried out on the three cell lines. See the main manuscript for more details about the LDH activity assay.* $^{***}P \leq 0.001$, $^{**}P \leq 0.01$, $^{*}P \leq 0.05$*; unpaired t-test.*

3.4 DISCUSSION and CONCLUSIONS

When cellular metabolism was interrogated using HP-pyruvate in intact cells, the results were only partly in agreement with those obtained using the

conventional LDH activity assay. In fact, the metabolic phenotype of LNCaP is significantly less glycolitic than in the other two, more aggressive cell lines, that is consistent with the LDH activity test. Conversely, the pyruvate to lactate conversion rate of in DU145 cells was faster than in the PC3 cells, in contradiction with the LDH activity obtained from the biochemical assay (Fig. 3.5.A and D The LDH activity biochemical assays have not reported in the thesis, see the published paper for more details about this topic). In order to clarify this, we can consider the other two sets of experiments (those carried out on lysed cells and those with lactate added to the medium). We has also to keep in mind that the pyruvate-to-lactate exchange rate observed in intact cells is the result of concomitant processes, namely the rate of metabolite transport through the cellular membrane, and the efficiency of the LDH enzyme.

In the experiments carried out on lysed cells, the contribution of MCT1 (MonoCarboxylate Transporter-1) mediated transport of pyruvate to the extra to the intracellular compartment was removed, while lactate was added to the medium in order to mimic its intracellular concentration. In these experiments, the exchange kinetics became almost the same in both cell lines (PC3 and DU145)(Fig. 3.5C), even if not significantly faster in PC3 cells, as expected from the LDH activity tests. Therefore, it is evident that the MCT transporters have an effect on the pyruvate to lactate conversion rate, but this is not sufficient to justify the apparent higher glycolotic phenotype of DU145 cells observed using HP-pyruvate. Therefore we have to consider that different isoforms of LDH exist (LDH-A and LDH-B), that have different affinity either for pyruvate or for lactate. Isoforms LDH-A and LDH-B are found in the mitochondrial compartment, plasma membrane, and cytosol[53]. LDH-A has a higher affinity for pyruvate, which means it preferentially converts pyruvate to lactate and NADH to NAD^+, whereas LDH-B has a higher affinity for lactate and preferentially converts lactate to pyruvate and NAD^+ to NADH[54,55].

Therefore, the faster ^{13}C label exchange between pyruvate and lactate observed in the PC3 cells, after the addition of lactate to the extracellular medium, might be due to higher LDH_B expression, that leads to the more efficient oxidation of lactate to pyruvate. The biochemical assays seemed also to support this hypothesis. In fact, the biochemical LDH assay measured the rate of lactate-to-pyruvate conversion, through the spectrophotometric observation of NADH formation, and the LDH activity was higher in PC3 than in DU145 cells.

The process of converting lactate into pyruvate by means of an LDH_B-dependent reaction is the so-called oxidative lactate metabolism [56] and, associated with MCT-1 facilitated lactate uptake, is at the core of a metabolic adaptation of cancer cells called metabolic symbiosis [57].

These observations seemed to point toward the view that the oxidation of lactate into pyruvate is more efficient in PC3 cells, while the LDH enzyme works preferentially as a pyruvate reductase in the DU145 cells.

Although a thorough investigation of the expression of the different isoenzymes (LDH_A and LDH_B) and MCTs (MC1 and MCT4) in the two, more aggressive prostate cancer cell lines (PC3 and DU145) would be needed, it can be concluded that the experiments reported herein have shown that the polarization obtained on [1-^{13}C]pyruvate, as obtained using the PHIP-SAH methodology is more than sufficient for investigation of the differences in the metabolic phenotype of prostate cancer cells characterized by different aggressiveness (LNCaP, PC3, and DU145). These findings pave the way for a number of possible NMR investigations of cellular metabolism that go well-beyond -the pyruvate/lactate transformation investigated in this work.

CHAPTER 4

EFFECT OF THE HYDROGENATION SOLVENT IN THE PHIP-SAH HYPERPOLARIZATION OF [1-^{13}C]PYRUVATE

The results presented in this chapter have been previously published as the following article:

Oksana Bondar, Eleonora Cavallari, Carla Carrera, Silvio Aime, Francesca Reineri / Effect of the hydrogenation solvent in the PHIP-SAH hyperpolarization of [1-13C]pyruvate/ November 2021, Catalysis Today, doi.org/10.1016/j.cattod.2021.11.030.

Abstract

Para-Hydrogen Induced Polarization-Side Arm Hydrogenation (PHIP-SAH) is an inexpensive tool to obtain hyperpolarized pyruvate (and other metabolites) that can be applied to in-vivo diagnostics, for the investigation of metabolic processes. This method is based on hydrogenation, using hydrogen enriched in the para-isomer, of unsaturated substrates, catalysed, usually, by a homogeneous rhodium(I) complex. In this chapter, the effect of the solvent on the hydrogenation efficiency and on the hyperpolarization level will be investigated. Coordinating solvents, such as acetone and methanol, can increase significantly either the efficiency or the hyperpolarization level, but they are not compatible with the intended metabolic applications. The phase extraction of the hyperpolarized product (sodium pyruvate) in an aqueous solution was obtained carrying out the hydrogenation reaction in chloroform and toluene. The traces of the organic solvents in the water phase were removed, by means of filtration through a lipophilic resin, thus improving the biocompatibility of the aqueous solution of the hyperpolarized product. At the end of the chapter the biological in-vivo application will be described.

4.1 INTRODUCTION

The vast majority of MRI studies addressing diagnostic applications make use of the ^{1}H signal of water while other molecules are not usually observed directly, due to their low abundance and to the intrinsic low sensitivity of MR based methods. The in-vivo application of hyperpolarized substances obtained by means of PHIP has been reported since the early days of the application of hyperpolarization techniques[58,59] and recent advancements have been surveyed in both hydrogenative[60,61] and non-hydrogenative PHIP[62]. Pyruvate is the most scrutinized hyperpolarized metabolite and it has been used

in the investigation of metabolism of different diseases[36,44,63,64]. Clinical trials are currently ongoing for cancer (prostate and breast cancer[39]). The possibility of obtaining HP (hyperpolarized) pyruvate using PHIP-based methods is quite appealing and this task is under intense scrutiny by means of both hydrogenative[46,65,66] and non-hydrogenative PHIP (i.e. SABRE)[67,68] based methods.

The removal of the hydrogenation catalyst continues to be a major issue for biological applications, in spite of early investigations have shown relatively low toxicity[69] and its removal has been pursued by means of metal scavengers[70] Phase transfer of the hyperpolarized product from a hydrophobic organic solvent, in which the hydrogenation is carried out, to an aqueous medium, has been exploited for both SABRE[71] and hydrogenative-PHIP[72]. These methods yielded positive results in the catalyst removal, which is mostly retained in the organic phase. However, hydrophobic solvents such as chloroform are also partially soluble in water[73], thus introducing serious problems about the bio-compatibility of the hyperpolarized substrate containing solution. In this chapter will be shown the results on the effect of different reaction solvents on hyperpolarization of an unsaturated derivative of pyruvate (propargyl-pyruvate) by means of hydrogenative PHIP (PHIP-SAH). After hydrolysis of the ester and successive phase extraction, an aqueous solution of the hyperpolarized molecule was obtained and the residual amount of the organic solvents measured. Next, the aqueous solution was filtered to remove the organic solvent residues by filtration.

4.2 Materials and methods

4.2.1 Sample preparation

In order to hydrogenate the propargylic ester of pyruvate, the hydrogenation catalyst ([1,4-bis(diphenylphosphino)butane](1,5-cyclooctadiene)rhodium(I)tetrafluoroborate], Sigma Aldrich, CAS: 79255-71-3) was used, without purification.

NMR sample tubes equipped with a gas-tight valve (Norell® NMR sample tubes) were used to carry out the hydrogenation reactions.

Deuterated solvents were bought from CortecNet and used without purification. The propargylic ester of [1-^{13}C]pyruvate was synthesized as reported in ref[25].

The catalyst/substrates solutions were prepared and loaded into the NMR sample tubes according to the following experimental set-up:

Acetone. A 7 mM solution of the catalyst was prepared by dissolving the commercial compound in deuterated acetone (Acetone-d_4). The solution was filtered through a poly(tetrafluoroethylene) (PTFE) (Whatman, UNIFLO) syringe filter, size of the pores 0.22 μm. 100 µL of this solution were transferred into each NMR sample tube and the solution was frozen in liquid nitrogen. The propargylic ester of [1-^{13}C]pyruvate (27 µmol in each sample tube, concentration in the hydrogenation mixture 270 mM) was added to this solution.

Chloroform. A 14 mM solution of the catalyst was prepared in deuterated chloroform ($CDCl_3$) and filtered on the PTFE filters. 100 µL of this solution were transferred into each NMR sample tube and the tubes were frozen in a liquid nitrogen bath. The propargylic ester of [1-^{13}C]pyruvate (27 µmol) was added to each tube. In the experiments carried out using ethanol as co-solvent, 5 % of EtOH (Ethanol BioUltra for molecular biology, >99.8 %, Sigma-Aldrich) was added as well.

Methanol. Due to the low solubility of the catalyst precursor in methanol, it was dissolved in chloroform, first, and the solution was filtered through the PTFE filter (see above). The catalyst containing solution was distributed into the NMR sample tubes (1.4 µmol/tube) and chloroform was evaporated by means of an argon flow. Deuterated methanol was added to each tube (100 µL, final concentration of the catalyst 14 mM) and the solution was frozen in liquid nitrogen. The propargylic ester of [1-^{13}C]pyruvate was added to the tubes (concentration in the reaction mixture 270 mM).

Toluene. Due to the low solubility of the catalyst in toluene, the same procedure reportetd for methanol was applied (1.0 µmol/tube). Toluene was added (100 µL toluene-h8) and the tubes were frozen into a liquid nitrogen bath. The propargylic ester of [1-^{13}C]pyruvate (26.6 µmol) was added to the tube, as well as 5% v/v (Ethanol BioUltra for molecular biology, >99.8%, Sigma-Aldrich).

In order to add para-hydrogen, the frozen NMR sample tube, loaded with the substrate/catalyst solution, was connected to a vacuum line and the air was removed by applying vacuum (<0.2 mbar). Para-hydrogen (BPHG Bruker Para-Hydrogen Generator 86 % enrichment) (2.1 bar) was added, while keeping the NMR tube in a liquid nitrogen bath. The tube was disconnected from the vacuum line and kept frozen in liquid nitrogen (77 K) in order to prevent any chemical reaction, until the start of the hyperpolarization experiment.

4.2.2 ^{13}C hyperpolarization

The spin order transfers from the para-hydrogen protons to ^{13}C of the carboxylate group was obtained by applying magnetic field cycle, explained before at the chapter 2 (section 2.2.3).

In all the experiments, the NMR tube was placed inside the magnetic

field set to 1.5 µT and the MFC profile was applied. The sample tube was removed from the shield, 250 µL of solvent was added and the NMR tube was transported into the NMR spectrometer where the ^{13}C-NMR spectrum (one shot, 90° flip angle, RG 9) was acquired. Thermal equilibrium spectra were acquired with 8 transients, using 90° pulses separated by 250 s intervals.

4.2.3 Hydrolysis of the ester and phase extraction

Hydrolysis was carried out using an aqueous base solution (NaOH 0.13N) containing sodium ascorbate (50 mM). For each experiment, 260 µL of this solution were charged into a PTFE tube (PTFE 1/16" x 0.75i.d. tube, VICI Jour). The tube was pressurized with Argon (1.5bar) and heated in a hot water bath (80°C). The injection of the aqueous base into the organic solution was obtained by opening the injection valve (Fig. S1). A few seconds after (7-8 s), an acidic buffer (HEPES 144 mM, 100 µL, pH 5.4) was added to obtain neutral pH. It must be noticed that pyruvate is quite unstable in basic solution [74] and it tends to degrade quickly. In the end, the aqueous phase was collected in a syringe, transferred into an NMR sample tube for the acquisition of the ^{13}C-NMR spectrum and diluted with 200-300 µL D_2O. Thermal ^{13}C spectra were also acquired on each sample, in order to allow shorter repetition time between the scans, a Gd(III) complex (Gd-DO3A, 3 mM) [48] was added to the aqueous solution, after the acquisition of the hyperpolarized signal. The paramagnetic complex allowed to shorten the relaxation time of the ^{13}C signal and the time delay between the scans was set to 2 s. The concentration of sodium pyruvate and of the other side-products in the aqueous phase were determined by adding the reference standard TSP (3-(Trimethylsilyl)propionic-2,2,3,3-d4 acid CAS 24493-21-8, 15 mM).

4.2.4 Filtration.

In order to remove the organic solvents (toluene and chloroform) still present in the aqueous solution after the phase extraction, a small amount (approximately 100 µL) of TENAX resin was used. The resin was placed in a 1ml syringe (Fig. S3) and retained using a PEEK filter (Idex Fluidics, Frit in Ferrule 2 µm PEEK). The aqueous solution was put on the top of the column and quickly eluted through the resin. The water solution was collected in an NMR tube and placed into the NMR spectrometer for the acquisition of the ^{13}C-NMR spectrum. Thermal spectra were also acquired following the addition of the Gd(III) solution (to speed up ^{13}C-NMR acquisition) and of the standard TSP, as described in the previous paragraph.

4.2.5 Calculation of TOF.

The turnover frequency (TOF) of the catalyst in the different solvents was calculated using the formula $\frac{[product]}{[cat]\cdot t}$, where [product] is the concentration of the alkene obtained from the mono-hydrogenation of the substrate, [cat] is the catalyst concentration and t is the hydrogenation time, as reported in the experimental section . The concentration of the product (allyl-pyruvate) and of the catalyst were measured from the thermal ^{1}H-NMR spectra, using an external reference.

4.3 RESULTS AND DISCUSSION

4.3.1 Hydrogenation efficiency in different solvents

The use of PHIP polarized substrates in diagnostic applications requires that a highly concentrated sample of the product is obtained in a very short time, in order to limit the hyperpolarization loss due to relaxation.

The hydrogenation method, i.e. the use of NMR tubes pressurized with para-enriched hydrogen, allowed to use a small amount of reagents and to reach good reaction yields, in the very short time required for PHIP hyperpolarization. Different hydrogenation methods have been reported, which are based on spraying the hydrogenation mixture in a reactor filled with para-hydrogen [75,76] or bubbling paraH2 through the hydrogenation solvent [77,78].The former one requires a dedicated system and a relatively large amount of reactants, whereas the latter may need high para-hydrogen pressure (>10 bar) [79] to reach high efficiency of the reactions. In the herein reported experiments, a concentrated solution (240 mM) of the alkyne (propargyl-pyruvate) was hydrogenated to alkene in few seconds (1-3 seconds).

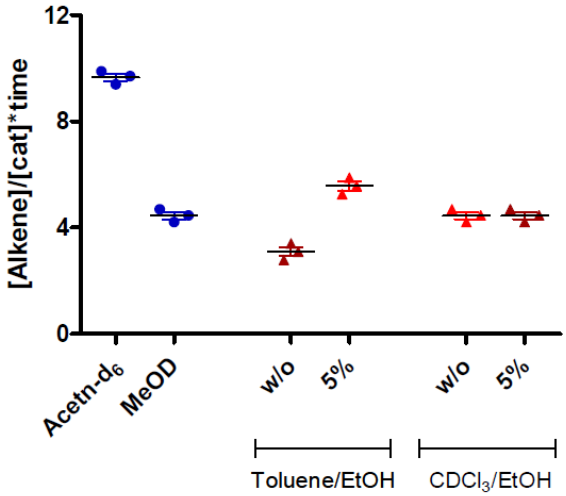

Figure 4.1: *TOF (turnover frequency) (moles of substrate that a mole of catalyst can convert in a unit time, 1s) for the catalyst (Rh(I) complex containing the chelating phosphine dppb (bis-(diphenilphosphino)butane)) in different solvents. The experimental conditions (hydrogen pressure, reaction temperature) and the hydrogenation method are described in the methods section.*

4. EFFECT OF THE HYDROGENATION SOLVENT IN THE PHIP-SAH HYPERPOLARIZATION OF [1-^{13}C]PYRUVATE

The concentration of the catalyst and the hydrogenation time were optimized for each hydrogenation solvent, in order to obtain complete hydrogenation of the substrate. The turnover frequency (TOF) of the catalyst in the different solvents was calculated (Fig. 4.1). The highest hydrogenation efficiency was obtained in acetone, in which complete conversion of the alkyne to the alkene was obtained in only 1 second, using half of the catalyst used in the experiments carried out in methanol (7 mM instead of 14 mM).

Acetone and methanol are both coordinating solvents and they are widely applied for the hydrogenation reactions catalysed by this type of rhodium complexes, containing chelating phosphines[80]. These solvents allow the formation of the catalytically active complexes (**I** in Fig. 4.2), upon the hydrogenation of the coordinated diene that frees the coordinating sites required for binding the substrate (Fig. 4.2). The formation of these active complexes can be detected in the ^{31}P-NMR spectra of the hydrogenation catalyst, following to the activation (i.e. the release of the coordinated diene). In these spectra, the signals of the phosphine ligand in the activated complex, in different solvents, can be clearly distinguished from those of the catalyst precursor (TableS1).

In the catalytic cycle, the so-called unsaturated route (Fig. 4.2)[81,82], the substrate coordinates to the metal center and displaces the solvent molecules (**I** to **II** in Fig. 4.2). The higher efficiency of the catalyst in acetone, as shown by the higher TOF, may be due to the fact that, being acetone a weaker ligand than methanol[83,84], it can be replaced more easily by the substrate, thus facilitating the hydrogenation reaction.

Unfortunately, acetone and methanol are completely miscible with water, therefore they are not compatible with in-vivo applications.

Vice-versa, chloroform and toluene are hydrophobic solvents, characterized by low solubility in water (toluene/water 0.052 WT% at 293K; chloroform/water 0.8 WT% at 293K)[84], therefore they can be used for

the phase-extraction step of PHIP hyperpolarized products.

So far, chloroform has been used to obtain the phase-extraction of PHIP hyperpolarized products[71,72] from the organic solution to the aqueous phase. It is a non-coordinating solvent and the activation of the catalyst precursor, by means of the hydrogenation of the coordinated diene (cyclooctadiene or norbornadiene), leads to the formation of non-catalytically active dimers.[85] Nevertheless, when the unsaturated substrate is added to the reaction mixture before the activation of the catalyst, the efficiency of the hydrogenation reaction is the same as the one observed in methanol (Fig. 4.1). The observed behaviour can be accounted for considering that, in the hydrogenation pathway (Fig. 4.2), the substrate can replace the product molecule directly (passage **V** to **II**, dotted arrow in Fig. 4.2) and the formation of the solvated specie (form **I**, Fig. 4.2) can be circumvented. The addition of a coordinating solvent (i.e. ethanol) does not improve the reaction efficiency, although the hyperpolarization level is increased, as it will be shown in the following section.

Toluene can coordinate to the metal centre, as it can be observed from the ^{31}P-NMR signals (Table S1), but unfortunately the hydrogenation efficiency of this complex is low, probably due to its scarce solubility in this solvent. The addition of a small percentage of ethanol (5% v/v) leads to an increase in both solubility and hydrogenation efficiency. It must be outlined that ethanol has been preferred to methanol, as co-solvent, due to its lower toxicity and better bio-compatibility

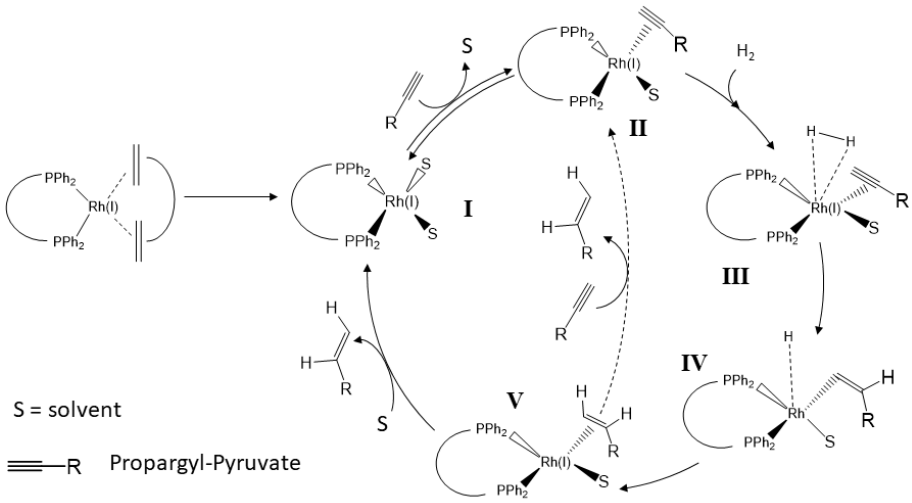

Figure 4.2: *Hydrogenation pathway for the Rh(I) complex containing the chelating phosphine dppb (bis-(diphenilphosphino)butane). In the passage shown by the dotted line, the intermediate **I** is circumvented, i.e. the adduct of catalyst and solvent is not formed. This is the case of chloroform, that is a non-coordinating solvent*

4.3.2 ^{1}H and ^{13}C Hyperpolarization on reaction products

Early on in the study of the PHIP phenomenon, it was realized that the hyperpolarized spectra of the product molecule depend crucially on the catalyst[85] because mixing between the singlet state of para-hydrogen and the other states (triplet states) occurs on hydrogenation intermediates[85]. The singlet/triplet mixing factor can be substantially different depending on the substrate, on the solvent and other experimental conditions. Higher S/T mixing leads substantially to loss of singlet order and hence lower hyperpolarization level on the products. More stable reaction intermediates would lead to longer

contact time of the hydrogen molecule on these intermediates and less efficient transfer of the singlet state to the products. In other words, para-hydrogen is not transferred to the product in pure singlet state, thus making the hydrogenation intermediates to have an effect on the S/T mixing, and in turn, introducing a relevant weight of the experimental conditions in the determination of the polarization level on products.

In order to estimate the efficiency of the singlet state transfer to the product, ^{1}H hyperpolarized spectra have been acquired in different solvents. In these experiments, hyperpolarization on protons has been taken as a readout of the singlet state transferred to the product. This can be considered a more direct readout than the ^{13}C polarization, which reports on the efficacy of spin order transfer techniques, i.e. RF pulses or magnetic field cycle.

In these experiments, called ALTADENA,[82] the molecule is hydrogenated at geomagnetic field, with all the protons resonating at the same Larmor frequency, and then transported into the high field of the NMR spectrometer for detection. During this passage, net magnetization on the ^{1}H-NMR signals of the product takes place.

The ^{1}H-NMR spectrum (Fig. 4.3) obtained from the ALTADENA experiments shows that hyperpolarization is distributed on all the protons of the allyl moiety.

Despite the higher catalyst efficiency observed in acetone, proton hyperpolarization in this solvent is significantly lower than in methanol. This can be explained considering the final step of the hydrogenation pathway (step **V** to **I** Fig. 4.2), in which the product is replaced by a solvent molecule, to allow a new molecule of the substrate to bind at the catalyst and start a new catalysis turnover. When the binding affinity of the solvent is higher, the displacement of the product molecule is energetically favored and this step is faster. This would result in a smaller singlet/triplet mixing on the intermediate **V** (Fig. 4.2) and

higher polarization on the product.

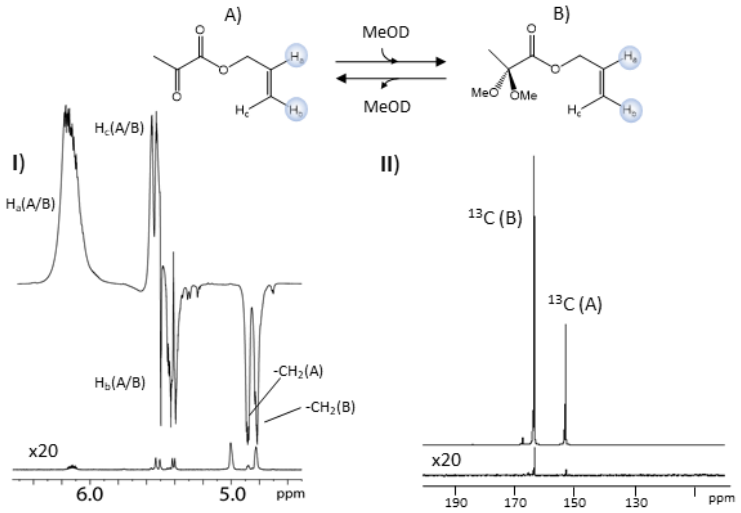

Figure 4.3: *In methanol, 15% of pyruvate ester is in the oxo-form (A) and 85% in the ketal form (B).* ***I)*** *^{1}H hyperpolarized (upper) and thermal (lower) spectra of allyl-pyruvate after hydrogenation, using para-enriched hydrogen, in methanol-d_4 (ALTADENA experiments).* ***II)*** *^{13}C hyperpolarized (upper) and thermal (lower) spectra of allyl pyruvate obtained in the same solvent, after the application of magnetic field cycle for spin order transfer from para-hydrogen protons to ^{13}C. From comparison between the hyperpolarized and thermal spectra, it can be easily noticed that the oxo- form (A) is significantly more polarized that the ketal form.*

Next ^{13}C hyperpolarization was obtained (Fig. 4.3), upon the application of the magnetic field cycle procedure. Consistently with the ALTADENA results, the ^{13}C hyperpolarization level was higher in methanol than in acetone. It must be noticed that the hyperpolarization level is different on the two isoforms of pyruvate-ester, being significantly higher on the

oxo-form (2-oxo-propanoate, 17.5 ± 0.9 % ^{13}C hyperpolarization, 15% of the total,), than on the acetalic-form (2,2-dimetoxy-propanoate, 6.4 ± 0.2% ^{13}C hyperpolarization). The two forms of pyruvate are 15% (2-oxo-propanoate) and 85% (2,2-dimetoxy-propanoate) of the total amount. The difference between the ^{13}C hyperpolarization of the two forms derives from the differences observed in the polarization of the ^{1}H signals. In fact, as shown in Fig. 4.3, the methylene protons appear more polarized on oxo-propanoate than on dimetoxy-propanoate. In pure toluene, hyperpolarization on ^{13}C is significantly lower than in the other solvents, but if a small percentage of ethanol is added (ethanol, 5% v/v), hyperpolarization is significantly increased. This can be due to the improved solubility of the catalyst in the toluene/ethanol mixture.

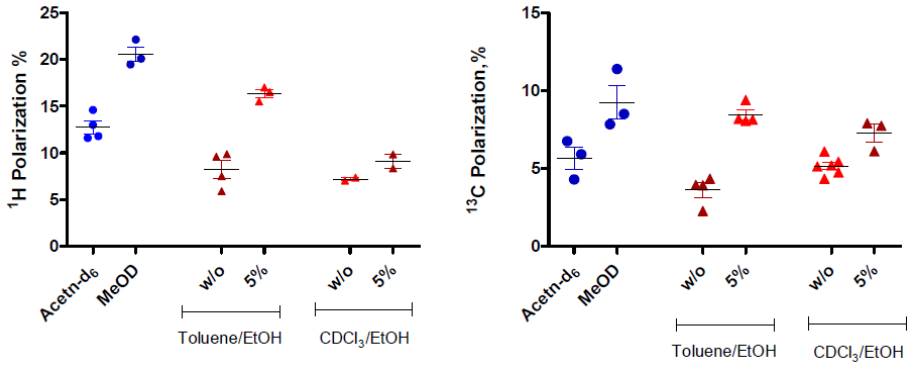

Figure 4.4: *Hyperpolarization level on ^{1}H and ^{13}C-NMR signals obtained in different solvents. ^{1}H hyperpolarization has been measured in ALTADENA experiments, while MFC (Magnetic Field Cycle) has been applied to obtain the spin order transfer from para-hydrogen protons to ^{13}C, in a different set of experiments.*

To study the effect of the ethanol addition as a co-solvent for the toluene

experiments with the different amount of the ethanol were performed. As can be observed from the results (Fig. 4.5) amount of the ethanol was not much effected at the polarization level but linearly decreased hydrogenation yield of the resulted ester. This can be explained that ethanol as co-solvent at the reaction is effected only solubility of the catalyst complex but not the coordination ability of the the solvent (Tabl. S1). On the basis of the obtained data for further work was chosen as a solvent solution the mixture of the toluene and 5 % of Ethanol.

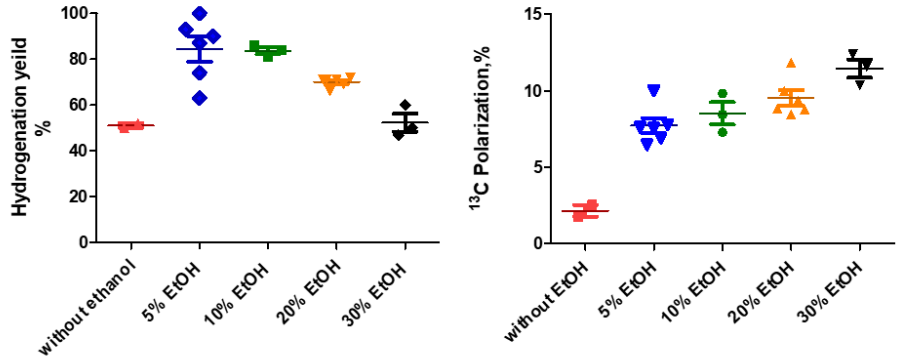

Figure 4.5: *Correlation between amount of Ethanol and Hydrogenation yield or Polarization level after the hydrogenation of [1-^{13}C] propargyl pyruvate with Para-hydrogen in toluene*

Chloroform is non-coordinating and it does not intervene directly in the reaction pathway. The observed hyperpolarization, on both ^{1}H and ^{13}C spectra, is slightly lower than in toluene. Also in this case, the addition of the co-solvent (ethanol, 5%) leads to an increase of the hyperpolarization of the ^{1}H and ^{13}C signals, although the effect of the co-solvent on hyperpolarization is lower than that observed in toluene (Fig. 4.4 and Tab. 4.1).

Solvent	**^{1}H Polarization**	**^{13}C Polarization Allyl-[1-^{13}C]pyruvate**	**^{13}C Polarization [1-^{13}C]Pyruvate**	**^{13}C Polarization [1-^{13}C]Pyruvate Filtered**
Acetone-d_6	12.7±1.4	5.7±1.2		
Methanol-d_4	20.6±1.4	9.2 ± 1.9 17.5±0.9 (oxo-form) 6.4±0.2 (acetalic-form)		
Toluene-h8	6.7 ± 1%	3.6 ± 0.9%		
Toluene/ EtOH (5%)	16.3 ± 0.8	8.4 ± 0.6	4.1 ± 0.3	3.4 ± 0.6
Chloroform-d	7.2 ± 0.2	5.2 ± 0.6 (n=6)	2.7 ± 0.6%	2.2 ± 0.3
Chloroform-d/ EtOH (5%)	9.1 ± 1	7.2 ± 1 (n=3) 6.2 ± 0.3*	3.5%*	
Chloroform/ EtOH (30%)		8.5 ± 0-4**	5.2%**	

Table 4.1: *Hyperpolarization level on ^{1}H and ^{13}C signals of parahydrogenated allyl-pyruvate. * ^{13}C hyperpolarization values reported in ref.[42] and ** in[43]*

4.3.3 Hydrolysis and phase extraction

For biological applications, hydrolysis of the allyl-ester and transfer of hyperpolarized pyruvate into the aqueous phase are the next steps. Phase transfer of the hyperpolarized product from the organic to the aqueous phase

can be obtained, provided that the hydrogenation reaction is carried out in an organic hydrophobic solvent, therefore toluene/ethanol (5%) and pure chloroform have been tested.

Despite that high polarization observed in methanol, being this solvent completely mixable with water, the aqueous solution of hyperpolarized pyruvate obtained by using methanol as hydrogenation solvent cannot be applied for biological studies. Analogously, special attention has to be devoted when the addition of ethanol to the organic phase is pursued to increase the efficiency of hydrogenation and hyperpolarization, as one has to keep in mind that high percentages of ethanol in the aqueous solution may not be compatible with the intended biological applications and in-vivo studies.

Hydrolysis of the ester is carried out by injecting an aliquot of a heated base solution in the NMR tube that contains the organic solution of the hydrogenation product. This step is followed, after few seconds (7-8 s), by the addition of the acidic buffer solution in order to reach physiologically acceptable pH values. The aqueous phase is withdrawn into a syringe and transferred into another sample tube for the acquisition of the NMR spectrum. All these passages, from the hydrolysis of the ester to the acquisition of the NMR spectrum, take a few tens of seconds (32-34 s). Due to the ongoing relaxation processes, the measured hyperpolarization level of the Pyruvate ^{13}C carboxylate signals resulted to be 4.1 $\pm$ 0.3% when the hydrogenation solvent was the toluene-h_8/ethanol mixture and 2.7 $\pm$ 0.6 % in the case of chloroform, respectively.

^{1}H-NMR spectra of the aqueous solutions were acquired to determine the concentration of all the chemical species present in the solution of the hyperpolarized substrate (Fig. S4, S5). Previously reported cellular studies[65] have shown that a toxicity effect associated to the presence of the organic solvent (chloroform) is evident when cells are incubated for

12-24 h in the aqueous solution of the products obtained by applying the hydrogenation/hydrolysis/phase extraction procedure above described. Impurities derived from the hydrogenation reaction (allyl-alcohol, ethanol) do not have any effect on cells viability.

The final concentrations of chloroform and toluene, in the aqueous solution of pyruvate, are 30± 2 mM and 15±2 mM, respectively. These values are higher than those recommended by the Environmental Protection Agencies for water quality criteria[86] (0.59 mM for chloroform and 10 mM for toluene), therefore a purification step must be added in order to reduce as much as possible. To do that, filtration of the aqueous solution using a lipophilic resin was applied as the final step, at the end of the hyperpolarization procedure. Tenax® TA[87,88]is a common porous organic polymer used for the absorption of volatile organic compounds. The use of a PEEK filter to retain the resin allowed to avoid hyperpolarization losses during filtration, whereas it was observed that, if stainless steel filters are used, the hyperpolarization loss during filtration is significant (Fig. S6). Filtration through the lipophilic resin allowed to completely remove toluene from the aqueous phase, while the chloroform concentration (0.5 ±0.1 mM) resulted lower than the value recommended by the water quality agencies.

Unfortunately, the filtration step caused a decrease in the ^{13}C polarization level that resulted to be 3.4 ± 0.6 % in the case of the toluene/ethanol (5% ethanol) solution was used and 2.2 ± 0.3 for chloroform as hydrogenation solvent, respectively. The decrease of the hyperpolarization level appears mainly due to the longer work-up of the solution. The filtration passage takes 18-20 seconds, therefore the time delay from the hydrolysis to the acquisition of the hyperpolarized spectrum becomes 50-52s. It can be reasonably expected that these polarization losses could be significantly reduced if an automatized procedure would be applied. Nevertheless, the

^{13}C hyperpolarization obtained in the case of hydrogenation in chloroform is still sufficient for in-vivo metabolic investigations, as reported in the following sections.

	[Pyruvate]	**[allyl-alcohol]**	**EtOH**	**Solvent**	**Solvent (filtration)**
Toluene/ EtOH	50 ± 5 mM	45 ± 5 mM	210 ± 50 mM	15 ± 3 mM	n.d.
$CDCl_3$	30 ± 5 mM	8 ± 1 mM	-	30 ± 2 mM	0.5 ± 0.1 mM

Table 4.2: *Concentration of the different chemical species in the aqueous phase*

4.3.4 MRI studies

In order to validate the applicability of the solution of HP-pyruvate to MRI studies, a few preliminary MR imaging investigations have been carried out. The aqueous solution of HP pyruvate obtained after hydrogenation in chloroform, phase-extraction and filtration through the Tenax resin was initially injected into a phantom consisting of three test-tubes: one containing a concentrated solution of thermally polarized ^{13}C-succinate and two containing water (Fig. 4.6a). After the injection of the hyperpolarized solution of [1-^{13}C]pyruvate, a ^{13}C-RARE image was acquired. The concentration of HP sodium pyruvate was 30 ± 6 mM (Fig. 4.6b) and the SNR was comparable to that observed on the thermally polarized 1.5M [1,4-2^{13}C]succinate (1.5 M, 256 scans) (Fig. 4.6c)

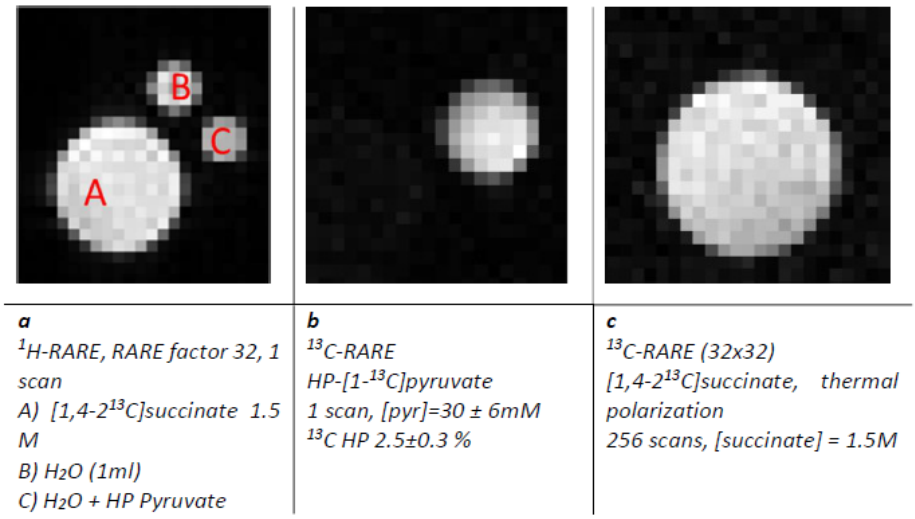

Figure 4.6: MRI images of the phantom

4.4 CONCLUSIONS

The hyperpolarization level on the parahydrogenation products depends strongly on the solvent used. This is due not only to the solubility of hydrogen in a given solvent, but also to the binding interaction of the solvent molecules to the hydrogenation catalyst. Coordinating solvents such as acetone, methanol and ethanol can lead to high efficiency, in terms of hydrogenation speed and polarization level. The higher polarization level obtained in coordinating solvents can be explained considering that the displacement of the product molecule from the metal center is faster, thus limiting the singlet/triplet mixing on intermediates.

Reactions that were carried out using variable concentrations of ethanol in chloroform or toluene have clearly shown the dependence of the ^{13}C polarization level and of the hydrogenation efficiency on the relative amount of

the co-solvent. However, high percentages of the co-solvent are not compatible with biological applications, and have to be avoided in the preparation of samples for in-vivo studies.

In order to allow the phase-extraction of hyperpolarized pyruvate, chloroform and toluene/ethanol (5% v/v) have been used. In these solvents, ^{13}C hyperpolarization on the allyl-ester are 5.2 ± 0.6% and 8.4 ± 0.6% respectively. After hydrolysis and phase extraction of sodium [1-^{13}C]pyruvate, the ^{13}C polarization is 2.7 ± 0.6% when hydrogenation is carried out in chloroform and 4.1 ± 0.3% when the toluene/ethanol mixture is used. Although the solubility of these organic solvents in water is low, their concentration in the aqueous solution is unneglectable. Filtration of the aqueous solution of the hyperpolarized product through a lipophilic resin (Tenax® TA) led to the complete removal of the organic solvents, still remaining a good hyperpolarization level almost unaffected, still sufficient for ^{13}C MRI studies.

CHAPTER 5

PHIP POLARIZED [1-^{13}C]PYRUVATE FOR ZERO AND ULTRA-LOW FIELD (ZULF) NMR DETECTION

Part of the material presented here is being published under the title:

Metabolic Reactions Studied by Zero-and Low-Field Nuclear Magnetic Resonance. Eills J., Picazo-Frutos R., **Bondar O.**, Cavallari E., Carrera C., Barker S. J., Utz M., Aime S., Reineri F., Budker D. and Blanchard J. W. (2022). arXiv preprint arXiv:2205.12380.

Due to features such as low cost and portability, ZULF NMR has recently gained considerable attention in the fields of chemistry, biology, medicine and fundamental physics tests. This chapter describes the basic principles, methodology and recent experimental and theoretical developments of ZULF NMR, as well as its application in spectroscopy. The future perspectives of ZULF NMR are also discussed.

5.1 INTRODUCTION

Conventional NMR makes use of high magnetic field that is necessary to polarize the nuclear spin, to resolve the chemical shift of different chemical species and to enable inductive detection of MR signals.[89]

NMR and MRI are widely used for studying the structure of chemical compounds and for diagnostics. The main drawbacks of MR based methods (NMR and MRI) are given by the high cost of superconducting magnets, that are bulky and non-portabe.

The use of ultralow magnetic field (or even zero field) reduces dramatically the size and the cost of the MR machine. Other advantages of Ultralow-field (ULF) nuclear magnetic resonance are the detection of MR signals in metal containers, that cannot be used for conventional NMR, and the high field homogeneity yielding narrow resonance lines and better determination of scalar and dipolar couplings[90,91].

Nevertheless, at zero field the chemical information given by the chemical shift is lost and the nuclear spin polarization is more than 10^6 times lower than that obtained using conventional high field NMR.

At zero-field, the information about the molecular structure can be derived from spin-spin interactions (i.e. scalar, dipolar and quadrupolar coulings). An external source of polarization is required, in order to obtain

a detectable nuclear magnetization of the sample. This is usually achieved by means of pre-polarization of the sample in an external magnetic field (1T or higher). Hyperpolarization techniques[2,6,25,92,93] are also an ideal partner for ZULF magnetic resonance because the intensity of the MR signal is not dependent on the magnetic field strength.

In this chapter, hyperpolarized substrates obtained by means of PHIP will be applied for ZULF NMR detection.

5.2 Components of a ZULF NMR spectrometer

In ZULF NMR, the geomagnetic field and other environmantal magnetic fields have to be shielded in order to reach a few nTs in the detection region. This can be obtained by means of passive shielding using a magnetic shielding material (permalloy or μ-metal) or actively using compensating magnetic fields applied by means of an electric current circulating in conductive coils.

Magnetization of the sample is usually obtained using a pre-polarizing magnet placed close to the detector, that allows to increase the thermal polarization of the sample.

The signal is then measured by an atomic magnetometer, which is a highly sensitive device for detecting the magnetic fields generated by the spins of the nuclei in the sample. These devices are made of a glass cell with filled alkali vapour (^{87}Rb).

The different parts of the ZULF NMR spectrometer are described at Fig. 5.1.

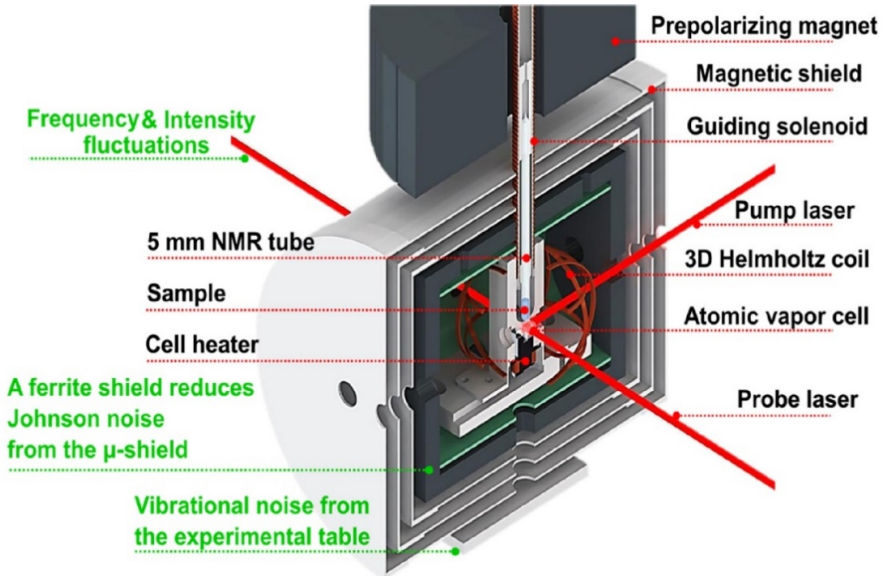

Figure 5.1: *Different components of the ZULF-NMR spectrometer (black text) and possible noise sources / sources of "shimming" (green text), adapted from*[94]*, current figure used from the web-page*[95].

5.2.1 Optically Pumped Magnetometer (OPM)

Atomic magnetometers are built on the basis of obtaining the absorption or emission of energy by vapors formed from one of the alkali metals, due to its irradiation with a laser of a precisely defined frequency, which changes the quantum state of the sample. The laser emits electromagnetic waves, creating a magnetically sensitive state in alkali metal vapors (alkali metals such as rubidium and cesium have only one electron at the outer level, which is largely distant from the nucleus. It is this electron that changes its state). Thus, passing to the vapour of polarized light. This sensitive change in the state of atoms is called optical pumping. Once the optical pumping state is established,

the light source no longer transmits polarized light into the vapour. Instead, polarized light passes through the vapor and is detected by the photodiode as a change in voltage (Fig. 5.2). If, however, a sample with its own magnetic field is introduced into this system, then this state will be violated and restoration will again be required by a laser that transmits polarized light into the vapor, and thus changes depending on the magnetic field of the sample will be recorded on the photodiode. More sophisticated optical magnetometers use two lasers, one of which calls pump beam (can be circularly polarised depending of the alcali metal at the vapor cell) and induce the magnetically sensitive state emits light of a certain length, another lazer - probe beam (typically is linearly polarised) - is using for measuring the changes in the magnetic field.

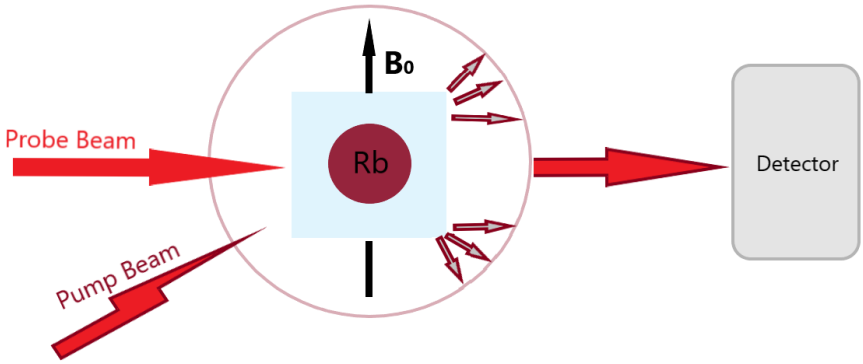

Figure 5.2: *General scheme of an optical atomic magnetometer.*

5.2.2 Sample prepolarization.

The most common pre-polarization method used in ZULF NMR makes use of a powerful Halbach magnet (˜ 2 T, Fig. 5.1). The sample is polarized into the high field and then mechanically transported to the shielded region for detection. This procedure is repeated many times in order to increase the

signal-to-noise ratio. To maintain polarization during the transport from the pre-polarizing magnet to the zero-field detector, a guide field is often used, generated by a solenoid coil around the shuttle path. A limitation of this technique is the transfer time (about 0.5 s), but for most compounds studied by ZULF NMR, the transfer time is much faster than the spin decoherence time. Therefore, only a small part of the polarization is lost during transportation.

An alternative way to polarize nuclei for ZULF detection has been reported recently[96]. This method relies on the application of an electromagnetic field around the sample, placed inside the mu-metal shield, close to the optical detector. This method is convenient for samples characterized by relaxation rates faster than the transfer rate from the pre-polarization to detection region because, using this setup, the sample remains next to the atomic vapour cell used for the detection.

In both cases, a sufficient degree of thermal polarization is achieved, which allows to obtain a ZULF NMR spectrum.

The higher the degree of pre-polarization, the greater the intensity of the received signal, which will improve the ratio of signal to noise. Thermal polarization in a 2 T magnetic field gives a polarization of only ˜ 9 ppm.

Hyperpolarization is an alternative method to increase the magnetization.

5.2.3 Signal detection.

In high field NMR, the Larmor frequency of the detected signals is in the order of hundreds of MHz, but, under ZULF conditions, nuclear spins precession is in the range betweeen a few Hz to kHz. In this frequency region the inductive detection, based on Faraday induction law, offers poor sensitivity and other magnetometric methods must be used.

Three different methods, suitable for the detection of MR signals at

ZULF, can be used: optically-pumped magnetometers (OPM), superconducting quantum interference devices (SQUID) and devices using nitrogen vacancy centers (NV) in diamond. SQUID can measure magnetic fields with a sensitivity greater than 1 fT averaged over one second, but they typically operate at liquid helium temperatures.

Negatively charged nitrogen-vacancy (NV^-) color centers in a diamond allows highly-sensitive detections of magnetic field, potentially providing an order of femtotesla magnetic detection. The electron spin of NV^- in solid-state material can be controlled at room temperature under an ambient magnetic field (for example, a geomagnetic field of approximately 50 µT). A single NV^- center in a nano-diamond enables the detection of the phenomena in the order of the nanometer scale, such as the magnetic field generated by a cell[97].

Atomic magnetometers (OPM), offering sensitivity similar to SQUIDs, work best between room temperature and elevated temperature (up to 200°C), have low power consumption (requiring power only to heat up a small cell and supply a low-power laser) and can be miniaturized,[98] and therefore their application is ZULF NMR is more convenient. Most optical magnetometers use alkali metal atoms (Rb, Cs, K) placed in glass cell. The cell is heated, as a result of which the rubidium atoms pass into a gaseous state. When the laser beam passes through the cell vapour of the alkali metal, pumping occurs, which is close to the absorption line of the atomic medium. Such a beam transfers angular momentum between photons and rubidium vapour atoms, so that the atomic spins enter a highly polarized state. The polarized atoms are now very sensitive to their external field and their spins will precess at a frequency proportional to the field strength. This altered state of polarized rubidium atoms can be measured with another laser, the "probe" beam, and the rotation or absorption of light from the probe beam, sensitive to the field experienced by the alkali metal atom, can be observed (Figure5.2. shows the individual light sources

for pumping and probing with orthogonal light rays). The magnitude of that change is a sensitive and accurate measure of magnetic field strength. In this way we can obtain ZULF spectra

Nowadays, OPM are commercial, for example the QuSpin zero field magnetometer (QZFM) from QSpin Inc.,[99] which is based on the change in atomic absorption at resonance in the zero field.[100] These sensors have found application in many fields of science and have been used in recent studies in the detection of ZULF.[100]

5.3 Magnetic Resonance signals at zero-field.

To be able to interpret the NMR spectra at zero magnetic field we can consider a spin system formed by two nuclei, namely A (e.g. ^{1}H) and X (i.e. ^{13}C). The nuclear spin Hamiltonian in isotropic media, in a magnetic field B is:

$$\hat{H} = 2\pi\hbar J_{AX} I_A I_X - \hbar B \left(\gamma_A I_A + \gamma_X I_X\right), \tag{5.1}$$

where J_{AX} is the scalar coupling between the two spins (J-coupling Hamiltonian) while the second part of the equation is the Zeeman Hamiltonian. In the absence of an external magnetic field B, the Hamiltonian reduces to the J-coupling. The four eigenstates of the J-coupling Hamiltonian, for two spins $\frac{1}{2}$, are given by singlet-triplet states S_0, T_0 and $T_{+/-}$. For the two states T_+ and T_-, the the energy level is +1/2J and for the state T0 the energy is -1/2J, therefore the gap between the states is equal to J. Therefore, the NMR spectrum shows one line at frequency J_{AX}.Figure 5.1.3a shows the zero-field spectrum of ^{13}C-formic acid, a heteronuclear two-spin system (the acidic proton can be neglected due to rapid chemical exchange). At zero magnetic field there is one observed nuclear spin transition, which occurs at 222 Hz, that corresponds to the value of the $^{1}J_{CH}$ scalar coupling.

More in general, in the absence of an applied magnetic field, the eigenstates of the Hamiltonian of a system $^{13}CH_N$ are eigenstates of $\boldsymbol{f}^2$ and f_z where $\boldsymbol{f}$ is the total angular momentum

$$f = \sum\nolimits_j I_j \tag{5.2}$$

In zero field, the energy levels are given by:

$$E(f,k) = J/2[f(f+1) - k(k+1) - s(s+1)] \tag{5.3}$$

Where k are the possible quantum numbers of the operator **k** describing the sum of equivalent proton spins and s is the spin of ^{13}C (1/2).

In the $\underline{AX_2}$ system we have a **single line at $3J_{XA}/2$**.

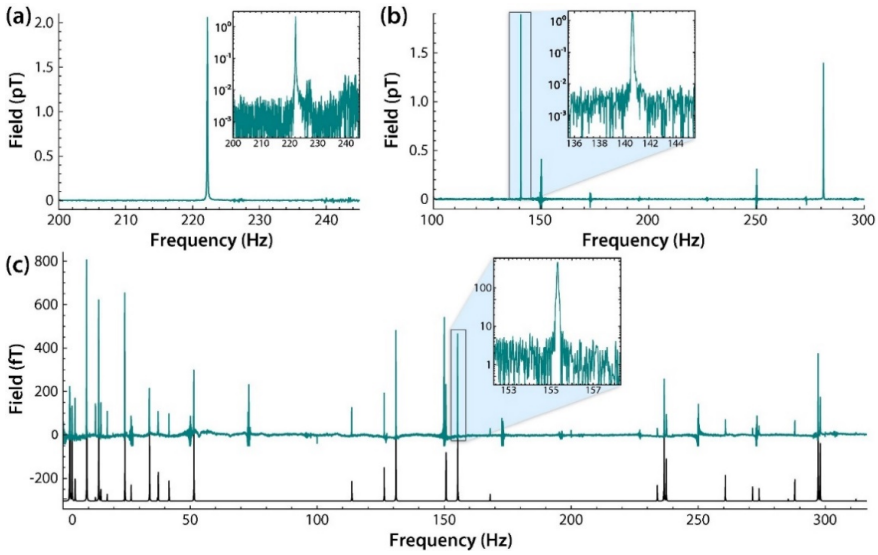

Figure 5.3: *ZULF NMR spectrum of a) formic acid; b) 2-13C acetonitrile and* [$^{13}C_2$,^{15}N] *-acetonitrile, picture is used from the article.*[101]

The zero-field spectrum of 2-^{13}C-acetonitrile, an AX_3 spin system, shows two peaks at $^1J_{CH}$ and 2^1J_{CH}. Being $^1J_{CH} \approx 141$ Hz, the two peaks are cen141

and 282 Hz, respectively.[102–104]

The spectrum of [$^{13}C_2$,^{15}N] -acetonitrile, a five-spins system is shown in Fig. 5.3(c). This system is more complicated and gives more peaks spread in the spectral range 0-300 Hz. Below the experimental spectrum, a simulated spectrum is shown to determine which peaks correspond to NMR signals and which peaks correspond to ambient / electron noise. Further analysis of the spectrum in terms of nuclear spin energy levels is given in[72].

5.4 Materials and Methods

All high-field NMR experiments (unless otherwise stated) were performed in a 1.4 T ^{1}H-^{13}C dual resonance SpinSolve NMR system (Magritek, Aachen, Germany).

Parahydrogen at >95% enrichment was generated by passing hydrogen gas (>99.999% purity) over a hydrated iron oxide catalyst in a cryostat operating at 30 K (Advanced Research Systems, Macungie, U.S.A.).

For magnetic field sweeps for polarization transfer, an MS-2 four-layer mu-metal magnetic shield (Twinleaf LLC, Princeton, U.S.A.) was used to provide a 10^4 shielding factor against external magnetic fields. No static shim fields were required, since the residual field within the shield was on the order of 5 nT. The time-dependent applied magnetic field was generated using the built-in B_y shim coil, with current supplied with an NI-9263 analog output card (National Instruments, Aachen, Germany) with 10 µs time precision. The guiding magnetic field for sample transport in and out of the magnetic shield was provided with a handmade solenoid, with current supplied with a Keysight U8001A current source (Keysight Technologies, Böblingen, Germany).

5.4.1 ZULF NMR of Propargyl-acetate and [1-^{13}C]propargyl-lactate.

The parahydrogenation reactions of propargyl-acetate (Fig. 5.5) and of propargyl [1-^{13}C]lactate Fig. 5.6 have been carried out by bubbling 5 bar para-hydrogen into a sample formed by 250 mM of the starting material (propargyl-acetate) and 13.8 mM of the Rh(I) catalyst (Rh(cod)dppb) in chloroform. The reaction was carried out at 60°C for 5 s, directly in the ZULF apparatus.

The ZULF setup used for the experiments is reported in figure 5.1 and two kinds of experiments (Fig. 5.4) have been carried out. In the first one, the parahydrogenation reaction has been carried out at zero field, then, a short "detection" pulse (50 µs, 1000 µT) has been applied, before the detection at zero field. In the second series of experiments, a magnetic field cycle, analogous to that applied for the spin order transfer from parahydrogen protons to ^{13}C, has been applied, before the zero-field detection. In this second case, the reaction has been done at 1 µT, then the magnetic field has been instantaneously (non-adiabatically) dropped to 50 nT and then exponentially increased again to 1 µT. In the end, the field has been switched off completely for the zero-field detection (Fig. 5.4).

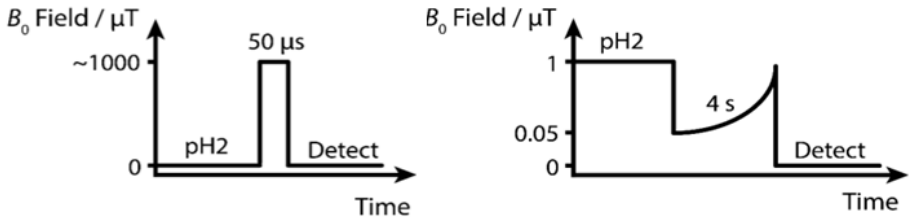

Figure 5.4: *Magnetic field applied in two types of experiments performed; "pulse-acquire" (left) and "field cycle" (right).*

5.4.2 ZULF NMR of [1-^{13}C]pyruvate and [1-^{13}C]lactate.

The precursor solution for all pyruvate experiments was 400 mM propargyl pyruvate and 20 mM rhodium catalyst [Rh(dppb)(COD)]BF_4 in a solvent of 95:5 (v/v) $CDCl_3$:ethanol-d_6, which was prepared by dissolving the catalyst in the solvent, and adding the propargyl pyruvate immediately (tens of seconds) before each experiment. The propargyl pyruvate precursor was synthesized in-house, and all other chemicals were purchased from Sigma Aldrich.

For pyruvate hydrogenation experiments, a 250 μL aliquot of precursor sample was loaded into a 5 mm low pressure/vacuum NMR tube via syringe injection and the tube was pressurized to 7 bar pH_2 pressure. The sample was heated to 120 °C with a heatgun, and then the tube was vigorously shaken for 4 s while under pressure. After shaking, the whole NMR tube was placed in the magnetic shield for a 4 s magnetic field sweep. After the field sweep, the solution was ejected from the NMR tube using a valve at the top and the internal gas pressure to push the solution through a 1/16 in PTFE capillary into a 10 mm NMR tube containing 300 μL 400 mM NaOH at 80 °C for the hydrolysis. The resulting mixture was allowed to settle for 2 s and the aqueous layer was extracted through a 1/16 in PTFE capillary into a syringe containing 300 μL acidified 500 mM phosphate buffer solution to neutralize the pyruvate solution at pH 7.

For the zero- and low-field experiments, this solution was injected into a 5 mm NMR tube, and this was dropped into the zero-field spectrometer for signal acquisition.

For the experiments to observe conversion to lactate, the syringe used to extract the aqueous phase from the 10 mm NMR tube contained 200 μL of acidified phosphate buffer solution, such that, after mixing, the solution ended

at pH 7. Another 100 μL of phosphate buffer solution contained 50 mg NADH and 25 μL lactate dehydrogenase (Sigma Aldrich, L7525), and this solution was held in the 5 mm NMR tube. The pyruvate solution was injected into the 5 mm NMR tube and mixed with the enzyme solution by vigorous shaking for 5 s, before being dropped into the zero-field spectrometer for signal acquisition.

A modified experimental procedure from the established protocol reported in Ref. [105] was adopted to increase the volume of the solution and maximize pyruvate concentration (and hence signal) for this proof-of-concept demonstration. For in vivo/in vitro studies, a protocol has to be established in order to attain a biologically compatible solution of the substrate at high concentration.

5.4.3 Ultralow field relaxation of [1-^{13}C]-pyruvate AND [1-^{13}C]-lactate

A solution of approximately 250 mM of the propargyl ester (propargyl-[1-^{13}C]lactate or propargyl-[1-^{13}C]pyruvate) and 13.8 mM of the catalyst [Rh(cod)dppb][BF_4] in 100 μL of 95:5 (v/v) $CDCl_3$:ethanol, was loaded into pressurizable NMR sample tubes, and these were pressurized with parahydrogen gas (86% enriched, to a pressure of 2 bar at liquid nitrogen temperature). The tubes were kept frozen (77 K) to prevent any chemical reaction, until the start of the hyperpolarization experiment. To initiate the hydrogenation reaction, the NMR tube was heated in a hot water bath at 80 °C for 7 s, shaken vigorously for 3 s, then opened to release the parahydrogen pressure. The tube was then placed in a mu-metal shield (Bartington TLMS-C200) equipped with a coaxial solenoid, through which a magnetic field cycle (MFC) was applied, to obtain the spin-order transfer from the parahydrogen protons to ^{13}C. The magnetic field profile applied in all the

experiments consists of a diabatic passage from 1.5 μT (initial magnetic field) to 50 nT, and then up to 10 μT in 4 s with an exponential profile.

To hydrolyse the ^{13}C-polarized ester (allyl-[1-^{13}C]-pyruvate/lactate) a hot 260 μL solution of 230 mM NaOH and 50 mM ascorbate was injected with 1.5 bar argon pressure. Hydrolysis of the ester occured in a few seconds and the aqueous phase containing the hydrolysed pyruvate/lactate was extracted, whereas the catalyst was retained in the organic phase. An acidic buffer (135 mM HEPES + 60 mM HCl) was added to the aqueous phase to obtain a neutral pH (7.4).

To investigate the effect of the external magnetic field on the relaxation of [1-^{13}C]lactate and [1-^{13}C]pyruvate, the hyperpolarized solutions were held at different magnetic fields (1, 2, 4, 8, and 36 μT) for 5 s before acquisition of the ^{13}C NMR spectrum at high field using a 14.1 T NMR Bruker Avance spectrometer. The magnetic fields were generated in the μ-metal shield by controlling the current through the solenoid coil, except 36 μT which was the laboratory magnetic field. Each measurement was performed using a freshly-prepared hyperpolarized sample.

5.5 ZULF NMR of parahydrogen hyperpolarized substrates

Despite their sensitivity at ULF, OPMs are 2-3 orders of magnitude less sensitive than inductive detection at ca. 7 T. The lower sensitivity of ZULF NMR has so far generally precluded applications of ZULF NMR, particularly for biomedical applications given the intrinsically low concentrations of biomolecules in biological systems. For these purposes, the application of hyperpolarization substrates is an ideal tool to circumvent the low sensitivity

issue. The feasibility of the ZULF detection of PHIP polarized signals has been tested, in the first subsection, on two molecules derived from hydrogenative-PHIP. In particular, the unsaturated propargyl derivatives of acetate and lactate have been used for the parahydrogenation reaction.

In the second subsection, the PHIP-SAH method has been applied to obtain hyperpolarized pyruvate that has been used for ZULF detection. In order to demonstrate that metabolic transformations can be observed with zero-field NMR, the conversion of pyruvate into lactate, has been observed in vitro, using an aqueous solution of the enzyme LDH (lactate dehydrogenase).

5.5.1 ZULF NMR of Propargyl-acetate and [1-^{13}C]propargyl-lactate.

Hyperpolarized signals were observed, as reported in Fig. 5.9, only in the first kind of experiments. They are related to the allyl-alcohol moiety of the ester (Fig. 5.5 and Fig. 5.6.). The hyperpolarized peaks at ˜230Hz are related to the -CH_2 group (two geminal protons) while the signal at ˜160Hz is due to the olefinic -CH group (Fig. 5.7).

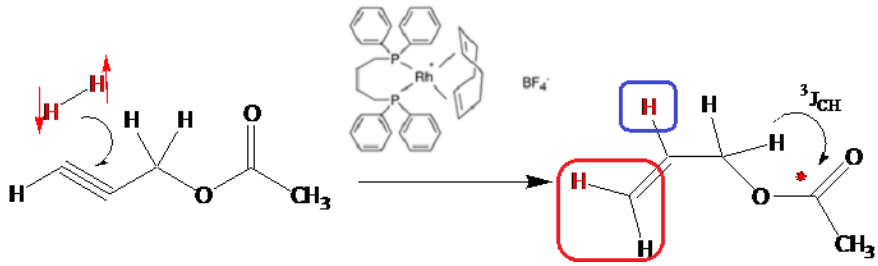

Figure 5.5: *Hydrgenation reaction of propargyl-acetate by PHIP method.*

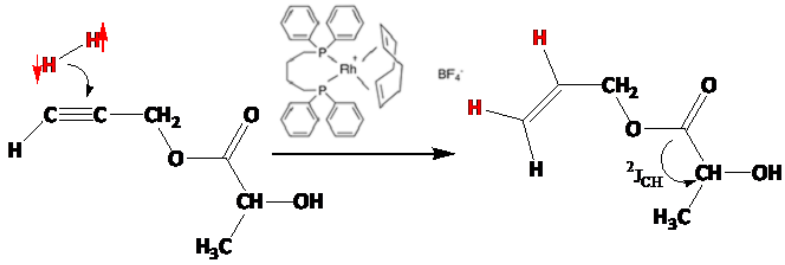

Figure 5.6: *hydrogenation reaction of the propargyl-lactate.*

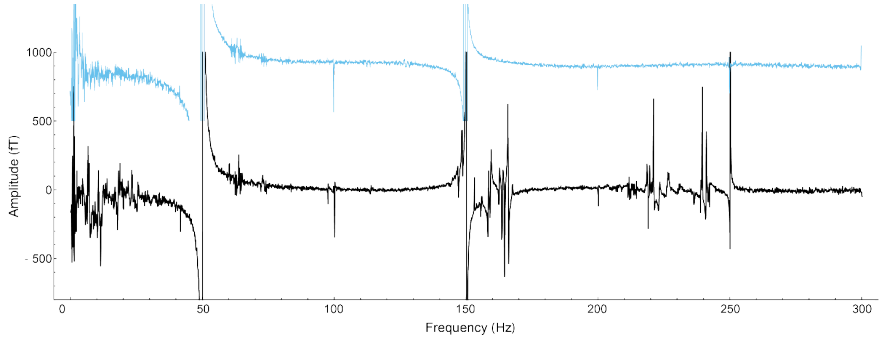

Figure 5.7: *ZULF NMR spectrum of 250 mM allyl-acetate formed via reaction with parahydrogen. A noise-spectrum is shown above in blue.*

In the low-frequency region (0-25 Hz) other enhanced peaks can be observed, that may be due to the smaller J-couplings ($^2J_{CH}$ and $^3J_{CH}$ couplings) in the allyl moiety.

Using the second kind of experiment, the hyperpolarized signals at higher frequencies (˜160 and ˜250 Hz), related to the allyl protons, are not observed, neither using the acetate (Fig. 5.8) not the [1-^{13}C]lactate (Fig. 5.9.) derivative, while the signals at lower frequency (0-15 Hz) are only vaguely detectable, due to the high noise level in this spectral region.

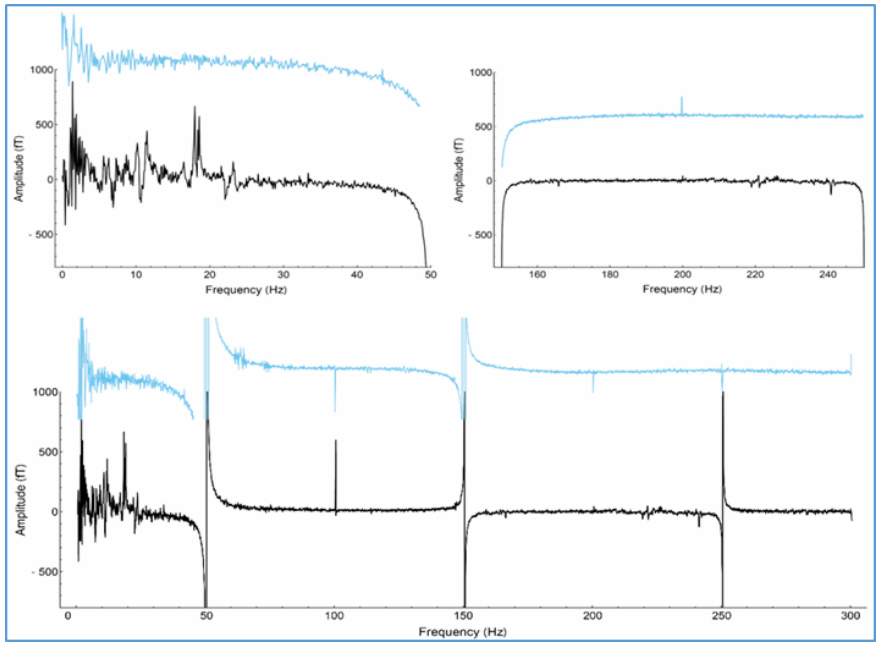

Figure 5.8: *ZULF NMR spectrum of 250 mM allyl acetate formed via reaction with para-hydrogen, after performing a magnetic field cycle experiment. A noise-spectrum is shown above each, in blue.*

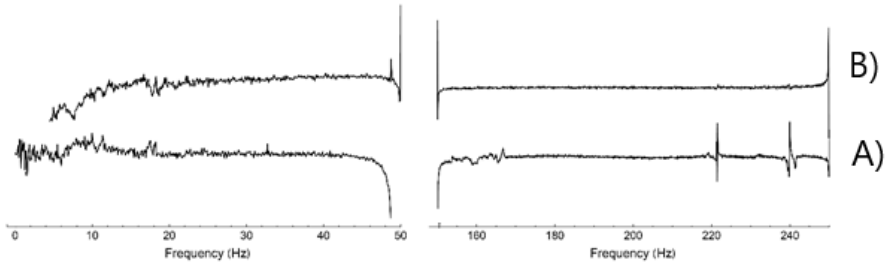

Figure 5.9: *ZULF NMR spectrum of 250 mM allyl-lactate formed via reaction with para-hydrogen, after performing a magnetic field cycle experiment.*

5.5.2 ZULF NMR of [1-^{13}C]pyruvate and [1-^{13}C]lactate.

After the experiments on hyperpolarized esters carried out at zero-field, the detection of MR signals of hyperpolarized metabolites (pyruvate and lactate) obtained by means of PHIP-SAH (chapter 2) has been carried out at ULF.

As observed in the experiments carried out using the PHIP polarized esters (allyl-acetate and allyl-lactate), the detection of signals in the lowest frequency region (0-15Hz) is often precluded by the high noise level.

In order to solve this problem and to increase the sensitivity of the OPM in the lowest frequency range, the ZULF NMR setup has been modified[1], as reported in Fig. 5.10a. In this setup, the sample is placed in a magnetic shield and measured using two optically pumped magnetometers [100]. A set of three orthogonal Helmholtz coils was present inside the shield to generate magnetic fields for control of the spin states and their dynamics. Furthermore, the sample was located within a long solenoid coil that pierced through the magnetic shield along the y axis, allowing for a magnetic field to be applied to the sample without significantly affecting the magnetometers [106]. The staggered arrangements of the magnetometers was chosen to reduce the common noise while maximizing the signal from the sample. As illustrated in figure 5.10b, the magnetic filed produced by the nuclear spins in the sample has opposite sign at the location of the two sensors. In contrast, many noise sources which are centered further from the detectors produce magnetic field that are more homogeneous at the position of the OPMs. By measuring the difference in the outputs from the two sensors, signals are combined constructively and noise is cancelled. Because the sensors have two sensitive axes, it was possible to independently measure magnetic fields corresponding to magnetization along x and z.

A set of three orthogonal Helmholtz coils are also present in the magnetic

[1] modification of the setup were done by people from the Dima Budker's group

field shield to generate magnetic fields for control of the spin state and dynamics. Furthermore, the sample is located within a long solenoid that pierces through the magnetic shield along the y axis, allowing for a magnetic field to be applied to the sample without significantly affecting the magnetometers.

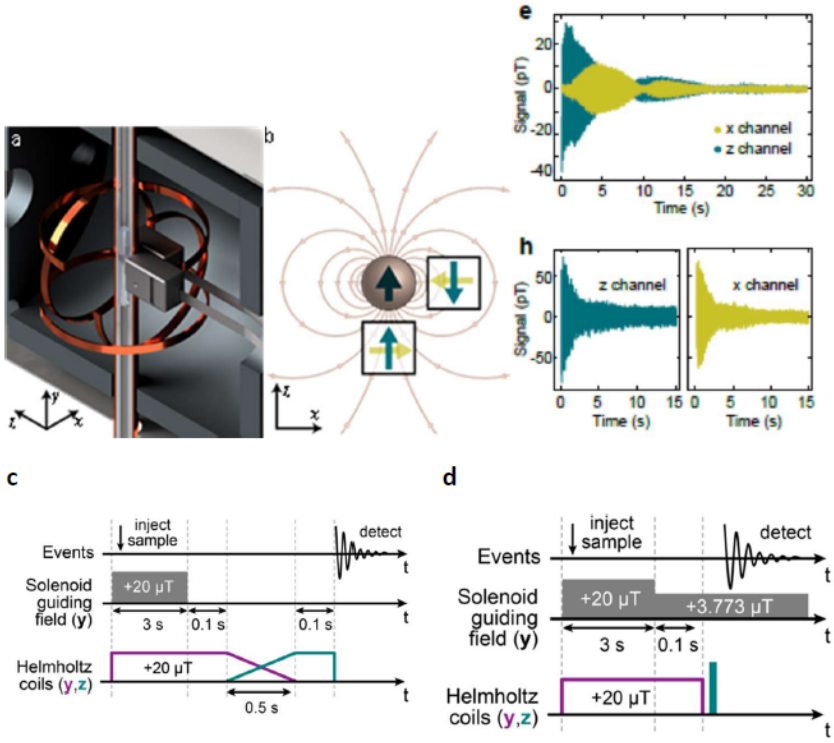

Figure 5.10: *Measurement of hyperpolarized metabolites. (a) Render of the experimental arrangement. (b) magnetic field of the sample (black arrow) and magnetic field detected by the detector along z (dark green) and along x (light green; (c) sequences used for the ULF experiments on hyperpolarized samples. (e) Zero-field signal in the x- and z-axes of the QuSpins generated from a sample of ^{13}C polarized metabolites. (h) Low-field time signal in the x- and z-axes of the QuSpins generated from a sample of ^{13}C polarized [1-^{13}C]pyruvate (lactate)*

In this part of the work, NMR experiments were performed in two field regimes: zero to ultralow field (ZULF), defined as the regime where the nuclear Larmor frequencies are small compared to the electron-mediated indirect spin-spin (J) coupling, and very low field (VLF), where the nuclear Larmor frequencies are larger than the J coupling, but chemical shifts are smaller than the resonance width. The experimental sequence for the ZULF NMR experiments is shown in Fig. 5.10c. The magnetization is rotated from its initial projection along the y axis to the z axis, after which the applied magnetic fields are suddenly turned off, resulting in the magnetic signal shown in Fig. 5.10e. Low-field NMR experiments can be performed by leaving the piercing solenoid on during signal acquisition. As depicted in Fig. 5.10d, the magnetization is kept along the y axis by a 20 μT field for sample injection, after which the field is reduced to a 3.8 μT detection field and the magnetization is rotated to the x-axis by a DC pulse along z, which results in the precessing magnetic signal shown in Fig. 5.10h.

5.5.3 Parahydrogen polarized Pyruvate detection at ZULF

[2]

An aqueous solution of hyperpolarized [1-^{13}C]pyruvate has been obtained according to the PHIP-SAH method.

The zero-field NMR spectrum of hyperpolarized [1-^{13}C]pyruvate (XA_3 spin system (one ^{13}C and three methyl protons), which exhibits peaks at J_{AX} and $2J_{AX}$, where J_{AX} is approximately 1.4 Hz, as can be observed in Figure 5.11.a.

[2] ZULF measurements were done by James Eills and Román Picazo Frutos as due to the COVID restrictions were not possible to visit physically their lab for in-person collaboration

At VLF (i.e. at 3.8 µT), the pseudo-high field condition is reached and the spectrum of the hyperpolarized ^{13}C carboxylate spin is a quartet. The small peak in the middle is presumed to be para-pyruvate, in which the J-coupling between the ^{13}C carboxylate and the protons is not observed.

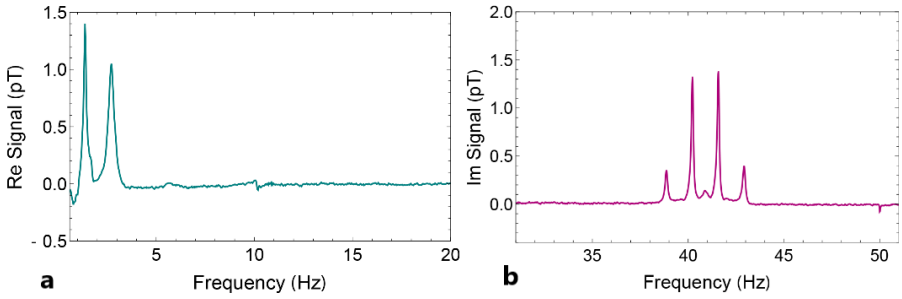

Figure 5.11: a) *NMR signal of the [1-^{13}C]pyruvate at the "zero" field;* ***b)*** *NMR signal of the [1-^{13}C]pyruvate at the VLF.*

In order to observed the conversion of pyruvate into lactate using ZULF-NMR, the aqueous solution of HP pyruvate was mixed with a buffered solution of NADH and lactate dehydrogenase (Sigma Aldrich, L7525), in a 5mm NMR tube. After mixing the enzyme solution with the HP metabolite, the NMR tube was dropped into the zero-field spectrometer for signal acquisition.

The zero field spectrum (Figure 5.12.a) of the pyruvate-to-lactate metabolic transformation shows the hyperpolarized signals of [1-^{13}C]pyruvate and [1-^{13}C]lactate. The peaks of each metabolite can be clearly identified form comparison with the simulated spectra, shown below in pink and teal.

The pyruvate-to-lactate conversion has also been observed at ULF (3.8 µT) NMR, where the 8-peak multiplet corresponding to lactate can be resolved in addition to the pyruvate 1:3:3:1 quartet (Fig. 5.12b) due to the ^{13}C coupling to the three protons. A small line can be observed at 41 Hz,

which corresponds to a small [1-^{13}C]parapyruvate impurity.[107] The production of lactate can also be seen at low field; a multiplet corresponding to lactate can be resolved in addition to the pyruvate quartet

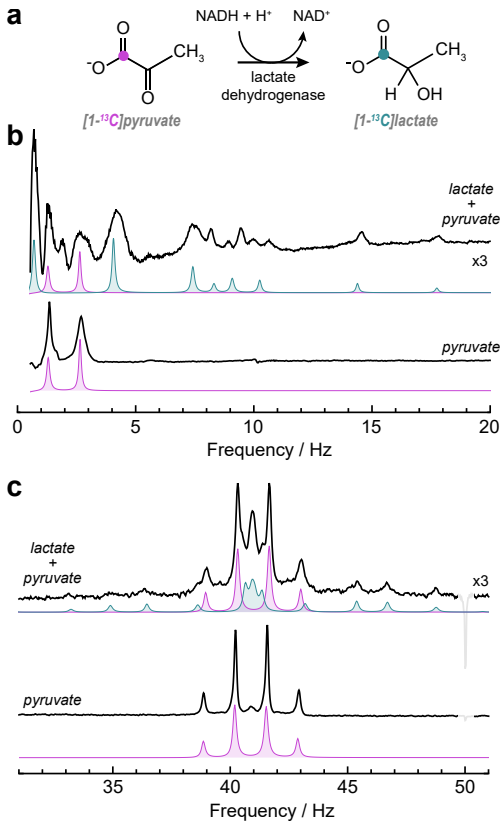

Figure 5.12: *a) The enzyme-catalysed conversion of pyruvate to lactate. (b) Zero-field NMR spectra of the reaction solution. (c) Pseudo-high-field NMR spectra of the reaction solution. For the pyruvate spectra the signal of hyperpolarized pyruvate was acquired directly. For the spectra that show lactate signals, lactate dehydrogenase and an excess of NADH was added to the hyperpolarized pyruvate solution prior to detection. All spectra are shown with 250 mHz line broadening. Simulations are shown beneath the spectra in pink and teal for pyruvate and lactate, respectively. The simulated spectra are vertically scaled to match the real spectra*

As can be observed from the spectrum, the lactate peaks are significantly

less intense than the pyruvate peaks, at ULF (3.8 µT), despite lactate is more concentrated than pyruvate, as observed in separated experiments carried out in the same conditions. This could be due to faster relaxation of lactate at this magnetic field. In order to validate this hypothesis, the hyperpolarization decay rate of [1-^{13}C]lactate and [1-^{13}C]pyruvate have been investigated at different ultra-low magnetic fields. To carry out these measurements, HP [1-^{13}C]lactate and [1-^{13}C]pyruvate have been kept, for 5 seconds, in a defined ULF that has been set into the magnetic shield. The experimental procedure is schematized in Fig. 5.13a. The ^{13}C hyperpolarization of the carboxylate signal, after storage at ULF, has been normalized to that observed after storage at geomagnetic field at the same time and the result can be seen in the figure 5.13b. From the hyperpolarization decay observed at different ultra-low field, it results that the intensity of the ^{13}C signal of pyruvate is not affected by the storage at ULF, while the relaxation of the ^{13}C carboxylate signal of lactate is significantly faster, apparently peaking around 2 µT.

The observed behaviour may be due to the scalar relaxation of the ^{13}C carboxylate spin that experiences a time-dependent J-coupling with the hydroxylic proton on lactate. This relaxation effect, (named Scalar Relaxation 1st kind, SR1K) is related to the exchange rate (k) of proton from OH^- group (350/s[108]. When the ^{13}C Larmor frequency corresponds to this exchange frequency, the relaxation rate is maximum. This hypothesis very well correlates with results obtained in LATEST MRI experiments, where we can see the highest intensity peak at 2 µT that is the same we've got in our measurements of relaxation for lactate (Fig. 5.13c).

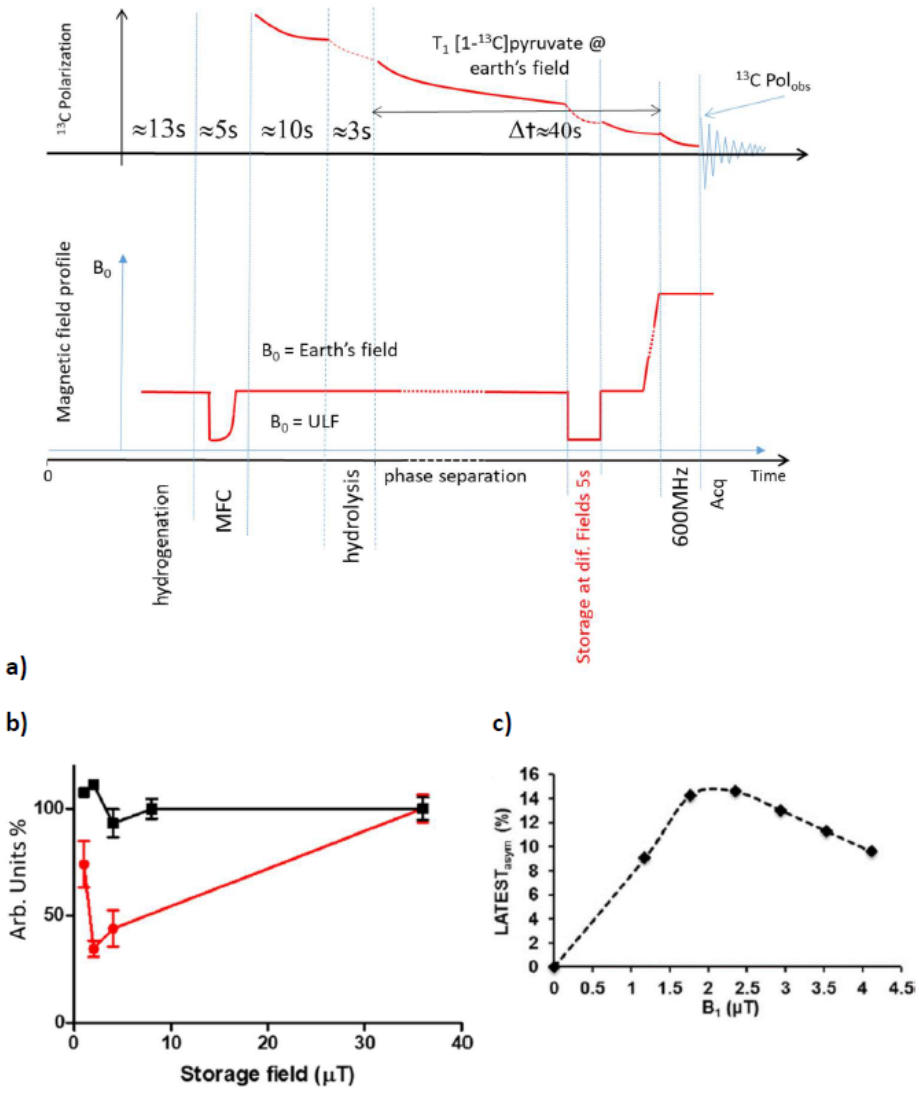

Figure 5.13: *a) timeline of the PHIP-SAH experiment with storage step at ULF: The passage from "high" field to "zero" is fast;* ***b)*** *effect of ULF on ^{13}C polarization: in red is lactate signal, in black – pyruvate;* ***c)*** *LATEST dependence on B_1 from a 50mM lactate phantom at pH 7*[108]

5.6 CONCLUSIONS

In this work it has been demonstrated that ParaHydrogen Polarized metabolites can be detected using ZULF NMR. The conversion of HP-pyruvate into lactate, catalyzed by the LDH enzyme, can be detected at zero and ultra-low field using a staggered arrangements of two optical magnetometers. This arrangement allows to reduce the noise in the lowest frequency region, making visible the HP signals derived from small J-couplings. The investigation of MR signals in the ZULF regime, thanks to the application of HP molecules, opens up a new field of investigations, since conventional NMR has been carried out, so far, using high magnetic field. The economic advantages given by the combined use of PHIP based hyperpolarization and ZULF are also evident. However, further research on OPM and PHIP polarization is still needed before that ZULF NMR could be used for metabolic investigations in biological systems. Nevertheless the herein reported studies are only the starting point for these new, promising field of research. As a possible future for this study we can imagine study of the metabolism in cells that gives promising future for cancer study and other types of research. The first fairly portable low-field MRI (Hyperfine)[109] already exists, a first step in the development of low-field tools for clinical use. The results obtained in recent years provide the potential to combine two financially and instrumentally accessible methods, such as PHIP and ZULF, in the future. The combination of these methods and possibly the construction of fully automated installations will allow them to be used both in conventional chemical laboratories and in laboratories where in-vitro and in-vivo experiments are carried out.

CONCLUSIONS

The work carried out during this PhD has been focused on the development and application of PHIP-SAH polarized substrates (and, in particular, of pyruvate) for metabolic investigations at high and ZULF magnetic field (results of what were shown at the chapter 5). In order to allow the application of these HP molecules for biological investigations, it is necessary that a high concentration of these substrates is obtained, together with hyperpolarization on ^{13}C (at least) sufficient to carry out MRI studies in-vivo or MRS in-cells. The first part of the work allowed to identify the main factors that determine the hyperpolarization level on the heteronucleus. On the basis of the results obtained, it clearly resulted that the method used for the transfer of spin order, from parahydrogen to the heteroatom, has to be improved. In fact the hyperpolarization on ^{13}C is only about 4.7 % while that observed on protons is ~ 20 %, in the allyl-pyruvate derivative. The ^{1}H hyperpolarization depends on the efficiency of the hydrogenation reaction, because mixing between the singlet and the triplet states occurs on reaction intermediates. About the

effect of the hydrogenation efficiency on the hyperpolarization level, the work carried out in chapter 4 showed that coordinating solvents, such as methanol and toluene, allow to obtain higher polarization because these take part into the hydrogenation catalysis. In particular, ^{13}C polarization observed in methanol was 9.2 %, taking the average between the two forms of pyruvate (oxo- and acetalic form), and 8.4 % in a toluene/ethanol mixture (5 % ethanol was used). Unfortunately, methanol cannot be used for biological applications. Conversely, the use of toluene allows the application of the phase extraction method, in which the hyperpolarized metabolite is extracted in the aqueous phase, while the catalyst is retained in the organic solvent. Traces of the organic solvent are present in the aqueous phase, following to phase extraction, that compromise the biocompatibility of the aqueous solution of the HP product. It has been demonstrated that these can be completely and quickly removed by means of filtration through a small amount of a lipophilic resin. Most importantly, the hyperpolarization level is not quite significantly affected by this passage and ^{13}C MRI and MRS experiments have been carried out in-vitro using the hyperpolarized pyruvate thus obtained.

SUPPLEMENTARY INFORMATION

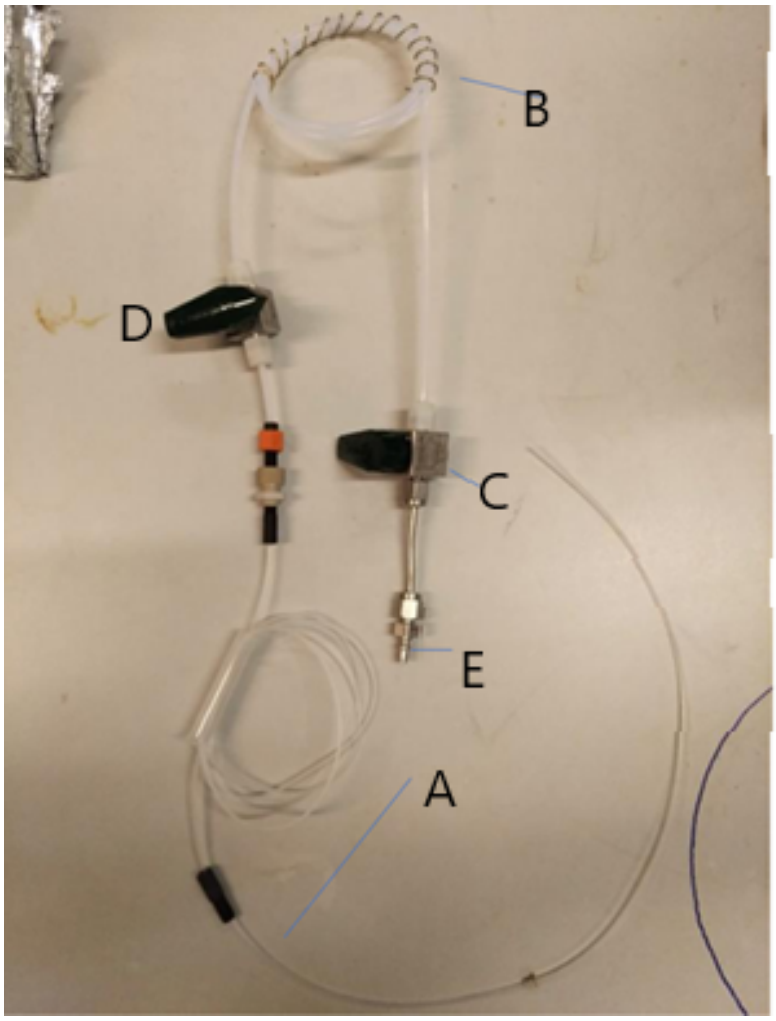

Figure S1: *Setup for hydrolysis: the base solution is loaded in tube A; Ar is connected to E, while D is kept closed, and tube B is pressurized using argon (1.5bar); valve D is closed. The setup is hold vertically and tube A is plunged in a hot water bath. For the injection of the aqueous base into the organic solution (hydrolysis step), the tip of tube A is placed a few mm above the organic solution of the product, then valve D is opened*

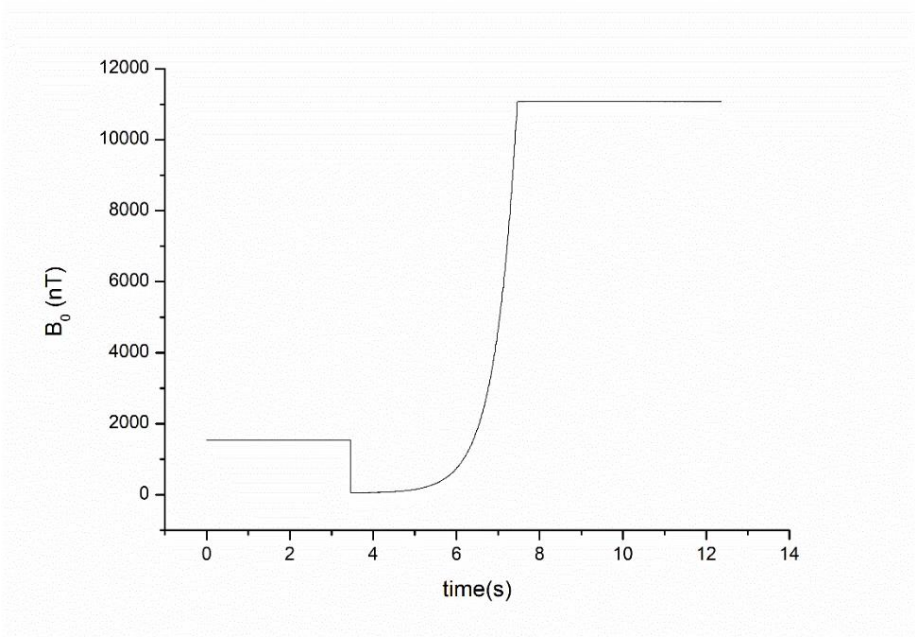

Figure S2: *Magnetic field profile used for magnetic field cycle. The measurement has been carried out by means of a three axis fluxgate magnetometer (Mag-03, Bartington, Witney, UK).*

Figure S3: *Filtration column connected to the NMR tube*

	δ ^{31}P (ppm) [Rh(cod)dppb]$^{+}$BF$_4$	J_{P-Rh} (Hz) [Rh(cod)dppb]$^{+}$BF$_4$	δ ^{31}P (ppm) [Rh(S$_2$)dppb]$^{+}$BF$_4$ S=Solvent	J_{P-Rh} (Hz) [Rh(S$_2$)dppb]$^{+}$BF$_4$ S=Solvent
Acetone-d6	24 ppm	144 Hz	50 ppm	195 Hz
Methanol-d4	24 ppm	144 Hz	53 ppm	200 Hz
Toluene	24 ppm	145 Hz	41 ppm	201 Hz
Toluene/Ethanol(5% v/v)	24 ppm	144 Hz	41 ppm	201 Hz
Ethanol-d6	24 ppm	144 Hz	52 ppm	200 Hz
$CDCl_3$	24 ppm	144 Hz	29 ppm; 46 ppm	-
$CDCl_3$/Ethanol(5% v/v)	24 ppm	144 Hz	29 ppm; 46 ppm	-

Table S1: *^{31}P-NMR signals of the catalyst in different solvents before activation ([Rh(cod)dppb]$^{+}$BF$_4$) and after hydrogenation of the coordinated diene. In coordinating solvents, the complex ([Rh(S$_2$)dppb]$^{+}$BF$_4$ is formed and the effect on the ^{31}P-NMR signal can be observed clearly. Chloroform is non-coordinating and other species (dimers) are formed.*

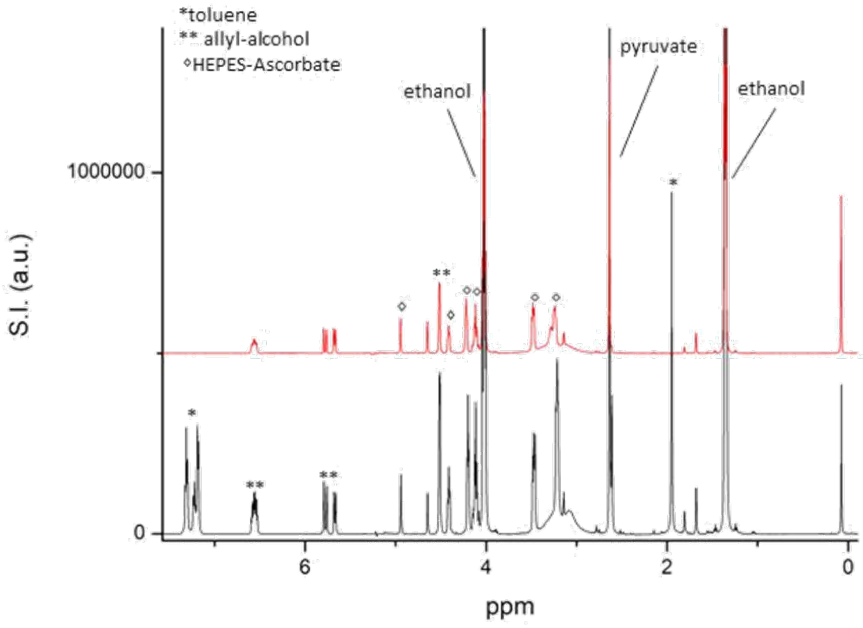

Figure S4: *Black line:* ^{1}*H-NMR of aqueous solutions of sodium[1-*^{13}*C]pyruvate obtained after hydrolysis following to the hydrogenation carried out in the toluene/ethanol solution. Red line:* ^{1}*H-NMR of aqueous solutions of sodium[1-*^{13}*C]pyruvate obtained after hydrolysis (as in the upper spectrum) and filtration through the Tenax column (see main text, Materials and methods section, for the experimental details).*

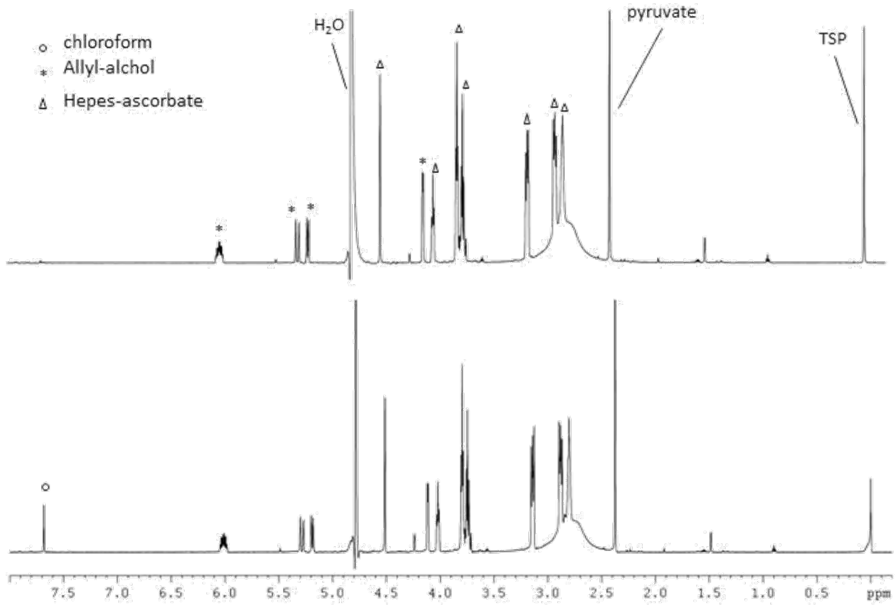

Figure S5: *Lower spectrum:* ^{1}*H-NMR spectrum of the aqueous solution of sodium [1-*^{13}*C]pyruvate obtained from hydrolysis of the ester (propargyl[1-*^{13}*C]pyruvate) hydrogenated in chloroform-d. Upper spectrum:* ^{1}*H-NMR spectrum of the aqueous solution of sodium [1-*^{13}*C]pyruvate obtained from hydrolysis of the ester (as in the upper spectrum) and filtration through the Tenax resin (*100 μL *in a syringe, retained by a PEEK filter, as reported in the main text, Materials and Methods).*

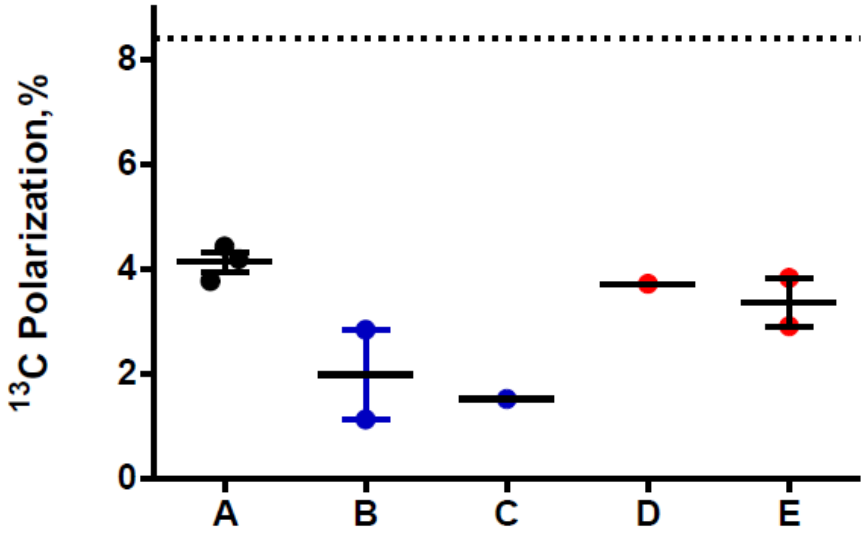

Figure S6: *^{13}C polarization on [1-^{13}C]pyruvate in the aqueous phase obtained after phase extraction from toluene/ethanol (ethanol 5% v/v). A) after hydrolysis, without filtration; B) after hydrolysis and passage through a SS filter (Idex Fluidics, Frit in Ferrule 1/16" PEEK Super Flangeless, SS Frit 2 µm); C) as in B, with Tenax resin; D) hydrolysis and passage through a PEEK filter (Idex Fluidics, Frit in Ferrule 1/16" PEEK Super Flangeless, PEEK Frit2 µm); E) as in D, with Tenax resin added*

BIBLIOGRAPHY

[1] S. R. Hartmann and E. L. Hahn, "Nuclear double resonance in the rotating frame," *Phys. Rev.*, vol. 128, pp. 2042–2053, Dec 1962. [Online]. Available: https://link.aps.org/doi/10.1103/PhysRev.128.2042

[2] D. R. Rich, T. R. Gentile, T. B. Smith, A. K. Thompson, and G. L. Jones, "Spin exchange optical pumping at pressures near 1 bar for neutron spin filters," *Applied Physics Letters*, vol. 80, no. 12, pp. 2210–2212, 2002.

[3] E. E. de Lange, J. P. Mugler III, J. R. Brookeman, J. Knight-Scott, J. D. Truwit, C. D. Teates, T. M. Daniel, P. L. Bogorad, and G. D. Cates, "Lung air spaces: Mr imaging evaluation with hyperpolarized 3he gas," *Radiology*, vol. 210, no. 3, pp. 851–857, 1999.

[4] L. R. Becerra, G. J. Gerfen, R. J. Temkin, D. J. Singel, and R. G. Griffin, "Dynamic nuclear polarization with a cyclotron resonance maser at 5 t," *Phys. Rev. Lett.*, vol. 71, pp. 3561–3564, Nov 1993. [Online]. Available: https://link.aps.org/doi/10.1103/PhysRevLett.71.3561

[5] G. J. Gerfen, L. R. Becerra, D. A. Hall, R. G. Griffin, R. J. Temkin, and D. J. Singel, "High frequency (140 ghz) dynamic nuclear polarization: polarization transfer to a solute in frozen aqueous solution," *The Journal of chemical physics*, vol. 102, no. 24, pp. 9494–9497, 1995.

[6] J. H. Ardenkjær-Larsen, B. Fridlund, A. Gram, G. Hansson, L. Hansson, M. H. Lerche, R. Servin, M. Thaning, and K. Golman, "Increase in signal-to-noise ratio of¿ 10,000 times in liquid-state nmr," *Proceedings of the National Academy of Sciences*, vol. 100, no. 18, pp. 10 158–10 163, 2003.

[7] K. Golman, R. i. Zandt, M. Lerche, R. Pehrson, and J. H. Ardenkjaer-Larsen, "Metabolic Imaging by Hyperpolarized 13C Magnetic Resonance Imaging for In vivo Tumor Diagnosis," *Cancer Research*, vol. 66, no. 22, pp. 10 855–10 860, 11 2006.

[8] K. Golman and J. S. Petersson, "Metabolic imaging and other applications of hyperpolarized 13c1," *Academic radiology*, vol. 13, no. 8, pp. 932–942, 2006.

[9] K. Golman, R. in 't Zandt, and M. Thaning, "Real-time metabolic imaging," *Proceedings of the National Academy of Sciences*, vol. 103, no. 30, pp. 11 270–11 275, 2006. [Online]. Available: https://www.pnas.org/doi/abs/10.1073/pnas.0601319103

[10] K. Golman, L. E. Olsson, O. Axelsson, S. Mansson, M. Karlsson, and J. Petersson, "Molecular imaging using hyperpolarized 13c," *The British journal of radiology*, vol. 76, no. suppl_2, pp. S118–S127, 2003.

[11] K. M. Brindle, "Imaging metabolism with hyperpolarized 13c-labeled cell substrates," *Journal of the American Chemical Society*, vol. 137, no. 20, pp. 6418–6427, 2015.

[12] G. Pileio, "Relaxation theory of nuclear singlet states in two spin-1/2 systems," *Progress in nuclear magnetic resonance spectroscopy*, vol. 56, no. 3, pp. 217–231, 2010.

[13] M. H. Levitt, "Long-lived states in nuclear magnetic resonance: an overview," 2020.

[14] R. W. Adams, J. A. Aguilar, K. D. Atkinson, M. J. Cowley, P. I. P. Elliott, S. B. Duckett, G. G. R. Green, I. G. Khazal, J. López-Serrano, and D. C. Williamson, "Reversible interactions with para-hydrogen enhance nmr sensitivity by polarization transfer," *Science*, vol. 323, no. 5922, pp. 1708–1711, 2009.

[15] K. D. Atkinson, M. J. Cowley, P. I. P. Elliott, S. B. Duckett, G. G. R. Green, J. López-Serrano, and A. C. Whitwood, "Spontaneous transfer of parahydrogen derived spin order to pyridine at low magnetic field," *Journal of the American Chemical Society*, vol. 131, no. 37, pp. 13 362–13 368, 2009.

[16] R. W. Adams, S. B. Duckett, R. A. Green, D. C. Williamson, and G. G. Green, "A theoretical basis for spontaneous polarization transfer in non-hydrogenative para hydrogen-induced polarization," *The Journal of chemical physics*, vol. 131, no. 19, p. 194505, 2009.

[17] K. D. Atkinson, M. J. Cowley, P. I. Elliott, S. B. Duckett, G. G. Green, J. Lopez-Serrano, and A. C. Whitwood, "Spontaneous transfer of para hydrogen derived spin order to pyridine at low magnetic field," *Journal of the American Chemical Society*, vol. 131, no. 37, pp. 13 362–13 368, 2009.

[18] A. N. Pravdivtsev, A. V. Yurkovskaya, H.-M. Vieth, K. L. Ivanov, and R. Kaptein, "Level anti-crossings are a key factor

for understanding para-hydrogen-induced hyperpolarization in sabre experiments," *ChemPhysChem*, vol. 14, no. 14, pp. 3327–3331, 2013.

[19] A. Svyatova, I. V. Skovpin, N. V. Chukanov, K. V. Kovtunov, E. Y. Chekmenev, A. N. Pravdivtsev, J.-B. Hövener, and I. V. Koptyug, "15n mri of slic-sabre hyperpolarized 15n-labelled pyridine and nicotinamide," *Chemistry–A European Journal*, vol. 25, no. 36, pp. 8465–8470, 2019.

[20] M. Fekete, F. Ahwal, and S. B. Duckett, "Remarkable levels of 15n polarization delivered through sabre into unlabeled pyridine, pyrazine, or metronidazole enable single scan nmr quantification at the mm level," *The Journal of Physical Chemistry B*, vol. 124, no. 22, pp. 4573–4580, 2020.

[21] D. A. Barskiy, R. V. Shchepin, A. M. Coffey, T. Theis, W. S. Warren, B. M. Goodson, and E. Y. Chekmenev, "Over 20% 15n hyperpolarization in under one minute for metronidazole, an antibiotic and hypoxia probe," *Journal of the American Chemical Society*, vol. 138, no. 26, pp. 8080–8083, 2016.

[22] J. R. Birchall, M. S. Kabir, O. G. Salnikov, N. V. Chukanov, A. Svyatova, K. V. Kovtunov, I. V. Koptyug, J. G. Gelovani, B. M. Goodson, W. Pham *et al.*, "Quantifying the effects of quadrupolar sinks via 15 n relaxation dynamics in metronidazoles hyperpolarized via sabre-sheath," *Chemical Communications*, vol. 56, no. 64, pp. 9098–9101, 2020.

[23] H. Park and Q. Wang, "State-of-the-art accounts of hyperpolarized 15 n-labeled molecular imaging probes for magnetic resonance spectroscopy and imaging," *Chemical Science*, 2022.

[24] C. R. Bowers and D. P. Weitekamp, "Parahydrogen and synthesis allow

dramatically enhanced nuclear alignment," *Journal of the American Chemical Society*, vol. 109, no. 18, pp. 5541–5542, 1987.

[25] T. C. Eisenschmid, R. U. Kirss, P. P. Deutsch, S. I. Hommeltoft, R. Eisenberg, J. Bargon, R. G. Lawler, and A. L. Balch, "Para hydrogen induced polarization in hydrogenation reactions," *Journal of the American Chemical Society*, vol. 109, no. 26, pp. 8089–8091, 1987.

[26] C. R. Bowers and D. P. Weitekamp, "Transformation of symmetrization order to nuclear-spin magnetization by chemical reaction and nuclear magnetic resonance," *Phys. Rev. Lett.*, vol. 57, pp. 2645–2648, Nov 1986. [Online]. Available: https://link.aps.org/doi/10.1103/PhysRevLett.57.2645

[27] M. G. Pravica and D. P. Weitekamp, "Net nmr alignment by adiabatic transport of parahydrogen addition products to high magnetic field," *Chemical physics letters*, vol. 145, no. 4, pp. 255–258, 1988.

[28] A. Viale and S. Aime, "Current concepts on hyperpolarized molecules in mri," *Current opinion in chemical biology*, vol. 14, no. 1, pp. 90–96, 2010.

[29] K. Münnemann, M. Kölzer, I. Blakey, A. K. Whittaker, and K. J. Thurecht, "Hyperbranched polymers for molecular imaging: designing polymers for parahydrogen induced polarisation (phip)," *Chemical Communications*, vol. 48, no. 10, pp. 1583–1585, 2012.

[30] M. Roth, J. Bargon, H. W. Spiess, and A. Koch, "Parahydrogen induced polarization of barbituric acid derivatives: 1h hyperpolarization studies," *Magnetic Resonance in Chemistry*, vol. 46, no. 8, pp. 713–717, 2008.

[31] S. Aime, W. Dastru, R. Gobetto, D. Santelia, and A. Viale, "Agents

for polarization enhancement in mri," *Molecular Imaging I*, pp. 247–272, 2008.

[32] R. V. Shchepin, A. M. Coffey, K. W. Waddell, and E. Y. Chekmenev, "Parahydrogen-induced polarization with a rh-based monodentate ligand in water," *The journal of physical chemistry letters*, vol. 3, no. 22, pp. 3281–3285, 2012.

[33] F. Reineri, A. Viale, S. Ellena, D. Alberti, T. Boi, G. B. Giovenzana, R. Gobetto, S. S. Premkumar, and S. Aime, "15n magnetic resonance hyperpolarization via the reaction of parahydrogen with 15n-propargylcholine," *Journal of the American Chemical Society*, vol. 134, no. 27, pp. 11 146–11 152, 2012.

[34] F. Reineri, A. Viale, W. Dastrù, R. Gobetto, and S. Aime, "How to design 13c para-hydrogen-induced polarization experiments for mri applications," *Contrast Media & Molecular Imaging*, vol. 6, no. 2, pp. 77–84, 2011.

[35] B. T. Reineri F. and A. S., "Parahydrogen induced polarization of 13c carboxylate resonance in acetate and pyruvate." *Nat Commun*, vol. 6, no. 5858, 2015.

[36] E. Cavallari, C. Carrera, S. Aime, and F. Reineri, "Studies to enhance the hyperpolarization level in phip-sah-produced c13-pyruvate," *Journal of Magnetic Resonance*, vol. 289, pp. 12–17, 2018.

[37] E. M. Serrao and K. M. Brindle, "Potential clinical roles for metabolic imaging with hyperpolarized [1-13c] pyruvate," *Frontiers in oncology*, vol. 6, p. 59, 2016.

[38] J. A. Bastiaansen, T. Cheng, H. Lei, R. Gruetter, and A. Comment, "Direct noninvasive estimation of myocardial tricarboxylic acid cycle flux in vivo using hyperpolarized 13c magnetic resonance," *Journal of molecular and cellular cardiology*, vol. 87, pp. 129–137, 2015.

[39] B. K. Gallagher FA, Kettunen MI, "Biomedical applications on hyperpolarized 13c magnetic resonance imaging," *Prog Nucl Magn Reson Spectrosc*, vol. 55, no. 285-295, 2009.

[40] Y. Xu, S. Ringgaard, C. Ø. Mariager, L. B. Bertelsen, M. Schroeder, H. Qi, C. Laustsen, and H. Stødkilde-Jørgensen, "Hyperpolarized 13c magnetic resonance imaging can detect metabolic changes characteristic of penumbra in ischemic stroke," *Tomography*, vol. 3, no. 2, pp. 67–73, 2017.

[41] M. I. Kettunen, D.-e. Hu, T. H. Witney, R. McLaughlin, F. A. Gallagher, S. E. Bohndiek, S. E. Day, and K. M. Brindle, "Magnetization transfer measurements of exchange between hyperpolarized [1-13c] pyruvate and [1-13c] lactate in a murine lymphoma," *Magnetic Resonance in Medicine: An Official Journal of the International Society for Magnetic Resonance in Medicine*, vol. 63, no. 4, pp. 872–880, 2010.

[42] J. Kurhanewicz, D. B. Vigneron, K. Brindle, E. Y. Chekmenev, A. Comment, C. H. Cunningham, R. J. DeBerardinis, G. G. Green, M. O. Leach, S. S. Rajan *et al.*, "Analysis of cancer metabolism by imaging hyperpolarized nuclei: prospects for translation to clinical research," *Neoplasia*, vol. 13, no. 2, pp. 81–97, 2011.

[43] S. B. Duckett and R. E. Mewis, "Application of para hydrogen induced polarization techniques in nmr spectroscopy and imaging," *Accounts of chemical research*, vol. 45, no. 8, pp. 1247–1257, 2012.

[44] E. Cavallari, C. Carrera, S. Aime, and F. Reineri, "13c mr hyperpolarization of lactate by using parahydrogen and metabolic transformation in vitro," *Chemistry–A European Journal*, vol. 23, no. 5, pp. 1200–1204, 2017.

[45] ——, "Metabolic studies of tumor cells using [1-13c] pyruvate hyperpolarized by means of phip-side arm hydrogenation," *ChemPhysChem*, vol. 20, no. 2, pp. 318–325, 2019.

[46] "The 13c hyperpolarized pyruvate generated by parahydrogen detects the response of the heart to altered metabolism in real time," *Sci Rep*, vol. 8, no. 8366, 2018. [Online]. Available: https://doi.org/10.1038/s41598-018-26583-2

[47] V. Breukels, K. C. F. Jansen, F. H. van Heijster, A. Capozzi, P. J. M. van Bentum, J. A. Schalken, A. Comment, and T. W. Scheenen, "Direct dynamic measurement of intracellular and extracellular lactate in small-volume cell suspensions with 13c hyperpolarised nmr," *NMR in Biomedicine*, vol. 28, no. 8, pp. 1040–1048, 2015.

[48] R. Francesca, D. Valeria, E. Cavallari, and S. Aime, "Assessing the transport rate of hyperpolarized pyruvate and lactate from the intra-to the extracellular space," *NMR in biomedicine*, vol. 29, no. 8, pp. 1022–1027, 2016.

[49] R. Balzan, L. Fernandes, L. Pidial, A. Comment, B. Tavitian, and P. R. Vasos, "Pyruvate cellular uptake and enzymatic conversion probed by dissolution dnp-nmr: the impact of overexpressed membrane transporters," *Magnetic Resonance in Chemistry*, vol. 55, no. 6, pp. 579–583, 2017.

[50] H. Zeng, Y. Lee, and C. Hilty, "Quantitative rate determination by dynamic nuclear polarization enhanced nmr of a diels- alder reaction," *Analytical chemistry*, vol. 82, no. 21, pp. 8897–8902, 2010.

[51] L. Higgins, H. Withers, A. Garbens, H. Love, L. Magnoni, S. Hayward, and C. Moyes, "Hypoxia and the metabolic phenotype of prostate cancer cells," *Biochimica et Biophysica Acta (BBA)-Bioenergetics*, vol. 1787, no. 12, pp. 1433–1443, 2009.

[52] G. F. e. a. Day S., Kettunen M., "Detecting tumor response to treatment using hyperpolarized 13c magnetic resonance imaging and spectroscopy." *Nat Med*, vol. 13, p. 1382–1387, 2007.

[53] R. Hussien and G. A. Brooks, "Mitochondrial and plasma membrane lactate transporter and lactate dehydrogenase isoform expression in breast cancer cell lines," *Physiological genomics*, vol. 43, no. 5, pp. 255–264, 2011.

[54] C. J. Valvona, H. L. Fillmore, P. B. Nunn, and G. J. Pilkington, "The regulation and function of lactate dehydrogenase a: therapeutic potential in brain tumor," *Brain pathology*, vol. 26, no. 1, pp. 3–17, 2016.

[55] M. Ždralević, A. Brand, L. Di Ianni, K. Dettmer, J. Reinders, K. Singer, K. Peter, A. Schnell, C. Bruss, S.-M. Decking *et al.*, "Double genetic disruption of lactate dehydrogenases a and b is required to ablate the "warburg effect" restricting tumor growth to oxidative metabolism," *Journal of Biological Chemistry*, vol. 293, no. 41, pp. 15 947–15 961, 2018.

[56] W. Zhu, L. Ma, J. Qian, J. Xu, T. Xu, L. Pang, H. Zhou, Y. Shu, and J. Zhou, "The molecular mechanism and clinical significance of ldha in her2-mediated progression of gastric cancer," *American journal of translational research*, vol. 10, no. 7, p. 2055, 2018.

[57] M. J. Rogatzki, B. S. Ferguson, M. L. Goodwin, and L. B. Gladden, "Lactate is always the end product of glycolysis," *Frontiers in neuroscience*, vol. 9, p. 22, 2015.

[58] K. Golman, O. Axelsson, H. Jóhannesson, S. Månsson, C. Olofsson, and J. Petersson, "Parahydrogen-induced polarization in imaging: Subsecond 13c angiography," *Magnetic Resonance in Medicine: An Official Journal of the International Society for Magnetic Resonance in Medicine*, vol. 46, no. 1, pp. 1–5, 2001.

[59] L. E. Olsson, C.-M. Chai, O. Axelsson, M. Karlsson, K. Golman, and J. S. Petersson, "Mr coronary angiography in pigs with intraarterial injections of a hyperpolarized 13c substance," *Magnetic Resonance in Medicine: An Official Journal of the International Society for Magnetic Resonance in Medicine*, vol. 55, no. 4, pp. 731–737, 2006.

[60] J.-B. Hövener, A. N. Pravdivtsev, B. Kidd, C. R. Bowers, S. Glöggler, K. V. Kovtunov, M. Plaumann, R. Katz-Brull, K. Buckenmaier, A. Jerschow *et al.*, "Parahydrogen-based hyperpolarization for biomedicine," *Angewandte Chemie International Edition*, vol. 57, no. 35, pp. 11 140–11 162, 2018.

[61] C. C. e. a. Reineri F., Cavallari E., "Hydrogenative-phip polarized metabolites for biological studies." *Magn Reson Mater Phy*, vol. 34, p. 25–47, 2021.

[62] P. J. Rayner and S. B. Duckett, "Signal amplification by reversible exchange (sabre): From discovery to diagnosis," *Angewandte Chemie International Edition*, vol. 57, no. 23, pp. 6742–6753, 2018.

[63] S. J. Nelson, J. Kurhanewicz, D. B. Vigneron, P. E. Z. Larson, A. L. Harzstark, M. Ferrone, M. van Criekinge, J. W. Chang, R. Bok, I. Park,

G. Reed, L. Carvajal, E. J. Small, P. Munster, V. K. Weinberg, J. H. Ardenkjaer-Larsen, A. P. Chen, R. E. Hurd, L.-I. Odegardstuen, F. J. Robb, J. Tropp, and J. A. Murray, "Metabolic imaging of patients with prostate cancer using hyperpolarized [1-¡sup¿13¡/sup¿c]pyruvate," *Science Translational Medicine*, vol. 5, no. 198, pp. 198ra108–198ra108, 2013.

[64] C. H. Cunningham, J. Y. Lau, A. P. Chen, B. J. Geraghty, W. J. Perks, I. Roifman, G. A. Wright, and K. A. Connelly, "Hyperpolarized 13c metabolic mri of the human heart: initial experience," *Circulation research*, vol. 119, no. 11, pp. 1177–1182, 2016.

[65] E. Cavallari, C. Carrera, T. Boi, S. Aime, and F. Reineri, "Effects of magnetic field cycle on the polarization transfer from parahydrogen to heteronuclei through long-range j-couplings," *The Journal of Physical Chemistry B*, vol. 119, no. 31, pp. 10 035–10 041, 2015.

[66] L. Dagys, A. P. Jagtap, S. Korchak, S. Mamone, P. Saul, M. H. Levitt, and S. Glöggler, "Nuclear hyperpolarization of (1-13 c)-pyruvate in aqueous solution by proton-relayed side-arm hydrogenation," *Analyst*, vol. 146, no. 5, pp. 1772–1778, 2021.

[67] B. J. Tickner, O. Semenova, W. Iali, P. J. Rayner, A. C. Whitwood, and S. B. Duckett, "Optimisation of pyruvate hyperpolarisation using sabre by tuning the active magnetisation transfer catalyst," *Catalysis science & technology*, vol. 10, no. 5, pp. 1343–1355, 2020.

[68] W. Iali, S. S. Roy, B. J. Tickner, F. Ahwal, A. J. Kennerley, and S. B. Duckett, "Hyperpolarising pyruvate through signal amplification by reversible exchange (sabre)," *Angewandte Chemie*, vol. 131, no. 30, pp. 10 377–10 381, 2019.

[69] H. R. Chan, P. Bhattacharya, A. Imam, A. Freundlich, T. Tran, W. H. Perman, A. P. Lin, K. Harris, E. Y. Chekmenev, M. Ingram *et al.*, "No clinical toxicity is seen in vivo from hyperpolarized pasadena mr reagents or catalyst," in *Proc. Intl. Soc. Mag. Reson. Med*, vol. 17, 2009, p. 2448.

[70] D. A. Barskiy, L. A. Ke, X. Li, V. Stevenson, N. Widarman, H. Zhang, A. Truxal, and A. Pines, "Rapid catalyst capture enables metal-free para-hydrogen-based hyperpolarized contrast agents," *The Journal of Physical Chemistry Letters*, vol. 9, no. 11, pp. 2721–2724, 2018.

[71] W. Iali, A. M. Olaru, G. G. Green, and S. B. Duckett, "Achieving high levels of nmr-hyperpolarization in aqueous media with minimal catalyst contamination using sabre," *Chemistry–A European Journal*, vol. 23, no. 44, pp. 10 491–10 495, 2017.

[72] F. Reineri, A. Viale, S. Ellena, T. Boi, V. Daniele, R. Gobetto, and S. Aime, "Use of labile precursors for the generation of hyperpolarized molecules from hydrogenation with parahydrogen and aqueous-phase extraction," *Angewandte Chemie*, vol. 123, no. 32, pp. 7488–7491, 2011.

[73] B. Nicholson, B. P. Maguire, and D. B. Bursill, "Henry's law constants for the trihalomethanes: effects of water composition and temperature," *Environmental science & technology*, vol. 18, no. 7, pp. 518–521, 1984.

[74] S. Margolis and B. Coxon, "Identification and quantitation of the impurities in sodium pyruvate," *Analytical Chemistry*, vol. 58, no. 12, pp. 2504–2510, 1986.

[75] A. M. Coffey, R. V. Shchepin, M. L. Truong, K. Wilkens, W. Pham, and E. Y. Chekmenev, "Open-source automated parahydrogen hyperpolarizer for molecular imaging using 13c metabolic contrast agents," *Analytical chemistry*, vol. 88, no. 16, pp. 8279–8288, 2016.

[76] J.-B. Hövener, E. Y. Chekmenev, K. C. Harris, W. H. Perman, L. W. Robertson, B. D. Ross, and P. Bhattacharya, "Pasadena hyperpolarization of 13c biomolecules: equipment design and installation," *Magnetic Resonance Materials in Physics, Biology and Medicine*, vol. 22, no. 2, pp. 111–121, 2009.

[77] A. S. Kiryutin, G. Sauer, S. Hadjiali, A. V. Yurkovskaya, H. Breitzke, and G. Buntkowsky, "A highly versatile automatized setup for quantitative measurements of phip enhancements," *Journal of Magnetic Resonance*, vol. 285, pp. 26–36, 2017.

[78] A. B. Schmidt, S. Berner, W. Schimpf, C. Müller, T. Lickert, N. Schwaderlapp, S. Knecht, J. Skinner, A. Dost, P. Rovedo *et al.*, "Liquid-state carbon-13 hyperpolarization generated in an mri system for fast imaging," *Nature communications*, vol. 8, no. 1, pp. 1–8, 2017.

[79] A. B. Schmidt, S. Berner, M. Braig, M. Zimmermann, J. Hennig, D. von Elverfeldt, and J.-B. Hövener, "In vivo 13c-mri using sambadena," *PloS one*, vol. 13, no. 7, p. e0200141, 2018.

[80] A. Meißner, E. Alberico, H.-J. Drexler, W. Baumann, and D. Heller, "Rhodium diphosphine complexes: a case study for catalyst activation and deactivation," *Catalysis Science & Technology*, vol. 4, no. 10, pp. 3409–3425, 2014.

[81] R. A. Sanchez-Delgado, N. Valencia, R. Marquez-Silva, A. Andriollo, and M. Medina, "Chemistry and catalytic properties of ruthenium and osmium complexes. 3. development of highly active systems for the homogeneous hydrogenation of aldehydes and ketones," *Inorganic Chemistry*, vol. 25, no. 8, pp. 1106–1111, 1986.

[82] M. Itoda, Y. Naganawa, M. Ito, H. Nonaka, and S. Sando, "Structural exploration of rhodium catalysts and their kinetic studies for efficient parahydrogen-induced polarization by side arm hydrogenation," *RSC advances*, vol. 9, no. 32, pp. 18 183–18 190, 2019.

[83] R. H. Crabtree, P. C. Demou, D. Eden, J. M. Mihelcic, C. A. Parnell, J. M. Quirk, and G. E. Morris, "Dihydrido olefin and solvento complexes of iridium and the mechanisms of olefin hydrogenation and alkane dehydrogenation," *Journal of the American Chemical Society*, vol. 104, no. 25, pp. 6994–7001, 1982.

[84] "IFA-Database of hazardous substances (GESTIS), https://gestis.dguv.de/."

[85] A. Preetz, C. Fischer, C. Kohrt, H.-J. Drexler, W. Baumann, and D. Heller, "Cationic rhodium-binap complexes: Full characterization of solvate-and arene-bridged dimeric species," *Organometallics*, vol. 30, no. 19, pp. 5155–5159, 2011.

[86] "https://www.federalregister.gov/documents/2017/01/11/2016-31262/national-primary-drinking-."

[87] P. Maria *et al.*, "Evaluation of anasorb cms and comparison with tenax ta for the sampling of volatile organic compounds in indoor and outdoor air by breakthrough measurements," *Analyst*, vol. 121, no. 3, pp. 303–307, 1996.

[88] L. Chu, S. Deng, R. Zhao, J. Deng, and X. Kang, "Comparison of adsorption/desorption of volatile organic compounds (vocs) on electrospun nanofibers with tenax ta for potential application in sampling," *PLoS One*, vol. 11, no. 10, p. e0163388, 2016.

[89] M. P. Ledbetter and D. Budker, "Zero-field nuclear magnetic resonance," *Physics Today*, vol. 66, no. 4, pp. 44–49, 2013.

[90] K. Buckenmaier, M. Rudolph, P. Fehling, T. Steffen, C. Back, R. Bernard, R. Pohmann, J. Bernarding, R. Kleiner, D. Koelle *et al.*, "Mutual benefit achieved by combining ultralow-field magnetic resonance and hyperpolarizing techniques," *Review of Scientific Instruments*, vol. 89, no. 12, p. 125103, 2018.

[91] S. Appelt, H. Kühn, F. W. Häsing, and B. Blümich, "Chemical analysis by ultrahigh-resolution nuclear magnetic resonance in the earth's magnetic field," *Nature Physics*, vol. 2, no. 2, pp. 105–109, 2006.

[92] J. Natterer and J. Bargon, "Parahydrogen induced polarization," *Progress in Nuclear Magnetic Resonance Spectroscopy*, vol. 31, no. 4, pp. 293–315, 1997.

[93] T. G. Walker and W. Happer, "Spin-exchange optical pumping of noble-gas nuclei," *Reviews of modern physics*, vol. 69, no. 2, p. 629, 1997.

[94] T. Wu, J. W. Blanchard, G. P. Centers, N. L. Figueroa, A. Garcon, P. W. Graham, D. F. J. Kimball, S. Rajendran, Y. V. Stadnik, A. O. Sushkov *et al.*, "Search for axionlike dark matter with a liquid-state nuclear spin comagnetometer," *Physical review letters*, vol. 122, no. 19, p. 191302, 2019.

[95] "https://blog.zulf.eu/BP3.php."

[96] M. C. Tayler, J. Ward-Williams, and L. F. Gladden, "Ultralow-field nuclear magnetic resonance of liquids confined in ferromagnetic and paramagnetic materials," *Applied Physics Letters*, vol. 115, no. 7, p. 072409, 2019.

[97] G. Balasubramanian, I. Chan, R. Kolesov, M. Al-Hmoud, J. Tisler, C. Shin, C. Kim, A. Wojcik, P. R. Hemmer, A. Krueger *et al.*, "Nanoscale imaging magnetometry with diamond spins under ambient conditions," *Nature*, vol. 455, no. 7213, pp. 648–651, 2008.

[98] D. Budker and M. Romalis, "Optical magnetometry," *Nature physics*, vol. 3, no. 4, pp. 227–234, 2007.

[99] J. Osborne, J. Orton, O. Alem, and V. Shah, "Fully integrated standalone zero field optically pumped magnetometer for biomagnetism," in *Steep dispersion engineering and opto-atomic precision metrology XI*, vol. 10548. International Society for Optics and Photonics, 2018, p. 105481G.

[100] J. W. Blanchard, T. Wu, J. Eills, Y. Hu, and D. Budker, "Zero-to ultralow-field nuclear magnetic resonance j-spectroscopy with commercial atomic magnetometers," *Journal of Magnetic Resonance*, vol. 314, p. 106723, 2020.

[101] A. W. Overhauser, "Polarization of nuclei in metals," *Phys. Rev.*, vol. 92, pp. 411–415, Oct 1953. [Online]. Available: https://link.aps.org/doi/10.1103/PhysRev.92.411

[102] M. Ledbetter, C. Crawford, A. Pines, D. Wemmer, S. Knappe, J. Kitching, and D. Budker, "Optical detection of nmr j-spectra at zero magnetic field," *Journal of magnetic resonance*, vol. 199, no. 1, pp. 25–29, 2009.

[103] M. C. Butler, M. P. Ledbetter, T. Theis, J. W. Blanchard, D. Budker, and A. Pines, "Multiplets at zero magnetic field: The geometry of zero-field nmr," *The Journal of chemical physics*, vol. 138, no. 18, p. 184202, 2013.

[104] T. Theis, J. W. Blanchard, M. C. Butler, M. P. Ledbetter, D. Budker,

and A. Pines, "Chemical analysis using j-coupling multiplets in zero-field nmr," *Chemical Physics Letters*, vol. 580, pp. 160–165, 2013.

[105] E. Cavallari, C. Carrera, G. Di Matteo, O. Bondar, S. Aime, and F. Reineri, "In-vitro nmr studies of prostate tumor cell metabolism by means of hyperpolarized [1-13c] pyruvate obtained using the phip-sah method," *Frontiers in oncology*, vol. 10, p. 497, 2020.

[106] V. Yashchuk, J. Granwehr, D. Kimball, S. Rochester, A. Trabesinger, J. Urban, D. Budker, and A. Pines, "Hyperpolarized xenon nuclear spins detected by optical atomic magnetometry," *Phys. Rev. Lett.*, vol. 93, no. 16, p. 160801, 2004.

[107] A. C. Rios, P. P. Bera, J. A. Moreno, and G. Cooper, "Pyruvate aldol condensation product: A metabolite that escaped synthetic preparation for over a century," *ACS omega*, vol. 5, no. 25, pp. 15 063–15 068, 2020.

[108] C. DeBrosse, R. P. R. Nanga, P. Bagga, K. Nath, M. Haris, F. Marincola, M. D. Schnall, H. Hariharan, and R. Reddy, "Lactate chemical exchange saturation transfer (latest) imaging in vivo: a biomarker for ldh activity," *Scientific reports*, vol. 6, no. 1, pp. 1–10, 2016.

[109] "https://https://hyperfine.io/."

LIST OF FIGURES

LIST OF TABLES

PUBLICATIONS AND ATTENDED CONFERENCES

1. Eills J., Picazo-Frutos R., **Bondar O.**, Cavallari E., Carrera C., Barker S. J., Utz M., Aime S., Reineri F., Budker D. and Blanchard J. W. (2022). Metabolic Reactions Studied by Zero-and Low-Field Nuclear Magnetic Resonance. arXiv preprint arXiv:2205.12380.

2. **Bondar O.**, Cavallari E., Carrera C., Aime S., and Reineri F. (2021). Effect of the hydrogenation solvent in the PHIP-SAH hyperpolarization of [1-13C] pyruvate. Catalysis Today.

3. Carrera C., Cavallari E., Digilio G., **Bondar O.**, Aime S., and Reineri F. (2021). ParaHydrogen polarized ethyl-[1-13C] pyruvate in water, a key substrate for fostering the PHIP-SAH approach to metabolic imaging. ChemPhysChem, 22(11), 1042-1048.

4. Cavallari E., Carrera C., Di Matteo G., **Bondar O.**, Aime S., and Reineri F. (2020). In-vitro NMR studies of prostate tumor cell metabolism by means of hyperpolarized [1-13C] pyruvate obtained using the PHIP-sah method. Frontiers in oncology, 10, 497.

5. XLVIII GIDRM National Congress, L'Aquila 11-13.09.2019 (poster presentation);

6. Virtual PERM2020 Conference, Online 27-29.07.2020;

7. First Conference on Zero and Ultra-Low Fields NMR, Online 1-4.09.2020 (poster presentation);

8. EUROMAR 2020, Online 7-8.12.2020 (conference paper);

9. Virtual PERM2021 Conference, Online 21-23.06.2021 (oral presentation).

10. HYP2021 Conference, Lyon 05-09.09.2021 (round table presentation).